ISSN: 2152-7385 Volume 10, Number 7, July 2019

Scientific Research Publishing

Applied Mathematics

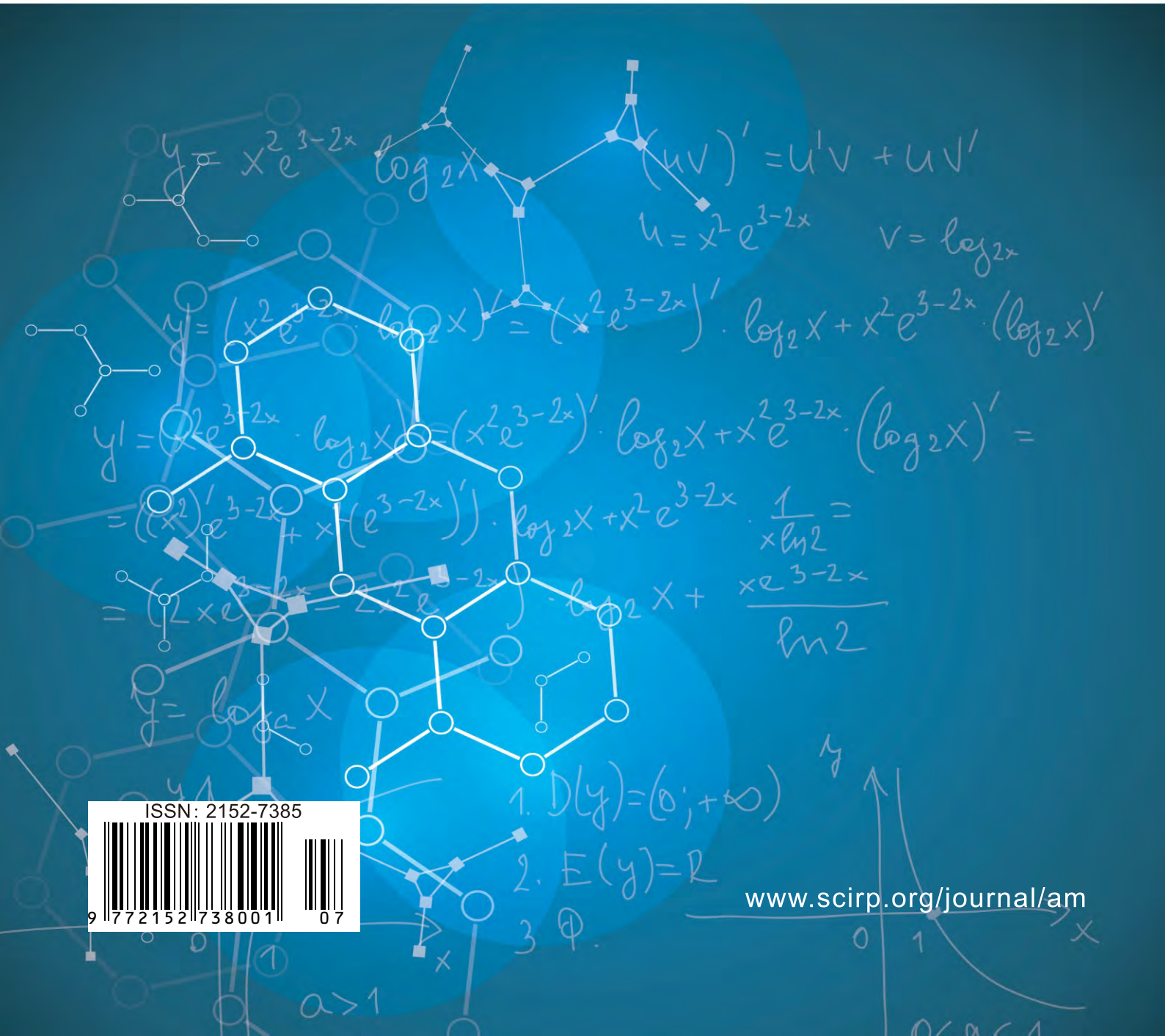

Journal Editorial Board

ISSN Print: 2152-7385 ISSN Online: 2152-7393

http://www.scirp.org/journal/am

Editorial Board

Scientific Research Publishing

Applied Mathematics, 2019, 10, 513-625
http://www.scirp.org/journal/am
ISSN Online: 2152-7393
ISSN Print: 2152-7385

Table of Contents

Volume 10 Number 7 July 2019

Applied Mathematics (AM)
Journal Information

SUBSCRIPTIONS

The *Applied Mathematics* (Online at Scientific Research Publishing, www.SciRP.org) is published monthly by Scientific Research Publishing, Inc., USA.

Subscription rates:
Print: $89 per copy.
To subscribe, please contact Journals Subscriptions Department, E-mail: sub@scirp.org

SERVICES

Advertisements
Advertisement Sales Department, E-mail: service@scirp.org

Reprints (minimum quantity 100 copies)
Reprints Co-ordinator, Scientific Research Publishing, Inc., USA.
E-mail: sub@scirp.org

COPYRIGHT

PRODUCTION INFORMATION

For manuscripts that have been accepted for publication, please contact:
E-mail: am@scirp.org

Applied Mathematics, 2019, 10, 513-520
http://www.scirp.org/journal/am
ISSN Online: 2152-7393
ISSN Print: 2152-7385

Switching Regimes in Economics: The Contraction Mapping and the ω-Limit Set

Pascal Stiefenhofer[1,2], Peter Giesl[1]

[1]Department of Mathematics, University of Sussex, Falmer, East Sussex, UK
[2]Brighton Business School, University of Brighton, Brighton, UK
Email: p.stiefenhofer@sussex.ac.uk, p.stiefenhofer@brighton.ac.uk, P.A.Giesl@sussex.ac.uk

How to cite this paper: Stiefenhofer, P. and Giesl, P. (2019) Switching Regimes in Economics: The Contraction Mapping and the ω-Limit Set. *Applied Mathematics*, **10**, 513-520.
https://doi.org/10.4236/am.2019.107035

Received: May 14, 2019
Accepted: June 30, 2019
Published: July 3, 2019

Abstract

This paper considers a dynamical system defined by a set of ordinary autonomous differential equations with discontinuous right-hand side. Such systems typically appear in economic modelling where there are two or more regimes with a switching between them. Switching between regimes may be a consequence of market forces or deliberately forced in form of policy implementation. Stiefenhofer and Giesl [1] introduce such a model. The purpose of this paper is to show that a metric function defined between two adjacent trajectories contracts in forward time leading to exponentially asymptotically stability of (non)smooth periodic orbits. Hence, we define a local contraction function and distribute it over the smooth and nonsmooth parts of the periodic orbits. The paper shows exponentially asymptotical stability of a periodic orbit using a contraction property of the distance function between two adjacent nonsmooth trajectories over the entire periodic orbit. Moreover it is shown that the ω-limit set of the (non)smooth periodic orbit for two adjacent initial conditions is the same.

Keywords

Non-Smooth Periodic Orbit, Differential Equation, Contraction Mapping, Economic Regimes, Non-Smooth Dynamical System

1. Introduction

Economic systems may not always satisfy the usual smoothness condition everywhere. In particular, a discontinuity in an economic system may occur due to a change in economic regime or policy implementation. In this paper, we consider an economic system defined by a planar ordinary differential equation with discontinuous right-hand side. Similar dynamical systems are considered in

various economic models [2] [3] [4] [5] [6]. For such models, there exists a well developed existence and uniqueness theory [7]. However, little is known about stability results of non-smooth periodic orbits. Moreover, such results depend on the explicit calculation of the periodic orbit and employ a global stability theory based on Poincaré's map. Since such explicit calculations may not always be possible, we want to establish existence and exponentially asymptotical stability of a nonsmooth periodic orbit without its calculation. The advantage of such a local stability theory would allow economists to derive analytic results for the purpose of economic policy analysis. The theory developed in Stiefenhofer and Giesl [1] allows us to do so. In this paper we study the distance function between two adjacent trajectories and show it's contraction property in forward time and calculate its ω-limit set. Section two discusses the dynamical system with a switching regime and recalls the theorem introduced in Stiefenhofer and Giesl [1]. Section three states the main results and provides the proofs. Section four is a conclusion.

2. The Model

We consider a differential equation

$$\dot{x} = f(x), \tag{1}$$

where f is a discontinuous function at $x_2 = 0$ and $x \in \mathbb{R}^2$ such that for $f := f^{\pm}$ we have

$$\dot{x} = f^{\pm}(x) = \begin{cases} f^{+}(x) & \text{if } x_2 > 0 \\ f^{-}(x) & \text{if } x_2 < 0 \end{cases} \tag{2}$$

This dynamical system is introduced in Stiefenhofer and Giesl [8]. On the right-hand side, we provide a condition for switching between economic regimes $f^{\pm}$. For simplicity, we consider only two regimes and an exogenously given switching condition between them. A stability theory for this dynamical system is provided by the following theorem.

Theorem 1 (Stiefenhofer and Giesl [1], Theorem 2 p. 11). *Let $\varnothing \neq K \subset \mathbb{R}^2$ be a compact, connected and positively invariant set with $f^{\pm}(x) \neq 0$ for all $x \in K^{\pm}$. Moreover, assume that $W^{\pm} : \mathbb{X}^{\pm} \to \mathbb{R}^2$ are continuous functions and let the orbital derivatives $\left(W^{\pm}\right)'$ exist and be continuous functions in $\mathbb{X}^{\pm}$ and continuously extendable up to $\mathbb{X}_0^{\pm}$. Let following conditions hold:*

1) $L_{W^{\pm}(x)} := \max_{\|v^{\pm}\| = e^{-W^{\pm}(x)}, v^{\pm} \perp f^{\pm}(x)} L_{W^{\pm}}(x, v^{\pm}) \leq -\nu < 0$

$$L_{W^{\pm}}(x, v^{\pm}) := e^{2W^{\pm}(x)} \left\{ \left(v^{\pm}\right)^{\mathrm{T}} \left[Df^{\pm}(x) \right] v^{\pm} + \left\langle \nabla W^{\pm}(x), f^{\pm}(x) \right\rangle \left\| v^{\pm} \right\|^2 \right\}$$

for all $x \in K^{\pm}$.

2) $$\frac{f_2^{\mp}(x_1,0)}{f_2^{\pm}(x_1,0)} \cdot \frac{\sqrt{\left(f_1^{\pm}(x_1,0)\right)^2 + \left(f_2^{\pm}(x_1,0)\right)^2}}{\sqrt{\left(f_1^{\mp}(x_1,0)\right)^2 + \left(f_2^{\mp}(x_1,0)\right)^2}} e^{W^{\mp}(x_1,0) - W^{\pm}(x_1,0)} < 1$$

for all $x \in K^0$ with $f_2^{\pm}(x_1,0) < 0$, $f_2^{\mp}(x_1,0) < 0$.

Then there is one and only one periodic orbit $\Omega \subset K$. Moreover, Ω is exponentially asymptotic stable with the real part of the Floquet exponent less or equal $-\nu$ except the trivial one and for its basin of attraction the inclusion $K \subset A(\Omega)$ holds.

Stiefenhofer and Giesl [1] derive the conditions 1 - 2 in theorem 1. Condition 1 states that two smooth trajectories contract if the weighted Lyapunov function $L_{W^{\pm}}$ is negative. This condition requires that the real part of the Floquet exponent be negative. While this condition does not depend on the periodic orbit itself, however, it requires to find a function $W^{\pm}(x)$. Condition 2 states a contraction property for the discontinuity points of the dynamical system, where the system switches. This condition depends on the vector field $f^{\pm}$ and some function $W^{\pm}$, and is hence independent of the periodic orbit itself. We now investigate the contraction property of the metric function between adjacent solutions, and calculate the ω-limit set of the periodic orbit. The details of how to derive these conditions are given in [8]. In principle, however, our method is a generalization of Borg [9], which introduces the concept of a contraction mapping between adjacent trajectories in the following way:

We want to show that $L(x) < 0$ is a sufficient condition for two adjacent trajectories to move towards each other. For example, consider the points $x \in \mathbb{R}^n$ and $x + \delta v \in \mathbb{R}^n$ in the phase space. Let $\delta > 0$, $v \perp f(x)$, and $\|v\| = 1$. Then in order for two adjacent trajectories through the points x and $x + \delta v$ to move towards each other it must hold that

$$0 > \langle f(x + \delta v), v \rangle \tag{3}$$

$$\approx \langle f(x) + \delta Df(x)v, v \rangle \tag{4}$$

$$= \delta \langle Df(x)v, v \rangle \text{ since } v \perp f(x). \tag{5}$$

where

$$L(x, v) := \langle Df(x)v, v \rangle. \tag{6}$$

Hence, if $L(x) < 0$ then locally, two adjacent trajectories move towards each other. See **Figure 1**. Borg provides the following theorem under slightly different assumptions:

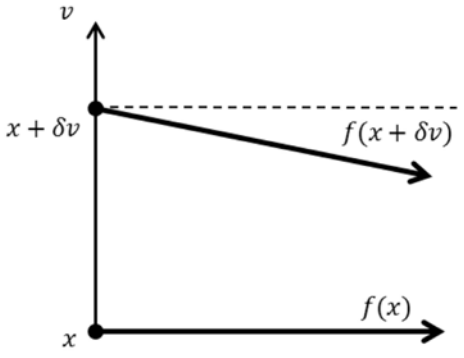

Figure 1. Borg's criterion [9].

Theorem 2 (Version of Borg [9]) *Let* $\varnothing \neq K \subset \mathbb{R}^n$ *be a compact, connected and positively invariant set which contains no equilibrium. Let* $L(x) < 0$ *hold for all* $x \in K$ *with*

$$L(x) := \max_{\|v\|=1, v \perp f(x)} (x, v) \tag{7}$$

where

$$L(x, v) := \langle Df(x)v, v \rangle. \tag{8}$$

Then there exists one and only one periodic orbit $\Omega \subset K$. Ω is exponentially asymptotically stable and its basin of attraction $A(\Omega)$ contains K.

3. Results

We now consider the time interval $t \in (t_{j-1}^+, t_j^+)$ in Figure 2 and show that the distance between two adjacent solutions decreases. We also show that for two nearby points x and $x+\eta$ in K that the ω-limit set is the same.

We define a time-dependent distance function $A^+ : \mathbb{R} \to \mathbb{R}_0^+$ between two adjacent points x and $x+\eta$ by

$$A^+(t) := \sqrt{\left(\left(S^+_{\mathcal{T}_x^{x+\eta}(t)}(x+\eta) - S_t^+ x \right)^{\mathrm{T}} \mathrm{e}^{2W^+(S_t^+ x)} \left(S^+_{\mathcal{T}_x^{x+\eta}(t)}(x+\eta) - S_t^+ x \right) \right)}, \tag{9}$$

where $S_{\mathcal{T}_x^{x+\eta}}(t)(x+\eta)$, $S_t^+ x$ are two adjacent (non)smooth trajectories, and $\mathcal{T}_x$ is a monotone increasing map for the time structure presented in Figure 2.

Theorem 3. *Let the assumptions of theorem* 1 *hold. Then there are constants* $\delta > 0$ *and* $C \geq 1$ *such that for all* $x \in K$ *and for all* $\eta \in \mathbb{R}^2$ *with* $\|\eta\| \leq \delta/2$

$$A(t) \leq A(t_{j-1}^+) \mathrm{e}^{-\mu t} \quad \text{for all } t \geq 0. \tag{10}$$

Moreover, we have

$$\omega(x) = \omega(x+\eta). \tag{11}$$

Proof.

We now show the contraction property of the distance function.

- We show that ν defined over a smooth time interval is strictly larger than μ defined over the same time interval including the subsequent time interval.

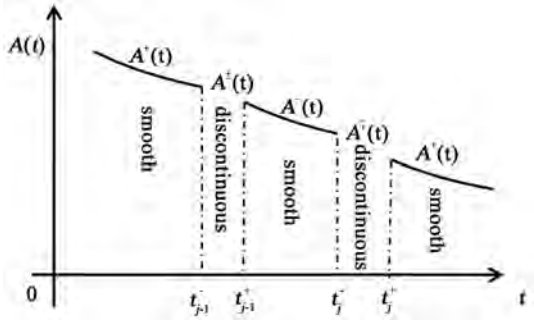

Figure 2. Time structure $t \in \mathbb{R}$.

- We show that the distance function is decreasing for all positive time.

By equations (2.17) and (2.30) in Stiefenhofer [8] we have

$$A(t) \le \mathrm{e}^{-\mu t} A^+\left(t_{j-1}^-\right) \text{ for all } t \in \left[t_{j-1}^-, t_{j-1}^+\right] \tag{12}$$

$$A(t) \le \mathrm{e}^{-\mu t} A^+\left(t_j^-\right) \text{ for all } t \in \left[t_j^-, t_j^+\right] \tag{13}$$

See time structure notation of the graph of $A(t)$ in **Figure 2**. Equations (12) and (13) show the contraction rate μ over each jumping interval in +/− and in −/+ direction. We now state similar equations for the smooth intervals with contraction rate ν. We have

$$A(t) \le \mathrm{e}^{-\nu t} A\left(t_{j-1}^+\right)^- \text{ for all } t \in \left(t_{j-1}^+, t_j^-\right) \tag{14}$$

$$A(t) \le \mathrm{e}^{-\nu t} A\left(t_j^+\right) \text{ for all } t \in \left(t_j^+, t_{j+1}^-\right)^-. \tag{15}$$

We consider the time interval $\left[t_1^-, t_1^+\right] \cup \left(t_1^+, t_2^-\right)$. Hence by equation (12) and equation (14) we obtain

$$\mathrm{e}^{-\nu\left(t_2^- - t_1^+\right)} A^+\left(t_1^+\right) \le \mathrm{e}^{-\mu\left(t_2^+ - t_1^+\right)} A^+\left(t_1^+\right)$$

$$\nu\left(t_2^- - t_1^+\right) \le \mu\left(t_2^+ - t_1^+\right)$$

$$\mu \le \nu\left(\frac{t_2^- - t_1^+}{t_2^+ - t_1^+}\right). \tag{16}$$

We define

$$S := \left(t_j^- - t_{j-1}^+\right) \ge c_2 \text{ for } j = 1,2,3,\cdots \tag{17}$$

$$J := \left(t_j^+ - t_j^-\right) \le c_1 \text{ for } j = 1,2,3,\cdots \tag{18}$$

where constants $c_1, c_2 > 0$ are defined by

$$c_1 := \delta > 0 \tag{19}$$

For the constant c_2 we consider $d := K \cap \{x_2 = 0\}$. From

$$\max_{x \in K} \left| f_1(x) \right| = s \tag{20}$$

and

$$t \cdot s = d \tag{21}$$

we obtain by $d \le \int_0^t f_1\left(x(\tau)\right) \mathrm{d}\tau$

$$c_2 := \frac{d}{\max_{x \in K} \left| f_1 \right|} \le t. \tag{22}$$

Equation (16) with bounds (17) and (18) and extension of time interval $t_2^+ - t_1^+ = \left(t_2^- - t_1^+\right) + \left(t_2^+ - t_2^-\right)$ yields

$$\mu = \nu\left(\frac{t_2^- - t_1^+}{\left(t_2^+ - t_1^+\right)\left(t_2^+ - t_2^-\right)}\right) \le \nu\left(\frac{c_2}{c_2 + c_1}\right) = \nu\left(\frac{1}{1 + \frac{c_1}{c_2}}\right) \tag{23}$$

Since $c_1 = \delta$ we can choose δ small enough so that μ gets as close to ν as we wish. From

$$A\left(t_1^+ + t\right) \le \mathrm{e}^{-\mu t} A\left(t_1^+\right) \text{ for all } t \in \left\{\left(t_1^+, t_2^- -\right) \cup \left[t_2^- - t_2^+\right]\right\} \tag{24}$$

$$A\left(t_1^+ + t\right) \le \mathrm{e}^{-\mu t} A\left(t_1^+\right) \text{ for all } t \in \left\{\left(t_2^+, t_3^- -\right) \cup \left[t_3^- - t_3^+\right]\right\} \tag{25}$$

we have

$$\begin{aligned} &A\left(t_1^+ + \tau\right) \le \mathrm{e}^{-\mu\tau} A\left(t_1^+\right) \\ &\text{for all } \tau \in \left\{\left(t_1^+, t_2^- -\right) \cup \left[t_2^- - t_2^+\right] \cup \left(t_2^+, t_3^- -\right) \cup \left[t_3^- - t_3^+\right]\right\} \end{aligned} \tag{26}$$

which generalizes to $\tau \ge 0$, by

$$\begin{aligned} &A\left(t_1^+ + \tau\right) \le \mathrm{e}^{-\mu\tau} A\left(t_1^+\right) \\ &\text{for all } \tau \in \left\{\left(t_{j-1}^+, t_j^- -\right) \cup \left[t_j^- - t_j^+\right] \cup \left(t_j^+, t_{j+1}^- -\right) \cup \left[t_{j+1}^- - t_3^+\right]\right\} \end{aligned} \tag{27}$$

This shows (10). It remains to show (11).

Now, we show that all points $x+\eta$ with $\eta \in \mathbb{R}^2$, $\eta \perp f(x)$, and $\|\eta\| \le \delta/2$ have the same ω-limit set as the point x. We first show the inclusion $\omega(x) \subset \omega(x+\eta)$. Assume there is a $w \in \omega(x)$. Then we have a strictly increasing sequence $t_i \to \infty$ satisfying $\|w - S_{t_i} x\| \to 0$ as $i \to \infty$. Because of condition (10) of proposition 3 and the properties of $\mathcal{T}$ in Figure 2 there is a sequence $\mathcal{T}(t_i)$ that satisfies

$$\mathcal{T}(t_i) \to \infty \text{ as } i \to \infty, \tag{28}$$

and

$$A^-(t_i) \le A^+\left(\mathcal{T}(t_i)\right) \mathrm{e}^{-\mu t_i} \text{ as } i \to \infty. \tag{29}$$

This proves that $S_{\mathcal{T}(t_i)}(x+\eta) \to w$ and $w \in \omega(x+\eta)$.

We now show that the inclusion $\omega(x+\eta) \subset \omega(x)$. Assume there is a $w \in \omega(x+\eta)$. Then we have a strictly increasing sequence $\theta_i \to \infty$ satisfying $\|w - S_{t_i} x\| \to 0$ as $i \to \infty$. Because of condition (10) of proposition 3 and properties of $\mathcal{T}$ in Figure 2 there is a sequence $\mathcal{T}^{-1}(\theta_i)$ that satisfies $\mathcal{T}^{-1}(\theta_i) \to \infty$ as $i \to \infty$. This proves that $S_{\mathcal{T}(t_i)}(x+\eta) \to w$ and $w \in \omega(x+\eta)$.

This concludes the proof of proposition 3.

Proposition 4. *Let the assumptions of theorem* 1 *be satisfied. Then for all* $x, y \in K$

$$\varnothing \ne \omega(x) = \omega(y) =: \Omega \tag{30}$$

Proof. Let $x_0 \in \Omega \setminus K^0$. Since for all $t \ge 0$ we have $S_t x_0 \subset K$, which is a compact set, hence

$$\varnothing \ne \omega(x_0) =: \Omega \subset K. \tag{31}$$

Now, pick an arbitrary point $x_0 \in \Omega \setminus K^0$. By proposition 3 we have $\omega(x) - \omega(y)$ for all y in a neighbourhood of x. Hence

$$K_1 := \left\{x \in K : \omega(x) = \omega(y_0)\right\} \tag{32}$$

$$K_2 := \{x \in K : \omega(x) \neq \omega(y_0)\} \tag{33}$$

are open sets. Since $K = K_1 \dot{\cup}_2$ and $p_0 \in K_1$ with K connected, it must be that K_2 is empty and $K_1 = K$.

4. Conclusion

Differential equations are ubiquitous in economics. Economic regimes, where there is a switching between them, fit particularly well within the framework of differential equations with discontinuous right-hand side, where the discontinuity represents the switching condition. In this paper, we assume an exogenous switching condition. However, this can without loss of generality be generalized by modelling the explicit economic context. The novelty of the stability theory discussed in this paper is that it is independent of the explicit solution of the system. This is a major advantage of our theory. However, it requires defining a weight function W, which may not always be easy. In particular, the paper shows that a distance function between two adjacent trajectories contracts in forward time over both, smooth and nonsmooth parts of the periodic orbit, where the dynamical system is discontinuous. It also shows that for two adjacent initial points the ω-limit set of nonsmooth period orbits is the same. Stiefenhofer and Giesl provide an example of the theory discussed in this paper [10] and compare it to global stability theory [11]. Further research should investigate the full basin of attraction of this model. Such a result would allow economists to fully characterize the set of initial conditions of exponentially asymptotically stable periodic orbits and to hence perform effective policy analysis.

Acknowledgements

We thank the Editor and the referee for their comments. EPSRC Research Grant (Engineering and Physical Science Research Council, 2011-2016), 1091684, Stability in Nonsmooth Systems with Applications to Biomechanics. This support is greatly appreciated.

Conflicts of Interest

The authors declare no conflicts of interest regarding the publication of this paper.

References

[1] Stiefenhofer, P. (2016) Stability Analysis of Non-Smooth Dynamical Systems with an Application to Biomechanics. PhD Thesis, University of Sussex, School of Mathematics and Physical Sciences, Brighton.

[2] Mallivaud, F. (1977) The Theory of Unemployment Reconsidered. Basil Blackwell, Oxford.

[3] Henry, C. (1972) Differential Equations with Discontinuous Right-Hand Side for Planning Procedure. *Journal of Economic Theory*, **4**, 545-551.

https://doi.org/10.1016/0022-0531(72)90138-X

[4] Benassy, J.P. (1978) A Neo-Keynesian Model of Price and Quantity Determination in Disequilibrium. In: Schwödiauer, G., Ed., *Equilibrium and Disequilibrium in Economic Theory*, Reidel, Dordrecht, 511-544. https://doi.org/10.1007/978-94-010-1155-6_27

[5] Ito, T. (1979) A Filippov Solution of a System of Differential Equations with Discontinuous Right-Hand Side. *Economic Letters*, **4**, 349-354. https://doi.org/10.1016/0165-1765(79)90183-6

[6] Löfgren, K.G. (1979) The Corridor and Local Stability of the Effective Excess Demand Hypothesis: A Result. *Scandinavian Journal of Economics*, **81**, 30-47. https://doi.org/10.2307/3439455

[7] Filippov, A.F. (1988) Differential Equations with Discontinuous Righthand Sides. Kluwer Academic Publishers, Dordrecht. https://doi.org/10.1007/978-94-015-7793-9

[8] Stiefenhofer, P. and Giesl, P. (2019) Economic Periodic Orbits: A Theory of Asymptotic Stability. *Nonlinear Analysis and Differential Equations*, **7**, 9-16. https://doi.org/10.12988/nade.2019.923

[9] Borg, G. (1960) A Condition for the Existence of Orbitally Stable Solutions of Dynamical Systems. In: *Kungliga Tekniska Högskolans Handlingar*, Kungliga Tekniska Högskolan, Stockholm, Vol. 153, 3-12.

[10] Stiefenhofer, P. and Giesl, P. (2019) A Global Stability Theory of Nonsmooth Periodic Orbits: Example I. *Applied Mathematical Sciences*, **13**, 511-520. https://doi.org/10.12988/ams.2019.9463

[11] Stiefenhofer, P. and Giesl, P. (2019) A Local Stability Theory of Nonsmooth Periodic Orbits: Example II. *Applied Mathematical Sciences*, **13**, 521-531. https://doi.org/10.12988/ams.2019.9464

Applied Mathematics, 2019, 10, 521-526
http://www.scirp.org/journal/am
ISSN Online: 2152-7393
ISSN Print: 2152-7385

Balancing Chemical Equations by Systems of Linear Equations

Ihsanullah Hamid

Department of Mathematics, University of Nangarhar, Jalalabad, Nangarhar, Afghanistan
Email: hamid@nu.edu.af

How to cite this paper: Hamid, I. (2019) Balancing Chemical Equations by Systems of Linear Equations. *Applied Mathematics*, **10**, 521-526.
https://doi.org/10.4236/am.2019.107036

Received: April 16, 2019
Accepted: July 9, 2019
Published: July 12, 2019

Abstract

In this paper, a formal and systematic method for balancing chemical reaction equations was presented. The results satisfy the law of conservation of matter, and confirm that there is no contradiction to the existing way(s) of balancing chemical equations. A chemical reaction which possesses atoms with fractional oxidation numbers that have unique coefficients was studied. In this paper, the chemical equations were balanced by representing the chemical equation into systems of linear equations. Particularly, the Gauss elimination method was used to solve the mathematical problem with this method, it was possible to handle any chemical reaction with given reactants and products.

Keywords

Chemical Reaction, Linear Equations, Balancing Chemical Equations, Matrix, Gauss Elimination Method

1. Introduction

Balancing of the chemical equation is one of the initial subjects taught in most preliminary chemistry courses. Balancing chemical reactions is an amazing subject of matter for mathematics and chemistry students who want to see the power of linear algebra as a scientific discipline [1]. Since the balancing of chemical reactions in chemistry is a basic and fundamental issue, it deserves to be considered on a satisfactory level [2]. A chemical equation is only a symbolic representation of a chemical reaction. Actually, every chemical equation is the story of some chemical reaction. Chemical equations play a main role in theoretical as well as in industrial chemistry [3]. A chemical reaction can neither create nor destroy atoms. So, all of the atoms represented on the left side of the arrow must also be on the right side of the arrow. This is called balancing the chemical equa-

tion [4]. The application of the law of conservation of matter is critical in chemistry education and is demonstrated in practice through balanced chemical equations [5]. Every student who has general chemistry as a subject is bound to come across balancing chemical equations. The substances initially involved in a chemical reaction are called reactants, but the newly formed substances are called the products. The products are new substances with properties that are different from those of reactants [6]. A chemical equation is said to be balanced, the number of atoms of each type on the left is the same as the number of atoms of corresponding type on the right [7].

Balancing chemical equation by inspection is often believed to be a trial and error process and, therefore, it can be used only for simple chemical reactions. But still it has limitations [8]. Balancing by inspection does not produce a systematic evaluation of all of the sets of coefficients that would potentially balance an equation. Another common method of balancing chemical reaction equations is the algebraic approach. In this approach, coefficients are treated as unknown variables or undetermined coefficients whose values are found by solving a set of simultaneous equations [9]. According to [5], the author clearly indicated that the algebraic approach to balancing both simple and advance chemical reactions typically encountered in the secondary chemistry classroom is superior to that of the inspection method. Also, in [10], the author emphasized very clearly that balancing chemical reactions is not chemistry; it is just linear algebra. From a scientific viewpoint, a chemical reaction can be balanced if only it generates a vector space. That is a necessary and sufficient condition for balancing a chemical reaction.

A chemical reaction, when it is feasible, is a natural process, the consequent equation is always consistent. Therefore, we must have nontrivial solution. And we should be able to obtain its assuming existences. Such an assumption is absolutely valid and does not introduce any error. If the reaction is infeasible, then, there exists only a trivial solution, *i.e.*, all coefficients are equal to zero [6]. In Mathematics and Chemistry, there are several mathematical methods for balancing chemical reactions. All of them are based on generalized matrix inverses and they have formal scientific properties that need a higher level of mathematical knowledge for their application [1]-[16]. Here, we are presenting the Gauss elimination method, it was possible to handle any chemical reaction with given reactants and products. Solved problems are provided to show that this methodology lends well for both simple and complex reactions.

2. Main Results

***Problem* 1**

Balance the following chemical reaction

$$C_2H_6 + O_2 \rightarrow CO_2 + H_2O \text{ -Not Balanced.}$$

The equation to balance is identified. This chemical reaction consists of three elements: Carbon(C); Hydrogen (H); Oxygen (O). The equation to balance is

identified our task is to assign the unknowns coefficients (x_1, x_2, x_3, x_4) to each chemical species. A balance equation can be written for each of these elements:

$$x_1C_2H_6 + x_2O_2 \rightarrow x_3CO_2 + x_4H_2O$$

Three simultaneous linear equations in four unknown corresponding to each of these elements. Then, the algebraic representation of the balanced

$$\text{Carbon}(\text{C}): 2x_1 = x_3 \Rightarrow 2x_1 - x_3 = 0$$

$$\text{Hydrogen}(\text{H}): 6x_1 = 2x_4 \Rightarrow 6x_1 - 2x_4 = 0$$

$$\text{Oxygen}(\text{O}): 2x_2 = 2x_3 + x_4 \Rightarrow 2x_2 - 2x_3 - x_4 = 0$$

First, note that there are four unknowns, but only three equations. The system is solved by Gauss elimination method as follows:

$$\left[\begin{array}{cccc|c} 2 & 0 & -1 & 0 & 0 \\ 6 & 0 & 0 & -2 & 0 \\ 0 & 2 & -2 & -1 & 0 \end{array}\right] \xrightarrow{R_2 \leftrightarrow R_2 - 3R_1} \left[\begin{array}{cccc|c} 2 & 0 & -1 & 0 & 0 \\ 0 & 0 & 3 & -2 & 0 \\ 0 & 2 & -2 & -1 & 0 \end{array}\right]$$

$$\xrightarrow{R_2 \leftrightarrow R_3} \left[\begin{array}{cccc|c} 2 & 0 & -1 & 0 & 0 \\ 0 & 2 & -2 & -1 & 0 \\ 0 & 0 & 3 & -2 & 0 \end{array}\right] \xrightarrow[R_1 \leftrightarrow 3R_1 + R_3]{R_2 \leftrightarrow 3R_2 + 2R_3} \left[\begin{array}{cccc|c} 6 & 0 & 0 & -2 & 0 \\ 0 & 6 & 0 & -7 & 0 \\ 0 & 0 & 3 & -2 & 0 \end{array}\right]$$

$$\xrightarrow[R_3 \leftrightarrow \frac{1}{3}R_3]{R_1 \leftrightarrow \frac{1}{6}R_1 \\ R_2 \leftrightarrow \frac{1}{6}R_2} \left[\begin{array}{cccc|c} 1 & 0 & 0 & -1/3 & 0 \\ 0 & 1 & 0 & -7/6 & 0 \\ 0 & 0 & 1 & -2/3 & 0 \end{array}\right]$$

The last matrix is of reduced row echelon form, so we obtain that the solution of the system of linear equations is:

$$x_1 - \frac{1}{3}x_4 = 0 \Rightarrow x_1 = \frac{1}{3}x_4$$

$$x_2 - \frac{7}{6}x_4 = 0 \Rightarrow x_2 = \frac{7}{6}x_4$$

$$x_3 - \frac{2}{3}x_4 = 0 \Rightarrow x_3 = \frac{2}{3}x_4$$

where x_4 a free variable, particular solution is can then obtain by assigning values to the x_4, for instance $x_4 = 6$ we can represent the solution set as:

$$x_1 = 2,\ x_2 = 7,\ x_3 = 4$$

Thus, the balanced chemical reaction equation is:

$$2C_2H_6 + 7O_2 \rightarrow 4CO_2 + 6H_2O$$

***Problem* 2**

Consider this chemical reaction which is infeasible

$$K_4Fe(CN)_6 + K_2S_2O_3 \rightarrow CO_2 + K_2SO_4 + NO_2 + FeS \text{ -Not Balanced.}$$

A balance equation can be written for each of these elements:

$$x_1K_4Fe(CN)_6 + x_2K_2S_2O_3 \rightarrow x_3CO_2 + x_4K_2SO_4 + x_5NO_2 + x_6FeS$$

From above equation, we will obtain the following set of equations:

$$\mathrm{K}: 4x_1 + 2x_2 = 2x_4$$

$$\mathrm{Fe}: x_1 = x_6$$

$$\mathrm{C}: 6x_1 = x_3$$

$$\mathrm{N}: 6x_1 = 2x_5$$

$$\mathrm{S}: 2x_2 = x_4 + x_6$$

$$\mathrm{O}: 3x_2 = 2x_3 + 4x_4 + 2x_5$$

From the systems of equations we obtain the contradictions $x_2 = 3x_1$ and $x_2 = \frac{44}{3}x_1$, that means that the system is inconsistent, *i.e.*, we have only a trivial solution $x_i = 0\left(1 \le i \le 6\right)$. Hence, that means the chemical reaction is infeasible.

***Problem* 3**

Consider the following chemical reaction with atoms which possess fractional oxidation numbers

$$\begin{aligned} &x_1\mathrm{C}_{2952}\mathrm{H}_{4664}\mathrm{N}_{812}\mathrm{O}_{832}\mathrm{S}_8\mathrm{Fe}_4 + x_2\mathrm{Na}_2\mathrm{C}_4\mathrm{H}_3\mathrm{O}_4\mathrm{SAu} + x_3\mathrm{Fe}\left(\mathrm{SCN}\right)_2 \\ &+ x_4\mathrm{Fe}\left(\mathrm{NH}_4\right)_2\left(\mathrm{SO}_4\right)_2\,6\mathrm{H}_2\mathrm{O} + x_5\mathrm{C}_4\mathrm{H}_8\mathrm{Cl}_2\mathrm{S} + x_6\mathrm{C}_8\mathrm{H}_{12}\mathrm{MgN}_2\mathrm{O}_8 \\ &\to x_7\mathrm{C}_{55}\mathrm{H}_{72}\mathrm{MgN}_4 + x_8\mathrm{Na}_{3.99}\mathrm{Fe}\left(\mathrm{CN}\right)_6 + x_9\mathrm{Au}_{0.987}\mathrm{SC}_6\mathrm{H}_{11}\mathrm{O}_5 \\ &+ x_{10}\mathrm{HClO}_4 + x_{11}\mathrm{H}_2\mathrm{S} \end{aligned}$$

For balancing of this kind of reaction the computer is useless. From the mass balance of the above chemical reaction one obtains this system of linear equations

$$2952x_1 + 4x_2 + 2x_3 + 4x_5 + 8x_6 = 55x_7 + 6x_8 + 6x_9$$

$$4664x_1 + 3x_2 + 20x_4 + 8x_5 + 12x_6 = 72x_7 + 11x_9 + x_{10} + 2x_{11}$$

$$812x_1 + 2x_3 + 2x_4 + 2x_6 = 4x_7 + 6x_8$$

$$832x_1 + 4x_2 + 14x_4 + 8x_6 = 5x_9 + 4x_{10}$$

$$8x_1 + x_2 + 2x_3 + 2x_4 + x_5 = x_9 + x_{11}$$

$$4x_1 + x_3 + x_4 = x_8$$

$$2x_2 = 3.99x_8$$

$$x_2 = 0.987x_9$$

$$2x_5 = x_{10}$$

$$x_6 = x_7$$

By using of the method of the elimination of the variables, from the chemical reaction and the system of linear equations immediately follows the required coefficients

$$\begin{aligned} &30448582\mathrm{C}_{2952}\mathrm{H}_{4664}\mathrm{N}_{812}\mathrm{O}_{832}\mathrm{S}_8\mathrm{Fe}_4 + 10833308052\mathrm{Na}_2\mathrm{C}_4\mathrm{H}_3\mathrm{O}_4\mathrm{SAu} \\ &+ 3899586588\mathrm{Fe}\left(\mathrm{SCN}\right)_2 + 1408848684\mathrm{Fe}\left(\mathrm{NH}_4\right)_2\left(\mathrm{SO}_4\right)_2\,6\mathrm{H}_2\mathrm{O} \\ &+ 5568665015\mathrm{C}_4\mathrm{H}_8\mathrm{Cl}_2\mathrm{S} + 1379870764\mathrm{C}_8\mathrm{H}_{12}\mathrm{MgN}_2\mathrm{O}_8 \\ &\to 1379870764\mathrm{C}_{55}\mathrm{H}_{72}\mathrm{MgN}_4 + 5430229600\mathrm{Na}_{3.99}\mathrm{Fe}\left(\mathrm{CN}\right)_6 \\ &+ 10975996000\mathrm{Au}_{0.987}\mathrm{SC}_6\mathrm{H}_{11}\mathrm{O}_5 + 11137330030\mathrm{HClO}_4 \\ &+ 16286436267\mathrm{H}_2\mathrm{S} \end{aligned}$$

Is it chemistry? No! It is linear algebra.

3. Results

Every chemical reaction can be represented by the systems of linear equations. A chemical reaction, when it is feasible, the consequent equation is always consistent. Therefore, we must have nontrivial solution. If the reaction is infeasible, then, there exists only a trivial solution, *i.e.*, all coefficients are equal to zero. A chemical reaction which possesses atoms with integers and fractional oxidation numbers was studied. And with this method, it was possible to handle any chemical reaction.

4. Conclusion

Balancing chemical reaction is not chemistry, but it is just linear algebra. This study investigates that every chemical reaction is represented by homogenous systems of linear equations only. This allows average, and even low achieving students, a real chance at success. It can remove what is often a source of frustration and failure and that turns students away from chemistry. Also, it allows the high achieving to become very fast and very accurate even with relatively difficult equations. This work presented a formal, systematic approach for balancing chemical equations. The method is based on the Gaussian elimination method. The mathematical method presented in this paper was applicable to all cases in chemical reactions. The results indicated that there is no any contradiction between the various methods that were applied to balance the chemical reaction equation and the suggested approach. Balancing chemical reactions which possess atoms with fractional oxidation numbers is possible only by using mathematical methods.

Conflicts of Interest

The author declares no conflicts of interest regarding the publication of this paper.

References

[1] Risteski, I.B. (2012) New Very Hard Problems of Balancing Chemical Reactions. *Bulgarian Journal of Science Education*, **21**, 574-580.

[2] Risteski, I.B. (2014) A New Generalized Algebra for the Balancing of Chemical Reactions. *Materials and Technology*, **48**, 215-219.

[3] Vishwambharrao, K.R., *et al.* (2013) Balancing Chemical Equations by Using Mathematical Model. *International Journal of Mathematical Research and Science*, **1**, 129-132.

[4] Larson, R. (2017) Elementary Linear Algebra. 8th Edition, CENGAGE Learning, the Pennsylvania State University, State College, 4.

[5] Charnock, N.L. (2016) Teaching Method for Balancing Chemical Equations: An Inspection versus an Algebraic Approach. *American Journal of Educational Research*, **4**, 507-511.

[6] Risteski, I.B. (2009) A New Singular Matrix Method for Balancing Chemical Equations and Their Stability. *Journal of the Chinese Chemical Society*, **56**, 65-79. https://doi.org/10.1002/jccs.200900011

[7] Zabadi, A.M. and Assaf, R. (2017) From Chemistry to Linear Algebra: Balancing Chemical Reaction Equation Using Algebraic Approach. *International Journal of Advanced Biotechnology and Research*, **8**, 24-33.

[8] Krishna, Y.H., *et al.* (2016) Balancing Chemical Equations by Using Matrix Algebra. *World Journal of Pharmacy and Pharmaceutical Sciences*, **6**, 994-999.

[9] Thorne, L.R. (2009) An Innovative Approach to Balancing Chemical Reaction Equations: A Simplified Matrix-Inversion Technique for Determining the Matrix Null Space. *The Chemical Educator*, **15**, 304-308.

[10] Risteski, I.B. (2010) A New Complex Vector Method for Balancing Chemical Equations. *Materials and technology*, **44**, 193-203.

[11] Akinola, R.O., Kutchin, S.Y., Nyam, I.A. and Adeyanju, O. (2016) Using Row Reduced Echelon Form in Balancing Chemical Equations. *Advances in Linear Algebra & Matrix Theory*, **6**, 146-157. https://doi.org/10.4236/alamt.2016.64014

[12] Gabriel, C.I. and Onwuka, G.I. (2015) Balancing of Chemical Equations Using Matrix Algebra. *Journal of Natural Sciences Research*, **5**, 29-36.

[13] Lay, D.C. (2012) Linear Algebra and Its Applications. 4th Edition, Addison-Wesley, Boston, 49-54.

[14] Leon, S.J. (2015) Linear Algebra with Applications. 9th Edition, University of Massachusetts, Dartmouth, 17-23.

[15] Poole, D. (2011) Linear Algebra: A Modern Introduction. 3rd Edition, Cole CENGAGE Learning, Brooks, 105-119.

[16] Weldesemaet, M.K. (2018) The Importance of Gauss-Jordan Elimination Methods for Balancing Chemical Reaction Equation. *International Journal of Engineering Development and Research*, **6**, 685-691.

Applied Mathematics, 2019, 10, 527-544
http://www.scirp.org/journal/am
ISSN Online: 2152-7393
ISSN Print: 2152-7385

Modeling of the Primary Acts of the Interaction between a Cell and an External Mechanical Field

Irina V. Ogneva[1,2*], Maria A. Usik[1,2], Nikolay S. Biryukov[1,2], Nikita O. Kremenetskii[3], Yuliya S. Zhdankina[2]

[1]Cell Biophysics Laboratory, State Scientific Center of the Russian Federation Institute of Biomedical Problems of the Russian Academy of Sciences, Moscow, Russia
[2]I. M. Sechenov First Moscow State Medical University, Moscow, Russia
[3]Ishlinsky Institute for Problems in Mechanics of the Russian Academy of Sciences, Moscow, Russia
Email: *iogneva@yandex.ru

How to cite this paper: Ogneva, I.V., Usik, M.A., Biryukov, N.S., Kremenetskii, N.O. and Zhdankina, Y.S. (2019) Modeling of the Primary Acts of the Interaction between a Cell and an External Mechanical Field. *Applied Mathematics*, **10**, 527-544.
https://doi.org/10.4236/am.2019.107037

Received: July 2, 2019
Accepted: July 16, 2019
Published: July 19, 2019

Abstract

The mechanism of interaction between a cell and an external mechanical field is still poorly understood, and the accumulated diverse experimental data are often scattered. Therefore, the aim of this work was to systematize the experimental data in a mathematical model of the interaction between a cell and an external mechanical field based on standard kinetic equations and Fick's diffusion equation. Assuming that the cortical cytoskeleton proteins play a key role in cell mechanosensitivity, we compared the results of mathematical modeling and experimental data concerning the content of cytoskeletal proteins at the early stages of a mechanical field change. In addition, the proposed mathematical model suggests the dynamics of changes of a key transcription factor, which is necessary for the expression of certain genes encoding cytoskeletal proteins.

Keywords

Cell Mechanosensititvity, Kinetic Equations, Cortical Cytoskeleton

1. Introduction

Human exploration of outer space faces a number of unsolved problems, including medical problems. Being in conditions of weightlessness, even during Earth orbit, leads to a number of negative effects, for example, on the musculoskeletal and cardiovascular systems [1] [2] [3]. Existing methods of countermeasures, for the most part, are palliative, which is associated with a lack of un-

derstanding of the etiology of the development of hypo-gravitational changes at the cellular and molecular levels. To date, questions remain about the interaction of a cell and a gravitational field: what is the mechanosensor and how the mechanotransduction paths are started.

Practically every intracellular structure can claim to be a mechanosensor. Thus, stretching of neurons or smooth muscle cells in a culture through the extracellular matrix leads to an increase in microtubule polymerization [4] [5]. Direct stretching of cell membranes, for example, using patch clamp technology, changes the cation-transport activity of mechanosensitive ion channels as a result of conformational changes of either the lipid bilayer [6] [7] or the portal domains of the channel itself [8] [9]. In addition, the submembrane cytoskeleton [10], as well as intracellular structures [11] [12], can also act as a mechanosensor.

The result of mechanotransduction is the formation of an adaptation pattern of proteins and gene expression. Thus, in cultured cells under conditions of altered gravity, there was a change in the cell profile, disorganization of microfilaments and, sometimes, microtubules [13]-[18], and changes in mitochondrial localization [19], which is determined by the state of the intermediate filaments. In addition, the changes are not limited to the protein content but also occur at the level of the expression of genes encoding cytoskeletal proteins and associated components of signaling cascades [20]-[26].

Our previous studies have suggested the role of the actin-binding proteins of the submembrane cytoskeleton in the primary mechanoreception of cells of various types, in particular skeletal muscle and myocardium. We assume that any change in the external conditions for the cell is reflected in the deformation of its cortical cytoskeleton. However, these strains are fundamentally different with increasing and decreasing loads. The first result is the dissociation of various actin-binding proteins from the cortical cytoskeleton: alpha-actinin-4 with a load decrease and alpha-actinin-1 with an increase [10] [27] [28]. With further development of this process, the deformation leads to the destruction of the structure and, at subsequent early stages of exposure, to an initial decrease in stiffness, which correlates with the content of actin non-muscle isoforms in the membrane fraction, which form the cortical cytoskeleton [29]. Furthermore, in the case of a decrease in external mechanical stress, there is a decrease in the expression of genes encoding cytoskeletal proteins and a further decrease in cortical cytoskeleton stiffness. In contrast, an increase in the external mechanical stress increases the mRNA content of the genes encoding cytoskeletal proteins and proteins directly and increases the stiffness [30] [31]. In general, the process of sensitivity to external stress by cells can be quite universal in the evolutionary series. Thus, *Drosophila melanogaster* lacks the isoform alpha-actinin-4; however, it is possible that supervillin plays a role in the process of mechanosensitivity [32].

Thus, the multiple components and variability of the mechanisms of cellular mechanosensitivity and mechanotransduction make it difficult to find the "hot

spots" of its regulation and, as a consequence, the development of effective protection methods. Therefore, we decided to build a mathematical model based on the classical kinetic equations of the concentrations of key proteins and mRNAs involved in the perception and transduction of external mechanical stress, taking into account their diffusion between the compartments.

2. Formulation of the Problem

Based on the experimental results described above, it is possible to suggest the following mechanism for triggering the formation of an adaptive response to changes in the external mechanical stress.

Suppose that a sensitive protein *SP* associated with microfilaments reacts to any change in mechanical stress. In addition, its antagonist, *aSP*, is also associated with microfilaments. Protein *SP* can exist both in connection with microfilaments and in free form. The binding to the microfilament network and dissociation from microfilaments at the initial state occur to maintain the initial level of free protein SP_{free} in both membrane SP_{freem0} and cytoplasmic compartment SP_{freec0}. Free-form SP_{free} can diffuse between compartments.

A change in the external mechanical stress leads to an increase in the content of free "sensitive" protein in the membrane fraction SP_{freem} with a reaction rate constant, which depends both on the external mechanical stress and on the membrane compartment characteristics $v^*_{MFm\to SPfreem}(g, z_{mc})$. An increase in the content of free SP_{freem} in the membrane leads to an increase in its content in the cytoplasm SP_{freec} due to diffusion. SP_{freec} activates some protein M^*_c. The activated protein M^*_c in turn activates the transcription factor TF^*_c to diffuse into the nucleus and alter the transcription efficiency of its target genes and the formation of the corresponding mRNA. There is feedback, and the efficiency of the formation of the "sensitive" protein mRNA, *rSP*, depends on the content of activated TF^*_n in the nucleus.

Suppose also that the efficiency of proteolysis and degradation of mRNA does not depend on the content and type of substrates and the rates of cleavage are constant—v_p and v_d for proteins and mRNA, respectively. In general, we assume that all reactions proceed at a constant rate, bearing in mind that the rate does not depend on the content of the substrate/reaction product.

We introduce the following notation:

t—time, index 0—the initial moment of time;

the indices *m* and *c*—the membrane and cytoplasmic compartments, respectively;

z_{mc} —the coordinate perpendicular to the cross section of the cell between the membrane and cytoplasmic compartments, along which the sensitive protein, its antagonist and the cytoskeletal proteins undergo diffusion,

z_{cn} —similarly, the coordinate perpendicular to the cell cross section between the cytoplasmic and nuclear compartments, along which the transcription factor is diffused;

D_{SP} —the diffusion coefficient of the molecules of the "sensitive" protein between the cell compartments;

D_{aSP} —the diffusion coefficient of antagonist molecules of the "sensitive" protein between the cell compartments;

SP_{free} —the content of the "sensitive" protein in the free state;

aSP_{free} —the content of the antagonist of the "sensitive" protein in a free state;

$v^*_{MF\to SPfree}\left(g, z_{mc}\right)$—reaction rate of the transition of the "sensitive" protein from the complex with microfilaments to the free state when the mechanical stress is changed,

rSP —the content of the "sensitive" protein mRNA;

$raSP$ —the content of the antagonist of the "sensitive" protein mRNA;

v_d —the reaction rate of mRNA degradation in the cytoplasm;

$v_{SPfreec}\left(rSP\right)$—the reaction rate of the synthesis of sensitive protein molecules, depending on the content of the corresponding mRNA rSP;

$v_{aSPfreec}\left(raSP\right)$—the reaction rate of the synthesis of antagonist molecules of the "sensitive" protein, depending on the content of the corresponding mRNA $raSP$;

v_p —is the reaction rate of proteolysis of protein molecules in the cytoplasm;

M^*_c —the content of the activated modifying factor in the cytoplasm;

$v_{M^*_c}\left(SP_{freec}\right)$—the reaction rate of the activation of the modifying protein depending on the content of the free "sensitive" protein in the cytoplasm SP_{freec};

TF^* —activated transcription factor;

$v_{TF^*_c}\left(M^*_c\right)$—reaction rate of formation of an activated transcription factor in the cytoplasm, depending on the content of the activated modifying protein M^*_c;

$v_{rSPs}\left(TF^*_n\right)$—the reaction rate of the synthesis of mRNA molecules of the "sensitive" protein, depending on the content of the activated transcription factor in the nucleus TF^*_n.

SP—the content of "sensitive" protein, which was evaluated experimentally;

aSP—the content of the antagonist "sensitive" protein, which was estimated experimentally;

MF—the content of major proteins that form microfilaments (actin isoforms);

MT—the content of the main proteins forming microtubules (tubulin);

IF—the content of basic proteins forming intermediate filaments (desmin);

D_{MF} —diffusion coefficient of microfilament monomer molecules between cell compartments;

D_{MT} —the diffusion coefficient of microtubule monomer molecules between cell compartments;

D_{IF} —diffusion coefficient of monomer molecules of intermediate filaments between the cell compartments;

rMF —the microfilament mRNA content;

rMT —the microtubule mRNA content;

rIF —the intermediate filament mRNA content;

$v_{aSPfreec}\left(raSP\right)$—the reaction rate of the synthesis of antagonist molecules of the "sensitive" protein, depending on the content of the corresponding mRNA $raSP$;

$v_{MFc}\left(rMF\right)$—the reaction rate of the synthesis of microfilament molecules, depending on the content of the corresponding mRNA rMF;

$v_{MTc}\left(rMT\right)$—the reaction rate of synthesis of microtubule molecules, depending on the content of the corresponding mRNA rMT;

$v_{IFc}\left(rIF\right)$—the reaction rate of synthesis of molecules of intermediate filaments, depending on the content of the corresponding mRNA rIF.

Then, for the proposed mechanism, the standard kinetic dependencies taking into account the diffusion between the compartments, the efficiency of synthesis and degradation for the concentrations of the analyzed proteins and mRNA are:

$$SP_{freem} = SP_{freem0} + D_{SP}\frac{\mathrm{d}SP_{freec}}{\mathrm{d}z_{mc}}\cdot t - D_{SP}\frac{\mathrm{d}SP_{freem}}{\mathrm{d}z_{mc}}\cdot t + v^{*}_{MFm\to SPfreem}\left(g, z_{mc}\right)\cdot t \tag{1}$$

$$SP_{freec} = SP_{freec0} + v_{SPfreec}\left(rSP\right)\cdot t - v_{p}\cdot t - D_{SP}\frac{\mathrm{d}SP_{freec}}{\mathrm{d}z_{mc}}\cdot t + D_{SP}\frac{\mathrm{d}SP_{freem}}{\mathrm{d}z_{mc}}\cdot t \tag{2}$$

$$M^{*}_{c} = M^{*}_{c0} + v_{M^{*}_{c}}\left(SP_{freec}\right)\cdot t - v_{p}\cdot t \tag{3}$$

$$TF^{*}_{c} = TF^{*}_{c0} + v_{TF^{*}_{c}}\left(M^{*}_{c}\right)\cdot t - D_{TF}\frac{\mathrm{d}TF^{*}_{c}}{\mathrm{d}z_{cn}}t - v_{p}\cdot t \tag{4}$$

$$rSP = rSP_{0} + v_{rSPs}\left(TF^{*}_{n}\right)\cdot t - v_{d}\cdot t \tag{5}$$

$$TF^{*}_{n} = TF^{*}_{n0} + D_{TF}\frac{\mathrm{d}TF^{*}_{c}}{\mathrm{d}z_{cn}}t - v_{p}\cdot t \tag{6}$$

$$aSP_{freem} = aSP_{freem0} + D_{aSP}\frac{\mathrm{d}aSP_{freec}}{\mathrm{d}z_{mc}}\cdot t - D_{aSP}\frac{\mathrm{d}aSP_{freem}}{\mathrm{d}z_{mc}}\cdot t \tag{7}$$

$$\begin{aligned} aSP_{freec} = {} & aSP_{freec0} + v_{aSPfreec}\left(raSP\right)\cdot t - v_{p}\cdot t - D_{aSP}\frac{\mathrm{d}aSP_{freec}}{\mathrm{d}z_{mc}}\cdot t \\ & + D_{aSP}\frac{\mathrm{d}aSP_{freem}}{\mathrm{d}z_{mc}}\cdot t \end{aligned} \tag{8}$$

Similar to the previous system, for comparison with the experimental results and to determine the type of dependencies, we write the expressions for those parameters that can be determined (divided into compartments):

Membrane + cortical cytoskeleton

$$SP_{m} = SP_{m0} + D_{SP}t\left(\frac{\mathrm{d}SP_{freec}}{\mathrm{d}z_{mc}} - \frac{\mathrm{d}SP_{freem}}{\mathrm{d}z_{mc}}\right) \tag{9}$$

$$aSP_{m} = aSP_{m0} + D_{aSP}t\left(\frac{\mathrm{d}aSP_{freec}}{\mathrm{d}z_{mc}} - \frac{\mathrm{d}aSP_{freem}}{\mathrm{d}z_{mc}}\right) \tag{10}$$

$$MF_{m} = MF_{m0} + D_{MF}t\left(\frac{\mathrm{d}MF_{c}}{\mathrm{d}z_{mc}} - \frac{\mathrm{d}MF_{m}}{\mathrm{d}z_{mc}}\right) \tag{11}$$

$$MT_m = MT_{m0} + D_{MT}t\left(\frac{\mathrm{d}MT_c}{\mathrm{d}z_{mc}} - \frac{\mathrm{d}MT_m}{\mathrm{d}z_{mc}}\right) \tag{12}$$

$$IF_m = IF_{m0} + D_{IF}t\left(\frac{\mathrm{d}IF_c}{\mathrm{d}z_{mc}} - \frac{\mathrm{d}IF_m}{\mathrm{d}z_{mc}}\right) \tag{13}$$

Cytoplasm

$$SP_c = SP_{c0} + v_{SPfreec}\left(rSP\right)\cdot t - v_p\cdot t - D_{SP}t\left(\frac{\mathrm{d}SP_{freec}}{\mathrm{d}z_{mc}} - \frac{\mathrm{d}SP_{freem}}{\mathrm{d}z_{mc}}\right) \tag{14}$$

$$aSP_c = aSP_{c0} + v_{aSPfreec}\left(raSP\right)\cdot t - v_p\cdot t - D_{aSP}t\left(\frac{\mathrm{d}aSP_{freec}}{\mathrm{d}z_{mc}} - \frac{\mathrm{d}aSP_{freem}}{\mathrm{d}z_{mc}}\right) \tag{15}$$

$$MF_c = MF_{c0} + v_{MFc}\left(rMF\right)\cdot t - v_p\cdot t - D_{MF}t\left(\frac{\mathrm{d}MF_c}{\mathrm{d}z_{mc}} - \frac{\mathrm{d}MF_m}{\mathrm{d}z_{mc}}\right) \tag{16}$$

$$MT_c = MT_{c0} + v_{MTc}\left(rMT\right)\cdot t - v_p\cdot t - D_{MT}t\left(\frac{\mathrm{d}MT_c}{\mathrm{d}z_{mc}} - \frac{\mathrm{d}MT_m}{\mathrm{d}z_{mc}}\right) \tag{17}$$

$$IF_c = IF_{c0} + v_{IFc}\left(rIF\right)\cdot t - v_p\cdot t - D_{IF}t\left(\frac{\mathrm{d}IF_c}{\mathrm{d}z_{mc}} - \frac{\mathrm{d}IF_m}{\mathrm{d}z_{mc}}\right) \tag{18}$$

$$rSP = rSP_0 + v_{rSPs}\left(TF_n^*\right)\cdot t - v_d\cdot t \tag{19}$$

$$raSP = raSP_0 + v_{raSPs}\left(TF_n^*\right)\cdot t - v_d\cdot t \tag{20}$$

$$rMF = rMF_0 + v_{rMFs}\left(TF_n^*\right)\cdot t - v_d\cdot t \tag{21}$$

$$rMT = rMT_0 + v_{rMTs}\left(TF_n^*\right)\cdot t - v_d\cdot t \tag{22}$$

$$rIF = rIF_0 + v_{rIFs}\left(TF_n^*\right)\cdot t - v_d\cdot t \tag{23}$$

Solving equations together, we obtain expressions for the content of various proteins. For the modifying protein and transcription factor:

$$M_c^* = M_{c0}^* + v_{M_c^*}\left(SP_{freec}\right)\cdot t - v_p\cdot t \tag{24}$$

$$TF_c^* = TF_{c0}^* - v_p\cdot t + v_{TF_c^*}\left(M_c^*\right)\cdot t - \left(TF_{c0}^* - v_p\cdot t + v_{TF_c^*}\left(M_c^*\right)\cdot t\right)\cdot \mathrm{e}^{-\frac{z_{cn}}{D_{TF}t}} \tag{25}$$

$$TF_n^* = TF_{n0}^* - v_p\cdot t + \left(TF_{c0}^* - v_p\cdot t + v_{TF_c^*}\left(M_c^*\right)\cdot t\right)\cdot \mathrm{e}^{-\frac{z_{cn}}{D_{TF}t}} \tag{26}$$

For "sensitive" protein:

$$\begin{aligned} rSP &= rSP_0 + v_{rSPs}\left(TF_n^*\right)\cdot t - v_d\cdot t \\ SP_{freec} &= SP_{freec0} - v_p\cdot t + v_{SP_{freec}}\left(rSP\right)\cdot t \\ &\quad - \left(SP_{freec0} - v_p\cdot t + v_{SP_{freec}}\left(rSP\right)\cdot t\right)\cdot \mathrm{e}^{-\frac{z_{mc}}{2D_{SP}t}} \\ &\quad + \frac{\mathrm{e}^{-\frac{z_{mc}}{2D_{SP}t}}}{2D_{SP}}\int_0^{z_{mc}} \frac{\mathrm{d}k_{MFm\to SPfreem}^*\left(g, z_{mc}\right)}{\mathrm{d}z_{mc}}\cdot \mathrm{e}^{\frac{z_{mc}}{2D_{SP}t}}\mathrm{d}z_{mc} \end{aligned} \tag{27}$$

$$SP_{freem} = SP_{freem0} + v^*_{MFm\to SPfreem}\left(g, z_{mc}\right)\cdot t + \left(SP_{freec0} - v_p\cdot t + v_{SP_{freec}}\left(rSP\right)\cdot t\right)\cdot \mathrm{e}^{-\frac{z_{mc}}{2D_{SP}t}} - \frac{\mathrm{e}^{-\frac{z_{mc}}{2D_{SP}t}}}{2D_{SP}}\int_0^{z_{mc}} \frac{\mathrm{d}k^*_{MFm\to SPfreem}\left(g, z_{mc}\right)}{dz_{mc}}\cdot \mathrm{e}^{\frac{z_{mc}}{2D_{SP}t}}\mathrm{d}z_{mc} \tag{28}$$

$$SP_c = SP_{c0} + \left(SP_{freec0} - v_p\cdot t + v_{SP_{freec}}\left(rSP\right)\cdot t\right)\cdot \mathrm{e}^{-\frac{z_{mc}}{2D_{SP}t}} + t\cdot\frac{\mathrm{d}}{\mathrm{d}z_{mc}}\left(\mathrm{e}^{-\frac{z_{mc}}{2D_{SP}t}}\cdot\int_0^{z_{mc}}\frac{\mathrm{d}k^*_{MFm\to SPfreem}\left(g, z_{mc}\right)}{\mathrm{d}z_{mc}}\cdot\mathrm{e}^{\frac{z_{mc}}{2D_{SP}t}}\mathrm{d}z_{mc}\right) \tag{29}$$

$$SP_m = SP_{m0} - v_p\cdot t + v_{SP_{freec}}\left(rSP\right)\cdot t - \left(SP_{freec0} - v_p\cdot t + v_{SP_{freec}}\left(rSP\right)\cdot t\right)\cdot \mathrm{e}^{-\frac{z_{mc}}{2D_{SP}t}} - t\cdot\frac{\mathrm{d}}{\mathrm{d}z_{mc}}\left(\mathrm{e}^{-\frac{z_{mc}}{2D_{SP}t}}\cdot\int_0^{z_{mc}}\frac{\mathrm{d}k^*_{MFm\to SPfreem}\left(g, z_{mc}\right)}{\mathrm{d}z_{mc}}\cdot\mathrm{e}^{\frac{z_{mc}}{2D_{SP}t}}\mathrm{d}z_{mc}\right) \tag{30}$$

For the antagonist of "sensitive" protein:

$$raSP = raSP_0 + v_{raSPs}\left(TF_n^*\right)\cdot t - v_d\cdot t \tag{31}$$

$$aSP_{freec} = aSP_{freec0} - v_p\cdot t + v_{aSP_{freec}}\left(raSP\right)\cdot t - \left(aSP_{freec0} - v_p\cdot t + v_{aSP_{freec}}\left(raSP\right)\cdot t\right)\cdot \mathrm{e}^{-\frac{z_{mc}}{2D_{aSP}t}} \tag{32}$$

$$aSP_{freem} = aSP_{freem0} + \left(aSP_{freec0} - v_p\cdot t + v_{aSP_{freec}}\left(raSP\right)\cdot t\right)\cdot \mathrm{e}^{-\frac{z_{mc}}{2D_{aSP}t}} \tag{33}$$

$$aSP_c = aSP_{c0} - v_p\cdot t + v_{aSP_{freec}}\left(raSP\right)\cdot t - \left(aSP_{freec0} - v_p\cdot t + v_{aSP_{freec}}\left(raSP\right)\cdot t\right)\cdot \mathrm{e}^{-\frac{z_{mc}}{2D_{aSP}t}} \tag{34}$$

$$aSP_m = aSP_{m0} + \left(aSP_{freec0} - v_p\cdot t + v_{aSP_{freec}}\left(raSP\right)\cdot t\right)\cdot \mathrm{e}^{-\frac{z_{mc}}{2D_{aSP}t}} \tag{35}$$

For microfilaments:

$$rMF = rMF_0 + v_{rMFs}\left(TF_n^*\right)\cdot t - v_d\cdot t \tag{36}$$

$$MF_c = MF_{c0} - v_p\cdot t + v_{MFc}\left(rMF\right)\cdot t - \left(MF_{c0} - v_p\cdot t + v_{MFc}\left(rMF\right)\cdot t\right)\cdot \mathrm{e}^{-\frac{z_{mc}}{2D_{MF}t}} \tag{37}$$

$$MF_m = MF_{m0} + \left(MF_{c0} - v_p\cdot t + v_{MFc}\left(rMF\right)\cdot t\right)\cdot \mathrm{e}^{-\frac{z_{mc}}{2D_{MF}t}} \tag{38}$$

For microtubules:

$$rMT = rMT_0 + v_{rMTs}\left(TF_n^*\right)\cdot t - v_d\cdot t \tag{39}$$

$$MT_c = MT_{c0} - v_p\cdot t + v_{MTc}\left(rMT\right)\cdot t - \left(MT_{c0} - v_p\cdot t + v_{MTc}\left(rMT\right)\cdot t\right)\cdot \mathrm{e}^{-\frac{z_{mc}}{2D_{MT}t}} \tag{40}$$

$$MT_m = MT_{m0} + \left(MT_{c0} - v_p \cdot t + v_{MTc}\left(rMT\right)\cdot t\right)\cdot \mathrm{e}^{-\frac{z_{mc}}{2D_{MT}t}} \tag{41}$$

For intermediate filaments:

$$rIF = rIF_0 + v_{rIFs}\left(TF_n^*\right)\cdot t - v_d \cdot t \tag{42}$$

$$IF_c = IF_{c0} - v_p \cdot t + v_{IFc}\left(rIF\right)\cdot t - \left(IF_{c0} - v_p \cdot t + v_{IFc}\left(rIF\right)\cdot t\right)\cdot \mathrm{e}^{-\frac{z_{mc}}{2D_{IF}t}} \tag{43}$$

$$IF_m = IF_{m0} + \left(IF_{c0} - v_p \cdot t + v_{IFc}\left(rIF\right)\cdot t\right)\cdot \mathrm{e}^{-\frac{z_{mc}}{2D_{IF}t}} \tag{44}$$

3. Simulation

In previous studies, we obtained systematic data concerning the contents of various cytoskeletal proteins in the membrane and cytoplasmic fractions of rat soleus muscle fibers [28] [29]. Therefore, for the simulation, we consider this type of cell under changes in the external mechanical field.

We consider the actin-binding proteins alpha-actinin-4 and alpha-actinin-1 as a "sensitive" protein and its antagonist, respectively, and beta-actin as a protein of microfilaments of the submembrane cytoskeleton because its content dominates over the content of gamma-actin in this cell type [28] (**Figure 1(a)**).

As a result of a change in the external mechanical stress, an adaptive pattern is formed: in the case of an increase, the cytoskeleton becomes more developed, in the case of a decrease, vice versa. Consider the option of decreasing external mechanical stress (**Figure 1(b)**).

We will follow the "sensitive" protein, its antagonist, and microfilaments and compare the results of the simulation with the experimental data.

Since the experiment evaluated the relative contents of proteins and mRNA as a whole in compartments, then z_{mc} is the "path length" between the cortical

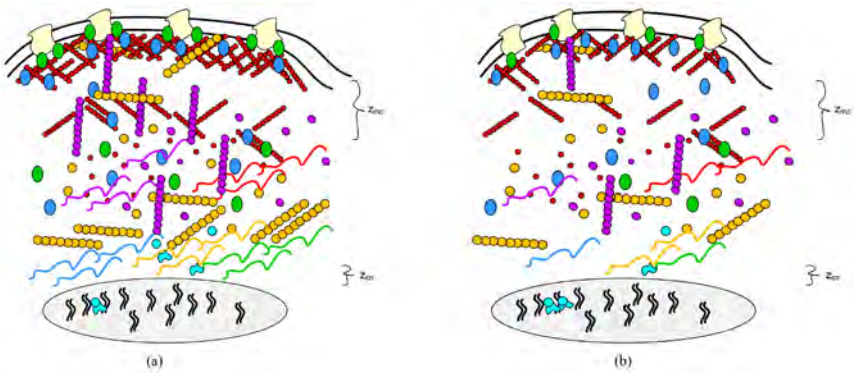

Figure 1. Schema of mechanosensitivity. (a)—an initial state; (b)—an adaptive pattern under decrease of the external mechanical tension. —cholesterol, —*SP*, —*rSP*, —*aSP*, —*raSP*, —*MF* as filaments, —*MF* as monomers, —*rMF*, —*MT* as filaments, —*MT* as monomers, —*rMT*, —*IF* as filaments, —*IF* as monomers, —*rIF*, $-M_c^*$, $-TF^*$.

cytoskeleton and the cytoplasm, and z_{cn} is the "path length" between the cytoplasm and chromatin (**Figure 1**).

We assume that for the fibers of the soleus muscle of rats:

$$z_{mc} = 18\times10^{-7}\,\text{m}, \quad z_{cn} = 2\times10^{-7}\,\text{m}.$$

Following [33], using the Stokes-Einstein equation, we assume that the diffusion coefficient is:

$$D = \frac{RT}{6\pi\eta r N_A}, \tag{45}$$

where $R = 8.31\,\text{J/mol}\cdot\text{K}$ —the universal gas constant, $T = 298\,\text{K}$ —the temperature, $\eta = 10^{-3}\,\text{Pa}\cdot\text{s}$ —the dynamic viscosity of the medium, $N_A = 6.02\times10^{23}\,\text{mol}^{-1}$, *r*—the hydrodynamic radius of the protein molecule.

Beta-actin, considered the main protein of microfilaments of the cortical cytoskeleton in rat soleus muscle, has 375 amino acid residues. Then, we will assume that its hydrodynamic radius is 5.28 × 10^{-9} m [33]. Assuming that *SP* and *aSP* are alpha-actinin-4 and alpha-actinin-1, having 911 and 892 amino acid residues, respectively, we will assume that for them, the hydrodynamic radii are the same and amount to 6.61 × 10^{-9} m, based on the extrapolation proposed by [33]. The transcription factor remains unknown in the proposed mechanism, but since many parameters are not determined accurately but are estimated, for simplicity of calculations, we will consider the hydrodynamic radius of the transcription factor as a certain average value, and we will use 6.0 × 10^{-9} m. Consequently, all the hydrodynamic radii necessary for calculations have close values, and we can assume that the diffusion coefficient has one order:

$$D_{MF} = D_{SP} = D_{aSP} = D_{TF} = 10^{-11}. \tag{46}$$

The rate of RNA polymerase II in eukaryotic cells is 10 - 70 nucleotides per second [34] [35]. Thus, we defined it as 40 nucleotides/s. Since the dependence of the efficiency of the recruitment of a transcriptional complex to DNA in this case is unknown, we will assume that for each of the proteins under consideration, it is a linear relationship with a specific recruitment coefficient in each case. Then:

$$\text{for } SP \text{ (alpha-actinin-4, 3885 bp)} — v_{rSPs}\left(TF_n^*\right) = 10^{-2} k_{rSPs}\cdot TF_n^* s^{-1}; \tag{47}$$

$$\text{for } aSP \text{ (alpha-actinin-1, 2956 bp)} — v_{raSPs}\left(TF_n^*\right) = 1.4\times10^{-2} k_{raSPs}\cdot TF_n^* s^{-1}; \tag{48}$$

$$\text{for } MF \text{ (beta-actin, 1293 bp)} — v_{rMF}\left(TF_n^*\right) = 3\times10^{-2} k_{rMF}\cdot TF_n^* s^{-1}, \tag{49}$$

where k_{rSPs}, k_{raSPs} and k_{rMF} are recruitment coefficients of the transcriptional complex to DNA depending on the content of the activated transcription factor in the nucleus for alpha-actinin-4, alpha-actinin-1 and beta-actin, respectively.

We assume that the half-life of mRNA of genes encoding cytoskeletal proteins, as well as for globin, is approximately 8 hours [36]. We assume that on average, it is approximately 28,800 seconds. Therefore, the reaction rate constant for mRNA degradation in the cytoplasm is:

$$v_d = 3.5\times10^{-5}\,\mathrm{s}^{-1} \tag{50}$$

The speed of ribosomes in eukaryotic cells is diverse, but we will assume that on average, including for cytoskeletal proteins, processing proceeds at a speed of 5 amino acid residues per second [37]. Then:

for SP (alpha-actinin-4, 911aa)— $v_{SPfreec}\left(rSP\right) = 5.5\times10^{-3} k_{SPfreec}\cdot rSPs^{-1}$; (51)

for aSP (alpha-actinin-1, 892aa)— $v_{aSPfreec}\left(raSP\right) = 5.6\times10^{-3} k_{aSPfreec}\cdot raSPs^{-1}$; (52)

for MF (beta-actin, 375aa)— $v_{MFc}\left(rMF\right) = 13.3\times10^{-3} k_{MFc}\cdot rMFs^{-1}$ (53)

where the $k_{SPfreec}, k_{aSPfreec}$ and k_{MFc} are coefficients that reflect the efficiency of translation for alpha-actinin-4, alpha-actinin-1 and beta-actin, respectively.

We assume that proteolysis is carried out using the proteasome. The rate of proteolysis depends on how long the protein has been synthesized but, on average, is 2.5 substrates/minute [38]. Let us assume that on average, for the analyzed proteins, the rate of proteolysis reaction of protein molecules in the cytoplasm is:

$$v_p = 4\times10^{-2}\,\mathrm{s}^{-1} \tag{54}$$

Since the dependence of the activation of the modifying protein on the content of free "sensitive" protein in the cytoplasm SP_{freec} and the dependence of the formation of an activated transcription factor in the cytoplasm, which depend on the content of the activated modifying protein M_c^*, remain unknown, we approximate, as above, with the linear dependence specific activation factors:

$$v_{M_c^*}\left(SP_{freec}\right) = a_{M_c^*}\cdot SP_{freec}s^{-1} \tag{55}$$

$$v_{TF_c^*}\left(M_c^*\right) = a_{TF_c^*}\cdot M_c^* s^{-1} \tag{56}$$

where $a_{M_c^*}$ and $a_{TF_c^*}$ are the activation coefficients of the modifying protein by the free "sensitive" protein and the transcription factor by the activated modified protein, respectively.

Consequently, the greatest uncertainty is $v^*_{MF\to SPfree}\left(g, z_{mc}\right)$, the reaction rate of the transition of the "sensitive" protein from the complex with microfilaments to the free state when the mechanical stress changes. Without loss of generality, we will assume that the variables are independent and then:

$$v^*_{MF\to SPfree}\left(g, z_{mc}\right) = v^*\left(g\right)\cdot v^*\left(z_{mc}\right) = v^*\left(g\right)\cdot\ D_{SP}\cdot t\cdot^{-\frac{z_{mc}}{2D_{SP}t}} \tag{57}$$

Considering gravity as a bulk force, we accept, as before [27], that:

$$v^*\left(g\right) = \rho\cdot g\cdot\cos\varphi, \tag{58}$$

where φ is the orientation angle, in this case, the soleus muscle in the field of gravity, g is the acceleration of gravity, and ρ is the density of the cortical cytoskeleton, depending on the initial number of formed filaments and their organization into the network. For the standard model used to reproduce the effects of weightlessness on Earth in rodents, antiorthostatic suspension, this angle

is 30˚ [39].

We take the initial values of the estimated parameters for 100% and substitute (45) - (58) into (24) - (38). We evaluated the process of perception of a mechanical stimulus and its transduction at several points—6, 12, 18, 24 and 72 hours—to compare the results of mathematical modeling and experimental data obtained by us earlier [28].

The dependences obtained for the content of the "sensitive" protein—alpha-actinin-4 (**Figure 2**), the antagonist of the "sensitive" protein—alpha-actinin-1 (**Figure 3**), and microfilaments—beta-actin (**Figure 4**) in comparison with experimental data show coincidence when varying only the constants of the efficiency of transcription ($k_{rSPs}, k_{raSPs}, k_{rMF}$ respectively) and translation ($k_{SPfreec}, k_{aSPfreec}, k_{MFc}$ respectively). However, there are differences at the 72-hour point: in the experiment, the alpha-actinin-1 content is 77% ± 7% of the control in the membrane fraction and 50.5% in the numerical experiment (**Figure 3(b)**); in the experiment, the beta-actin content in the cytoplasmic fraction does not differ from the control; in the numerical experiment, it is reduced (66.4% of the control) (**Figure 4(c)**). In addition, at the 12 o'clock point in the experiment, the beta-actin content in the membrane fraction is already reduced and amounts to 51% ± 4% of the control; in a numerical experiment, it does not differ from the control (103%) (**Figure 4(b)**).

The dynamics of the transcription factor change (**Figure 5**) indicates an increase in its content in the nucleus after 6 hours by 35% and a subsequent increase up to 24 hours (235% relative to the control) and then a decrease after 72 hours compared to the maximum accumulation (up to 190%).

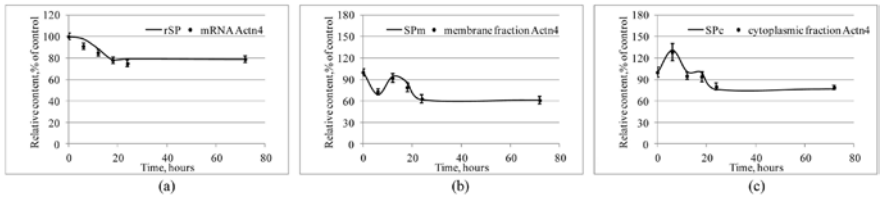

Figure 2. Relative content of the "sensitive" protein and its mRNA (simulation data) and comparison with the relative content of alpha-actinin-4 (Actn4) and mRNA (experimental data). (a)—mRNA comparison; (b)—membrane fraction of protein comparison; (c)—cytoplasmic fraction of protein comparison.

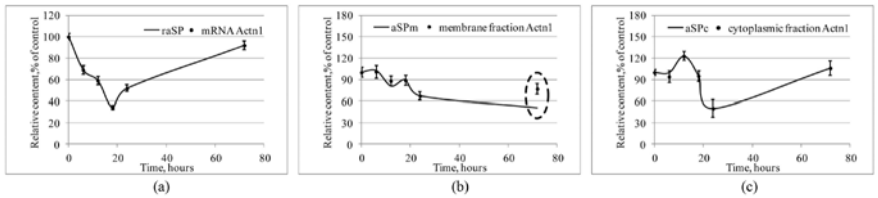

Figure 3. Relative content of the antagonist of the "sensitive" protein and its mRNA (simulation data) and comparison with the relative content of alpha-actinin-1 (Actn1) and mRNA (experimental data). (a)—mRNA comparison; (b)—membrane fraction of protein comparison; (c)—cytoplasmic fraction of protein comparison.

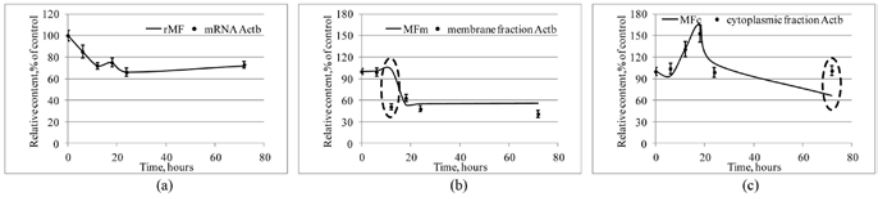

Figure 4. Relative content of microfilament protein and its mRNA (simulation data) and comparison with the relative content of beta-actin and mRNA (experimental data). (a)—mRNA comparison; (b)—membrane fraction of protein comparison; (c)—cytoplasmic fraction of protein comparison.

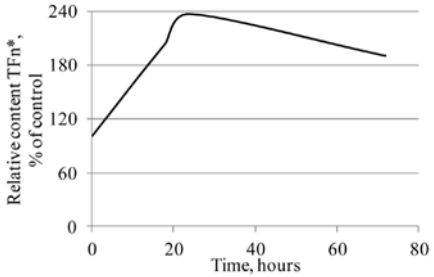

Figure 5. Relative content of the transcription factor in the nuclei (simulation data).

Simulation data were fitted by curve; experimental data are marked by dots. The simulation was performed under parameters (45) - (58) and constants for 6h $k_{rSPs} = -5.28\times10^{-5}$, $k_{SPfreec} = -18\times10^{-2}$, for 12 h— $k_{rSPs} = -4.4\times10^{-5}$, $k_{SPfreec} = -16\times10^{-2}$, for 18 h— $k_{rSPs} = -4.39\times10^{-5}$, $k_{SPfreec} = -2\times10^{-2}$, for 24 h— $k_{rSPs} = 3.36\times10^{-5}$, $k_{SPfreec} = -1.53\times10^{-3}$, for 72 h— $k_{rSPs} = 1.75\times10^{-5}$, $k_{SPfreec} = 8.85\times10^{-4}$. The figure was built in the Excel 2007 for Windows.

Simulation data were fitted by curve; experimental data are marked by dots. The simulation was performed under parameters (45) - (58) and constants for 6h $k_{rSPs} = -1.62\times10^{-4}$, $k_{SPfreec} = 10^{-4}$, for 12 h— $k_{rSPs} = -1.11\times10^{-4}$, $k_{SPfreec} = 2.23\times10^{-3}$, for 18 h— $k_{rSPs} = 2.84\times10^{-5}$, $k_{SPfreec} = 2.01\times10^{-3}$, for 24 h— $k_{rSPs} = -5.33\times10^{-5}$, $k_{SPfreec} = -2.44\times10^{-3}$, for 72 h— $k_{rSPs} = -5.33\times10^{-5}$, $k_{SPfreec} = -2.41\times10^{-3}$. The dotted ovals show differences between the simulation and experimental data. The figure was built in the Excel 2007 for Windows.

The simulation was performed under parameters (45) - (58). The figure was built in the Excel 2007 for Windows.

4. Discussion

The problem of perception by living cells of a mechanical stimulus is not only of practical importance associated with the exploration of deep space but also fundamental since life has evolved under the conditions of a permanently acting mechanical factor—gravity. Despite the many studies, there is currently no universal idea of how a cell perceives an external mechanical field and how it transduces its changes to form an adaptation pattern.

In our previous works, we obtained experimental data that suggest the key role of actin-binding proteins in the cells' perception of various types of me-

chanical stimulus. For mammals, we assume that these proteins can be two calcium-dependent alpha-actinin forms: alpha-actinin-1 and alpha-actinin-4 [10] [27] [28]. However, for example, in *Drosophila*, there is only one alpha-actinin isoform, but our previous data suggest that another actin-binding protein, supervillin, may be the second participant [32]. Therefore, in this work, we designated this pair of proteins as a sensitive protein SP and an antagonist of the sensitive protein *aSP*.

In system biology, mathematical modeling is often used to estimate the values of unknown parameters. The model of population dynamics of Lotka-Volterra is used especially widely in various kinetic models, for example, when modeling the development of bacterial infection [40]. In this paper, the use of kinetic regularities and the second Fick's law, the diffusion equation, assuming that increasing or decreasing mechanical stress leads to dissociation of *aSP* or *SP* from the cortical cytoskeleton, let us numerically receive the same results as in the experiments.

We estimated the values of the parameters after 6, 12, 18, 24 and 72 hours. In almost all cases, by varying only the constants of the efficiency of transcription and translation, we obtained theoretical data that coincided with the experimental data. The exception was the content of the antagonist of the sensitive protein in the membrane fraction (alpha-actinin-1) after 72 hours of exposure: in the experiment, the minimum content was at the previous point, 24 hours [28], while modeling was at 72 hours. However, the error values of the experimental data do not show a significant difference between the values at 24 and 72 hours [28]. In addition, a significant difference between the experimental data and those obtained in a numerical experiment occurred in the membrane fraction of microfilaments after 12 hours, as well as in the cytoplasmic fraction, after 72 hours. However, it should be noted that in the experiment, we evaluated the content of actin isoforms (beta and gamma-) separately, while in a numerical experiment, for simplicity, we followed the total content of proteins forming microfilaments, comparing the data with beta-actin. However, because the content of beta-actin in muscle cells substantially dominates the content of gamma-actin, this approach can be justified. In general, this model, developed for early acts of cellular mechanoreception, gives results that coincide with experimental data up to 72 hours of exposure.

In addition, it is known that one of the candidates for the role of the sensitive protein *SP*, alpha-actinin-4, can penetrate into the nucleus [41] and bind to the promoter regions of the genes. However, it is still unknown, in the case of changes in external mechanical stress, whether alpha-actinin-4 itself regulates the expression of its potential targets or indirectly regulates them through a transcription factor. Therefore, we introduced a transcription factor modifier into the model, which can be activated by *SP*, and, in turn, activate the corresponding transcription factor. In a numerical experiment, the dynamics of changes in the content of the transcription factor in the nucleus were estimated,

and according to these results, we can assume that the maximum of its accumulation occurs at 24 hours, where its content exceeds the control level by almost 2.5 times. In addition, its content in the nuclei begins to increase after 6 hours of exposure.

Alpha-actinin-4, according to experimental data, has approximately the same initial content in the membrane and cytoplasmic compartments. After 6 hours of exposure in the membrane compartment, its content decreases by 27% and increases in the cytoplasm by 30% [28] [29]. In the numerical experiment, we obtained the same data. However, at the same time, after 6 hours of exposure, according to the simulation data, the content of the activated transcription factor in the nucleus increases by 35%. Comparing these data, we can assume that when the external mechanical stress changes, alpha-actinin-4 does not directly regulate the expression of the genes assessed but indirectly regulates them through the activation of an appropriate transcription factor.

Of course, such an assumption after mathematical modeling needs experimental verification, but it can be assumed that the disclosure of the detailed mechanism of interaction between the cell and the external mechanical field will help in the development of effective preventive measures that are necessary, for example, during deep space exploration.

5. Conclusions

The results obtained indicate that the model of perception of an external mechanical stimulus by living cells, based on a system of kinetic equations and the second Fick law, adequately describes the process, and the simulation results correlate with the experimental data.

The time dependencies estimated in a numerical experiment suggest that alpha-actinin-4 triggers a signaling cascade, leading to an increase in the content of certain transcription factors whose targets are both alpha-actinin-4 and alpha-actinin-1 and beta-actin. In other words, the answer to the question of whether alpha-actinin-4 regulates gene expression directly when mechanical stress changes (given its ability to penetrate into the nucleus and bind to some promoters) is as follows: according to a numerical experiment, it is more likely that another transcription factor will appear.

Author Contributions

Irina V. Ogneva—idea, conceptualization, data curation, formal analysis, funding acquisition, investigation, methodology, project administration, resources, software, supervision, validation, visualization, writing.

Maria A. Usik—formal analysis, investigation, methodology, visualization, writing.

Nikolay S. Biryukov—investigation, methodology, validation.

Nikita O. Kremenetsky—investigation, validation.

Yuliya S. Zhdankina—investigation, methodology, validation.

Funding

This work was financially supported by the program for fundamental research SSC RF-IBMP RAS; program "Postgenomic technologies and perspective solutions in the biomedicine" of the RAS Presidium; Russian Academic Excellence Project 5-100.

Disclosure of Potential Conflicts of Interest

The authors declare that they have no conflict of interest.

Data Availability Statement

All data generated or analyzed during this study are included in this article.

References

[1] Riley, D.A., Bain, J.L.W., Thompson, J.L., Fitts, R.H., Widrick, J.J., Trappe, S.W. and Trappe, T.A. (2000) Decreased Thin Filament Density and Length in Human Atrophic Soleus Muscle fibers after Spaceflight. *Journal of Applied Physiology*, **88**, 567-572. https://doi.org/10.1152/jappl.2000.88.2.567

[2] Vico, L. and Hargens, A. (2018) Skeletal Changes during and after Spaceflight. *Nature Reviews Rheumatology*, **14**, 229-245. https://doi.org/10.1038/nrrheum.2018.37

[3] Watenpaugh, D.E. and Hargens, A.R. (1996) The Cardiovascular System in Microgravity. In: *Handbook of Physiology. Environmental Physiology*, Bethesda, MD, 631-674.

[4] Dennerll, T.J., Joshi, H.C., Steel, V.L., Buxbaum, R.E. and Heidemann, S.R. (1988) Tension and Compression in the Cytoskeleton of PC-12 Neurites. II: Quantitative Measurements. *The Journal of Cell Biology*, **107**, 665-674. https://doi.org/10.1083/jcb.107.2.665

[5] Putnam, A.J., Schultz, K. and Mooney, D.J. (2001) Control of Microtubule Assembly by Extracellular Matrix and Externally Applied Strain. *American Journal of Physiology*, **280**, C556-C564. https://doi.org/10.1152/ajpcell.2001.280.3.C556

[6] Sukharev, S. and Corey, D.P. (2004) Mechanosensitive Channels: Multiplicity of Families and Gating Paradigms. *Science Signaling*, **2004**, re4. https://doi.org/10.1126/stke.2192004re4

[7] Maroto, R., Raso, A., Wood, T.G., Kurosky, A., Martinac, B. and Hamill, O.P. (2005) TRPC1 Forms the Stretch-Activated Cation Channel in Vertebrate Cells. *Nature Cell Biology*, **7**, 179-185. https://doi.org/10.1038/ncb1218

[8] Sukharev, S., Betanzos, M., Chiang, C.S. and Guy, H.R. (2001) The Gating Mechanism of the Large Mechanosensitive Channel MscL. *Nature*, **409**, 720-724. https://doi.org/10.1038/35055559

[9] Howard, J. and Bechstedt, S. (2004) Hypothesis: A Helix of Ankyrin Repeats of the NOMPC-TRP Ion Channel Is the Gating Spring of Mechanoreceptors. *Current Biology*, **14**, R224-R226. https://doi.org/10.1016/j.cub.2004.02.050

[10] Ogneva, I.V. (2013) Cell Mechanosensitivity: Mechanical Properties and Interaction with Gravitational Field. *BioMed Research International*, **2013**, Article ID: 598461. https://doi.org/10.1155/2013/598461

[11] Maniotis, A.J., Chen, C.S. and Ingber, D.E. (1997) Demonstration of Mechanical Connections between Integrins, Cytoskeletal Filaments and Nucleoplasm that Sta-

bilize Nuclear Structure. *Proceedings of the National Academy of Sciences of the United States of America*, **94**, 849-854. https://doi.org/10.1073/pnas.94.3.849

[12] Huang, H., Kamm, R.D. and Lee, R.T. (2004) Cell Mechanics and Mechanotransduction: Pathways, Probes, and Physiology. *American Journal of Physiology-Cell Physiology*, **287**, C1-C11. https://doi.org/10.1152/ajpcell.00559.2003

[13] Sakar, D., Nagaya, T., Koga, K. and Seo, H. (1999) Culture in Vector-Averaged Gravity Environment in a Clinostat Results in Detachment of Osteoblastic ROS 17/2.8 Cells. *Occupational and Environmental Medicine*, **43**, 22-24.

[14] Uva, B.M., Masini, M.A., Sturla, M., Prato, P., Passalacqua, M., Giuliani, M., Tagliafierro, G. and Strollo, F. (2002) Clinoration-Induced Weightlessness Influences the Cytoskeleton of Glial Cells in Culture. *Brain Research*, **934**, 132-139. https://doi.org/10.1016/S0006-8993(02)02415-0

[15] Gaboyard, S., Blachard, M.P., Travo, B.T., Viso, M., Sans, A. and Lehouelleur, J. (2002) Weightlessness Affects Cytoskeleton of Rat Utricular Hair Cells during Maturation *in Vitro*. *NeuroReport*, **13**, 2139-2142. https://doi.org/10.1097/00001756-200211150-00030

[16] Plett, P.A., Abonour, R., Frankovitz, S.M. and Orschell, C.M. (2004) Impact of Modeled Microgravity on Migration, Differentiation and Cell Cycle Control of Primitive Human Hematopoietic Progenitor Cells. *Experimental Hematology*, **32**, 773-781. https://doi.org/10.1016/j.exphem.2004.03.014

[17] Kacena, M.A., Todd, P. and Landis, W.J. (2004) Osteoblasts Subjected to Spaceflight and Simulated Space Shuttle Launch Conditions. *In Vitro Cellular & Developmental Biology - Animal*, **39**, 454-459. https://doi.org/10.1290/1543-706X(2003)039<0454:OSTSAS>2.0.CO;2

[18] Crawford-Young, S.J. (2006) Effects of Microgravity on Cell Cytoskeleton and Embryogenesis. *The International Journal of Developmental Biology*, **50**, 183-191. https://doi.org/10.1387/ijdb.052077sc

[19] Schatten, H., Lewis, M.L. and Chakrabarti, A. (2001) Spaceflight and Clinorotation Cause Cytoskeleton and Mitochondria Changes and Increases in Apoptosis in Cultured Cells. *Acta Astronautica*, **49**, 399-418. https://doi.org/10.1016/S0094-5765(01)00116-3

[20] Gershovich, P.M., Gershovich, J.G. and Buravkova, L.B. (2008) Simulated Microgravity Alters Actin Cytoskeleton and Integrin-Mediated Focal Adhesions of Cultured Human Mesenchymal Stromal Cells. *Journal of Gravitational Physiology*, **15**, 203-204.

[21] Zayzafoon, M., Gathings, W.E. and McDonald, J.M. (2004) Modeled Microgravity Inhibits Osteogenic Differentiation of Human Mesenchymal Stem Cells and Increases Adipogenesis. *Endocrinology*, **145**, 2421-2432. https://doi.org/10.1210/en.2003-1156

[22] Meyers, V.E., Zayzafoon, M., Gonda, S.R., Gathings, W.E. and McDonald, J.M. (2004) Modeled Microgravity Disrupts Collagen I/Integrin Signaling during Osteoblastic Differentiation of Human Mesenchymal Stem Cells. *Journal of Cellular Biochemistry*, **93**, 697-707. https://doi.org/10.1002/jcb.20229

[23] Meyers, V.E., Zayzafoon, M., Douglas, J.T. and McDonald, J.M. (2005) RhoA and Cytoskeletal Disruption Mediate Reduced Osteoblastogenesis and Enhanced Adipogenesis of Human Mesenchymal Stem Cells in Modeled Microgravity. *Journal of Bone and Mineral Research*, **20**, 1858-1866. https://doi.org/10.1359/JBMR.050611

[24] Dai, Z.Q., Wang, R., Ling, S.K., Wan, Y.M. and Li, Y.H. (2007) Simulated Microgravity Inhibits the Proliferation and Osteogenesis of Rat Bone Marrow Mesen-

chymal Stem Cells. *Cell Proliferation*, **40**, 671-684. https://doi.org/10.1111/j.1365-2184.2007.00461.x

[25] Patel, M.J., Liu, W., Sykes, M.C., Ward, N.E., Risin, S.A., Risin, D. and Jo, H. (2007) Identification of Mechanosensitive Genes in Osteoblasts by Comparative Microarray Studies Using the Rotating Wall Vessel and the Random Positioning Machine. *Journal of Cellular Biochemistry*, **101**, 587-599. https://doi.org/10.1002/jcb.21218

[26] Pan, Z., Yang, J., Guo, C., Shi, D., Shen, D., Zheng, Q., Chen, R., Xu, Y., Xi, Y. and Wang, J. (2008) Effects of Hindlimb Unloading on *ex Vivo* Growth and Osteogenic/Adipogenic Potentials of Bone Marrow Derived Mesenchymal Stem Cells in Rats. *Stem Cells and Development*, **17**, 795-804. https://doi.org/10.1089/scd.2008.0254

[27] Ogneva, I.V. and Biryukov, N.S. (2013) Mathematical Modeling Cardiomyocyte's and Skeletal Muscle Fiber's Membrane: Interaction with External Mechanical Field. *Applied Mathematics*, **4**, 1-6. https://doi.org/10.4236/am.2013.48A001

[28] Ogneva, I.V., Biryukov, N.S., Leinsoo, T.A. and Larina, I.M. (2014) Possible Role of Non-Muscle Alpha-Actinins in Muscle Cell Mechanosensitivity. *PLoS ONE*, **9**, e96395. https://doi.org/10.1371/journal.pone.0096395

[29] Ogneva, I.V. and Biryukov, N.S. (2016) Lecithin Prevents Cortical Cytoskeleton Reorganization in Rat Soleus Muscle Fibers under Short-Term Gravitational Disuse. *PLoS ONE*, **11**, e0153650. https://doi.org/10.1371/journal.pone.0153650

[30] Ogneva, I.V., Maximova, M.V. and Larina, I.M. (2014) Structure of Cortical Cytoskeleton in Fibers of Mouse Muscle Cells after Being Exposed to a 30-Day Space Flight on Board the BION-M1 Biosatellite. *Journal of Applied Physiology*, **116**, 1315-1323. https://doi.org/10.1152/japplphysiol.00134.2014

[31] Ogneva, I.V., Gnyubkin, V., Laroche, N., Maximova, M.V., Larina, I.M. and Vico, L. (2015) Structure of the Cortical Cytoskeleton in Fibers of Postural Muscles and Cardiomyocytes of Mice after 30-Day 2g-Centrifugation. *Journal of Applied Physiology*, **118**, 613-623. https://doi.org/10.1152/japplphysiol.00812.2014

[32] Ogneva, I.V., Belyakin, S.N. and Sarantseva, S.V. (2016) The Development of Drosophila Melanogaster under Different Duration Space Flight and Subsequent Adaptation to Earth Gravity. *PLoS ONE*, **11**, e0166885. https://doi.org/10.1371/journal.pone.0166885

[33] Nygaard, M., Kragelund, B.B., Papaleo, E. and Lindorf-Larsen, K. (2017) An Efficient Method for Estimating the Hydrodynamic Radius of Disordered Protein Conformations. *Biophysical Journal*, **113**, 550-557. https://doi.org/10.1016/j.bpj.2017.06.042

[34] Neuman, K.C., Abbondanzieri, E.A., Landick, R., Gelles, J. and Block, S.M. (2003) Ubiquitous Transcriptional Pausing Is Independent of RNA Polymerase Backtracking. *Cell*, **115**, 437-447. https://doi.org/10.1016/S0092-8674(03)00845-6

[35] Darzacq, X., Shav-Tal, Y., de Turris, V., Brody, Y., Shenoy, S.M., Phair, R.D. and Singer, R.H. (2007) *In Vivo* Dynamics of RNA Polymerase II transcription. *Nature Structural & Molecular Biology*, **14**, 796-806. https://doi.org/10.1038/nsmb1280

[36] Shyu, A.B., Greenberg, M.E. and Belasco, J.G. (1989) The c-Fos mRNA Is Targeted for Rapid Decay by Two Distinct mRNA Degradation Pathways. *Genes & Development*, **3**, 60-72. https://doi.org/10.1101/gad.3.1.60

[37] Palmiter, R.D. (1975) Quantitation of Parameters that Determine the Rate of Ovalbumin Synthesis. *Cell*, **4**, 189-197. https://doi.org/10.1016/0092-8674(75)90167-1

[38] Princiotta, M.F., Finzi, D., Qian, S.B., Gibbs, J., Schuchmann, S., Buttgereit, F., Bennink, J.R. and Yewdell, J.W. (2003) Quantitating Protein Synthesis, Degradation, and Endogenous Antigen Processing. *Immunity*, **18**, 343-354.

https://doi.org/10.1016/S1074-7613(03)00051-7

[39] Morey-Holton, E., Globus, R.K., Kaplansky, A. and Durnova, G. (2005) The Hindlimb Unloading Rat Model: Literature Overview, Technique Update and Comparison with Space Flight Data. *Advances in Space Biology and Medicine*, **10**, 7-40. https://doi.org/10.1016/S1569-2574(05)10002-1

[40] Lakhani, V., Tan, L., Mukherjee, S., Stewart, W.C.L., Swords, W.E. and Das, J. (2018) Mutations in Bacterial Genes Induce Unanticipated Changes in the Relationship between Bacterial Pathogens in Experimental Otitis Media. *Royal Society Open Science*, **5**, Article ID: 180810. https://doi.org/10.1098/rsos.180810

[41] Goffart, S., Franko, A., Clemen, C.S. and Wiesner, R.J. (2006) Alpha-Actinin 4 and BAT1 Interaction with the Cytochrome *c* Promoter Upon Skeletal Muscle Differentiation. *Current Genetics*, **49**, 125-135. https://doi.org/10.1007/s00294-005-0043-0

Applied Mathematics, 2019, 10, 545-560
http://www.scirp.org/journal/am
ISSN Online: 2152-7393
ISSN Print: 2152-7385

Asymptotic Normality of the Nelson-Aalen and the Kaplan-Meier Estimators in Competing Risks

Didier Alain Njamen Njomen

Department of Mathematics and Computer Science, Faculty of Science, University of Maroua, Maroua, Cameroon
Email: didiernjamen1@gmail.com, didier-njamen@univ-maroua.cm

How to cite this paper: Njomen, D.A.N. (2019) Asymptotic Normality of the Nelson-Aalen and the Kaplan-Meier Estimators in Competing Risks. *Applied Mathematics*, **10**, 545-560.
https://doi.org/10.4236/am.2019.107038

Received: December 30, 2018
Accepted: July 19, 2019
Published: July 22, 2019

Abstract

This paper studies the asymptotic normality of the Nelson-Aalen and the Kaplan-Meier estimators in a competing risks context in presence of independent right-censorship. To prove our results, we use Robelledo's theorem which makes it possible to apply the central limit theorem to certain types of particular martingales. From the results obtained, confidence bounds for the hazard and the survival functions are provided.

Keywords

Censored Data, Right-Censoring, Counting Process, Competing Risks, Nelson-Aalen and Kaplan-Meier Estimators, Asymptotic Properties of Estimators, Confidence Bands

1. Introduction and Background

The model of competing risks has been widely studied in the literature, see e.g., Heckman and Honoré [1], Commenges [2], Com-nougué [3], Fine and Gray [4], Crowder [5], Fermanian [6], Latouche, A. [7], Geffray [8], Belot [9], Njamen and Ngatchou ([10], [11]), Njamen ([12], [13]). In most approaches, the competing risks are assumed to be either all independent or all dependent. Here, the independent component of the potential risks constitutes an independent censoring variable while the other risks are kept as possibly dependent. This approach is used by Geffray [8]. Namely, we consider a population in which each subject is exposed to m mutually exclusive competing risks which may be dependent. For $j \in \{1,\cdots,m\}$, the failure time from the j^{th} cause is a non-negative random variable (r.v.) τ_j. The competing risks model postulates

that only the smallest failure time is observable, it is given by the r.v. $T=\min\left(\tau_1,\cdots,\tau_m\right)$ with distribution function (d.f.) denoted by *F*. The cause of failure associated to T is then indicated by a r.v. η which takes value *j* if the failure is due to the j^{th} cause for a $j\in\left\{1,\cdots,m\right\}$ *i.e.* $\eta=j$ if $T=\tau_j$. The following modeling technique is extracted in Njamen and Ngatchou [10]: we assume that T is, in its turn, at risk of being independently right-censored by a non-negative r.v. C with d.f. *G*. Consequently, the observable r.v. are

$$\left(Z=\min\left(T,C\right),\xi=\eta\delta\right),$$

where $\delta=\mathbb{1}_{\{T\le C\}}$ and where $\mathbb{1}_{(.)}$ denotes the indicator function. As T and C are independent, the r.v. Z has d.f. H given by $1-H=\left(1-F\right)\left(1-G\right)$. Let $\tau_H=\sup\left\{t:H\left(t\right)<1\right\}$ denote the right-endpoint of H beyond which no observation is possible. The subdistribution functions $F^{(j)}$ pertaining to the different risks or causes of failure are defined for $j=1,\cdots,m$ and $t\ge 0$ by

$$F^{(j)}\left(t\right)=\mathbb{P}\left[T\le t,\eta=j\right],\ j=1,\cdots,m \tag{1}$$

When the independence of the different competing risks may not be assumed, the functions $F^{(j)}$ for $j=1,\cdots,m$ are the basic estimable quantities.

The Kaplan-Meier estimator was developed for situations in which only one cause of failure and the independent right-censoring are considered. Aalen and Johansen [14] were the first to extend the Kaplan-Meier estimator to several causes of failure in the presence of independent censoring. In the present situation, the d.f. F may be consistently estimated by the Kaplan-Meier estimator denoted by b $\hat{F}_n$. For $j=1,\cdots,m$, the subdistribution functions $F^{(j)}$ may be consistently estimated by means of the Aalen-Johansen estimators denoted respectively by $\hat{F}_n^{(j)}$, for $j=1,\cdots,m$. Indeed, when the process of the states occupied by an individual in time is a time-inhomogeneous Markov process, Aalen and Johansen [14] introduced an estimator of the transition probabilities between states in presence of independent random right-censoring. The competing risks set-up corresponds to the case of a time-inhomogeneous Markov process with only one transient state and several absorbing states (that can be labeled $1,\cdots,m$). Aalen and Johansen [14] obtained the joint consistency of $\hat{F}_n^{(j)}$ to $F^{(j)}$ for $j=1,\cdots,m$ uniformly over fixed compact intervals $\left[0,\sigma\right]$ for $\sigma<\tau_H$. They also obtained the joint weak convergence of the processes $\sqrt{n}\left(\hat{F}_n^{(j)}-F^{(j)}\right)$ on fixed compact intervals $\left[0,\sigma\right]$ for $\sigma<\tau_H$.

The asymptotic properties of the Kaplan-Meier estimator on the distribution function have been studied by several authors (see Peterson [15], Andersen and al. [16], Shorack and Wellner [17], Breslow and Crowley [18]).

In this paper, in a region where there is at least one observation, we are interested in providing asymptotic properties of the Nelson-Aalen and Kaplan-Meier nonparametric estimators of the functions $\Lambda^{*(j)}$ and $S^{*(j)}$. For $j=1,\cdots,m$ in the presence of independent right-wing censorship in the context of competitive risks set out in Njamen and Ngatchou ([10], [11]).

The rest of the paper is organized as follows: Section 2 describes preliminary

results and rappels used in the paper. In Section 3, we obtain two laws: In Section 3.1, we give limit law of Nelson-Aalen's nonparametric estimator for competing risks as defined in Njamen and Ngatchou [10] and Njamen [12]. In Sect. 3.2, we give limit law of Kaplan-Meier's nonparametric estimator in competing risks as defined in Njamen and Ngatchou [10] and Njamen [13]. In Section 4, we give the trust Bands, including the Hall-Wellner trust Bands and the Nair precision equal bands.

2. Preliminary and Rappels

For $t \geq 0$, we introduce the following subdistribution functions $H^{(0)}$ and $H^{(1)}$ of H by:

$$H^{(0)}(t) = \mathbb{P}[Z \leq t, \xi = 0],$$

and

$$H^{(1)}(t) = \mathbb{P}[Z \leq t, \xi \neq 0]$$

and for $j = 1, \cdots, m$

$$H^{(1,j)}(t) = \mathbb{P}[Z \leq t, \xi = j].$$

The relations $F(t) = \sum_{j=1}^{m} F^{(j)}(t)$ and $H^{(1)}(t) = \sum_{j=1}^{m} H^{(1,j)}(t)$ hold for $t \geq 0$ since the different risks are mutually exclusive. The relation $H(t) = H^{(0)}(t) + H^{(1)}(t)$ is also valid for $t \geq 0$. The relations that connect the observable distribution functions $H^{(0)}$, $H^{(1)}$ and $H^{(1,j)}$ to the unobservable distributions F, G and $F^{(j)}$ are given by:

$$H^{(0)}(t) = \int_0^t (1-F)\,\mathrm{d}G,$$

$$H^{(1)}(t) = \int_0^t (1-G^-)\,\mathrm{d}F,$$

and

$$H^{(1,j)}(t) = \int_0^t (1-G^-)\,\mathrm{d}F^{(j)}.$$

The cumulative hazard function of T and the partial cumulative hazard function of T related to cause j for $j \in \{1, \cdots, m\}$ are given for $t \geq 0$ respectively by the following expressions:

$$\Lambda(t) = \int_0^t \frac{\mathrm{d}F}{1-F^-} = \int_0^t \frac{\mathrm{d}H^{(1)}}{1-H^-}, \tag{2}$$

$$\Lambda^{(1,j)}(t) = \int_0^t \frac{\mathrm{d}F^{(j)}}{1-F^-} = \int_0^t \frac{\mathrm{d}H^{(1,j)}}{1-H^-}. \tag{3}$$

Let us set estimators for the different quantities. Let $(Z_i, \xi_i)_{i=1,\cdots,n}$ be n independent copies of the random vector (Z, ξ). We define the empirical counterparts of $H^{(0)}$, $H^{(1)}$, $H^{(1,j)}$ and H, for $j \in 1, \cdots, m$ by:

$$H_n^{(0)}(t) = \frac{1}{n}\sum_{i=1}^{n} \mathbb{1}_{\{Z_i \leq t, \xi_i = 0\}},$$

$$H_n^{(1)}(t)=\frac{1}{n}\sum_{i=1}^{n}\mathbb{1}_{\{Z_i\le t,\xi_i\neq 0\}},$$

$$H_n^{(1,j)}(t)=\frac{1}{n}\sum_{i=1}^{n}\mathbb{1}_{\{Z_i\le t,\xi_i=j\}},$$

$$H_n(t)=\frac{1}{n}\sum_{i=1}^{n}\mathbb{1}_{\{Z_i\le t\}}.$$

The relations $H_n(t)=H_n^{(0)}(t)+H_n^{(1)}(t)$ and $H_n^{(1)}(t)=\sum_{j=1}^{m}H_n^{(1,j)}(t)$ are valid for $t\ge 0$. As T is independently randomly right-censored by C, a well-known estimator for F is the Kaplan-Meier estimator defined for $t\ge 0$ by:

$$\hat{F}_n(t)=1-\prod_{i=1}^{n}\left(1-\frac{\mathbb{1}_{\{Z_i\le t,\xi_i\neq 0\}}}{n\left(1-H_n^{-}(Z_i)\right)}\right),$$

where the left-continuous modification of any d.f. L is denoted by L^{-}. The Nelson-Aalen estimators of Λ and of $\Lambda^{(1,j)}$ for $j=1,\cdots,m$ respectively are defined for $t\ge 0$ by:

$$\Lambda_n(t)=\int_0^t\frac{\mathrm{d}H_n^{(1)}}{1-H_n^{-}},\tag{4}$$

$$\Lambda_n^{(1,j)}(t)=\int_0^t\frac{\mathrm{d}H_n^{(1,j)}}{1-H_n^{-}}.\tag{5}$$

The Aalen-Johansen estimator for $F^{(j)}$ is defined for $t\ge 0$ by:

$$\hat{F}_n^{(j)}(t)=\int_0^t\frac{1-\hat{F}_n^{-}}{1-H_n^{-}}\mathrm{d}H_n^{(1,j)}.$$

For all $t\ge 0$, the following equalities hold:

$$1-H_n(t)=\left(1-\hat{F}_n(t)\right)\left(1-\hat{G}_n(t)\right)$$

$$\Lambda_n(t)=\int_0^t\frac{\mathrm{d}\hat{F}_n}{1-\hat{F}_n^{-}},$$

where $\hat{G}_n$, the Kaplan-Meier estimator of G, is defined for $t\ge 0$ by:

$$\hat{G}_n(t)=1-\prod_{i=1}^{n}\left(1-\frac{\mathbb{1}_{\{T_i\le t,\xi_i=0\}}}{n\left(1-H_n^{-}(Z_i)\right)}\right).$$

3. Results

In this section, we continue the works of Njamen and Ngatchou [10], Njamen [12] and Njamen and Ngatchou [11]. In fact, Njamen and Ngatchou ([10], p. 9), studies the consistency of Nelson-Aalen's non-parametric estimator in competing risks, while Njamen ([12], pp. 11-12) studies respectively the simple convergence and the uniform convergence in probability of Nelson-Aalen's nonparametric estimator in competing risks; and Njamen and Ngatchou ([11], p. 13) study the bias and the uniform convergence of the non-parametric estimator survival function in a context of competing risks. It is also shown there that this

estimator is asymptotically unbiased. For this purpose, we use the martingale approach as the authors mentioned above.

3.1. Limit Law of Nelson-Aalen's Nonparametric Estimator for Competing Risks

In what follows, we study the asymptotic normality of Nelson-Aalen's non-parametric estimator in competitive risks. For that, considering, for all $j \in \{1,\cdots,m\}$ and $t \geq 0$, one has the Nelson-Aalen type cumulative hazard function estimator (Nelson, [19]; Aalen, [20], Njamen and Ngatchou, [10]) defined by

$$\hat{\Lambda}_n(t) = \int_0^t \frac{J(u)}{Y(u)} \mathrm{d}N(u), \tag{6}$$

where $J(t) = \mathbb{1}_{\{Y(t)>0\}}$.

The cumulative risk in a region where there is at least one observation is given for all $j \in \{1,\cdots,m\}$, by (see Njamen, [12]. p. 9)

$$\Lambda^{*(j)} = \int_0^t L^{*(j)} \lambda^{*(j)}(s) \mathrm{d}s, \tag{7}$$

with $L_i^{*(j)}(t) = \mathbb{1}_{\{Z_i \geq t\}}$ which indicates whether the individual i is still at risk just before time t (the individual has not yet undergone the event). Its estimator was defined in Njamen and Ngatchou ([10], p. 7).

The following theorem gives the limit law of the Neslson-Aalen estimator $\hat{\Lambda}_n^{*(j)}$ in competing risks of Njamen (2017, p. 9). This is the first fundamental result of this article.

Theorem 1.

In a region where there is at least one observation, it is assumed that $F_i^{*(j)}(t) < 1$ for $i \in \{1,\cdots,n\}$ and $j \in \{1,\cdots,m\}$. Then, for all $t \geq 0$,

$$\sqrt{n}\left(\hat{\Lambda}_n^{*(j)}(t) - \Lambda^{*(j)}(t)\right) \xrightarrow{\mathcal{L}} U_i^{*(j)}(t), \tag{8}$$

where $U_i^{*(j)}$ is a centered Gaussian martingale of variance such that:

$$\begin{cases} U_i^{*(j)}(0) = 0 \\ \mathbb{V}\left(U_i^{*(j)}(t)\right) = \int_0^t \dfrac{\alpha_i^{*(j)}(u)}{y_i^{*(j)}(u)} \mathrm{d}u, \end{cases} \tag{9}$$

where for all $s \geq 0$,

$$y_i^{*(j)}(s) = \left[1 - F_i^{*(j)}(s)\right]\left[1 - G_i^{*(j)}(s^-)\right] \tag{10}$$

with $G_i^{*(j)}$ standing for the distribution function of $C_i^{*(j)}$ and $\alpha_i^{*(j)}$ the instant risk function.

To prove this theorem, we need the Robelledo theorem. In fact, the Rebolledo theorem below makes it possible to apply the central limit theorem for certain types of particular martingales.

Theorem 2. (Rebolledo's Theorem)

Let $M^n = \sum_{i=1}^n M_i$ a sequence of martingales where $M_i = K_i - A_i$, K_i

denotes a counting process and A_i its compensator. Consider the processes $I_n(t)=\int_0^t f_n(s)\mathrm{d}M^n(s)$, and for all $\varepsilon>0$, $I_{n,\varepsilon}(t)=\int_0^t f_n(s)\mathbb{1}_{\{|f_n(s)|>\varepsilon\}}\mathrm{d}M^n(s)$. Suppose that f_n and f are predictable and locally bounded $\mathcal{F}_{s^-}$ processes such that

$$\sup_s\left|f_n-f(s)\right|\to 0\quad (n\to\infty).$$

Suppose also that the processes K_i, A_i, f_n are bounded. Let's for all $t>0$, $\alpha(t)=\int_0^t f^2(s)\mathrm{d}s$. If

1) $\langle I_n\rangle_t\xrightarrow{\mathbb{P}}\alpha(t),(n\to\infty)$;

2) for all $\varepsilon>0$, $\langle I_{n,\varepsilon}\rangle_t\xrightarrow{\mathbb{P}}0,(n\to\infty)$.

Then,

$$\left(I_n(t),t>0\right)\Rightarrow\left(\int_0^t f(s)\mathrm{d}W(s),t>0\right),\quad (n\to\infty),$$

where $\Rightarrow$ denotes the weak convergence in the space of continuous functions on the right, having a left-hand boundary with the topology of Skorokhod and where W is a Brownian motion.

To prove Theorem 1, it is sufficient to check whether the previous conditions of Rebolledo's Theorem are satisfied:

Proof. For all $j\in\{1,\cdots,m\}$ and $t\geq 0$, $M_i^{*(j)}(t)$ also decomposes into

$$M_i^{*(j)}(t)=K_i^{*(j)}(t)-\int_0^t\mathrm{d}\Lambda_i^{*(j)}(s)\mathrm{d}s,$$

which in turn can be written in terms of $\alpha_j(t)$ by

$$M_i^{*(j)}(t)=K_i^{*(j)}(t)-\int_0^t\alpha_i^{*(j)}(s)L_i^{*(j)}(s)\mathrm{d}s,$$

which finally, can be rewritten as

$$\mathrm{d}K_i^{*(j)}(t)=\alpha_i^{*(j)}(t)L_i^{*(j)}(t)\mathrm{d}t+\mathrm{d}M_i^{*(j)}(t),$$

where $\mathrm{d}M_i^{*(j)}(t)$ can be seen as a random noise process. The martingale $M_i^{*(j)}(t)$ above represents the difference between the number of failures due to a specific cause *j* observed in the time interval $[0,t]$, *i.e.* $K_i^{*(j)}(t)$ (see Njamen, [12], p.6), and the number of failures predicted by the model for the j^{th} cause. This definition fulfills the Doob-Meyer decomposition.

This martingale is used in Fleming and Harrington ([21], p. 26) and in Breuils ([22], p. 25).

Now, to explain the asymptotic nature of the results, we defined, for all $t\geq 0$, $j\in\{1,\cdots,m\}$, to pose:

$$N^{(n)}(t)=\sum_{i=1}^n K_i^{*(j)}(t),\ Y^{(n)}(t)=\sum_{i=1}^n L_i^{*(j)}(t),\ J^{(n)}=\mathbb{1}_{\left\{Y^{(n)}(t)>0\right\}},$$

In a subgroup $A^{(j)}$, where there is at least one observation, the survival function of $Z_i=\min(T_i,C_i)$ is defined for all $t\geq 0$ by:

$$S_Z^{*(j)}(t)=\left(1-F_i^{*(j)}(t)\right)\left(1-G_i^{*(j)}(t^-)\right).$$

Recall also that $F_i^{*(j)}$ is the distribution function of T_i, $G_i^{*(j)}$ is that of C_i's and $\left[1-\left(1-F_i^{*(j)}\right)\right]\left[1-G_i^{*(j)}\right]$ that of the Z_i's. From the Glivenko-Cantelli theorem, one has:

$$\sup_{s\in[0,t]}\left|\frac{Y^{(n)}(s)}{n}-\left[1-F_i^{*(j)}(s)\right]\left[1-G_i^{*(j)}\left(s^-\right)\right]\right|\xrightarrow{\mathbb{P}}0\quad(n\to\infty).\tag{11}$$

Otherwise,

$$J^{(n)}(t)=\mathbb{1}_{\left\{Y^{(n)}(t)>0\right\}},$$

one has:

$$1-J^{(n)}(t)=\mathbb{1}_{\left\{Y^{(n)}(t)=0\right\}}=\mathbb{1}_{\left\{B\left(n,\left[1-F_i^{*(j)}(t)\right]\left[1-G_i^{*(j)}\left(t^-\right)\right]\right)=0\right\}}\xrightarrow{\mathbb{P}}0\,(n\to\infty),$$

from which one obtains (see Theorem 3, p. 11 of Njamen, [12]),

$$J^{(n)}(t)\xrightarrow{\mathbb{P}}1\quad(n\to\infty).$$

Differentiating the martingale $M_i^{*(j)}(t)=K_i^{*(j)}-\int_0^t L_i^{*(j)}(s)\alpha_i^{*(j)}(s)\mathrm{d}s$, one has:

$$\mathrm{d}M_i^{*(j)}(t)=\mathrm{d}K_i^{*(j)}(t)-L_i^{*(j)}(t)\alpha_i^{*(j)}(t)\mathrm{d}t,$$

and from

$$\mathrm{d}\left\langle M_i^{*(j)}\right\rangle_t=\mathbb{V}ar\left(\mathrm{d}M_i^{*(j)}(t)\middle/\mathcal{F}_{t^-}\right),$$

one obtains

$$\begin{aligned}\mathrm{d}\left\langle M_i^{*(j)}\right\rangle_t&=\mathbb{V}ar\left(\mathrm{d}K_i^{*(j)}(t)-L_i^{*(j)}(t)\alpha_i^{*(j)}(t)\mathrm{d}t\middle/\mathcal{F}_{t^-}\right)\\&=\mathbb{V}ar\left(\mathrm{d}K_i^{*(j)}(t)\middle/\mathcal{F}_{t^-}\right)=L_i^{*(j)}(t)\alpha_i^{*(j)}(t)\mathrm{d}t.\end{aligned}$$

Consequently, the increasing process of

$$D_t=\int_0^t\frac{J^{(n)}(u)}{Y^{(n)}(u)}\mathrm{d}M_i^{*(j)}(u),\ t\geq 0,$$

is given by

$$\left\langle D\right\rangle_t=\int_0^t\frac{\left(J^{(n)}\right)^2(u)}{\left(Y^{(n)}\right)^2(u)}\mathrm{d}\left\langle M\right\rangle_u,\ t\geq 0.$$

Next, for all $t\geq 0$ and $j=\{1,\cdots,m\}$, one has

$$\begin{aligned}\left\langle\sqrt{n}\sum_{i=1}^n\int_0^t\frac{J^{(n)}(u)}{Y^{(n)}(u)}\mathrm{d}M_i^{*(j)}(u)\right\rangle_t&=\sum_{i=1}^n n\int_0^t\frac{\left(J^{(n)}\right)^2(u)}{\left(Y^{(n)}\right)^2(u)}L_i^{*(j)}(u)\alpha_i^{*(j)}(u)\mathrm{d}u\\&=\int_0^t n\frac{\left(J^{(n)}\right)^2(u)}{\left(Y^{(n)}\right)^2(u)}\sum_{i=1}^n L_i^{*(j)}(u)\alpha_i^{*(j)}(u)\mathrm{d}u\\&=\int_0^t n\frac{\left(J^{(n)}\right)^2(u)}{\left(Y^{(n)}\right)^2(u)}Y^{(n)}(u)\alpha_i^{*(j)}(u)\mathrm{d}u\\&=\int_0^t n\frac{J^{(n)}(u)}{Y^{(n)}(u)}\alpha_i^{*(j)}(u)\mathrm{d}u.\end{aligned}$$

Also, for all $t \geq 0$ and for all $j \in \{1, \cdots, m\}$, the process

$$\sqrt{n}\left(\hat{\Lambda}_n^{*(j)}(t) - \Lambda^{*(j)}(t)\right) = \sqrt{n}\sum_{i=1}^{n}\int_0^t \frac{J^{(n)}(u)}{Y^{(n)}(u)} \mathrm{d}M_i^{*(j)}(u) = R_n(t), \quad \forall i \in \{1, \cdots, n\},$$

is a martingale. We apply the central limit theorem for the martingales (Rebolledo's Theorem). In this purpose, we show that the condition of this theorem is satisfied by $R_n(t)$.

One has, for all $i \in \{1, \cdots, n\}$,

$$\langle R_n \rangle_t = \int_0^t n \frac{J^{(n)}(u)}{Y^{(n)}(u)} \alpha_i^{*(j)}(u) \mathrm{d}u, \quad \forall j \in \{1, \cdots, m\},$$

and also by the proof of the Theorem 3 of Njamen ([12], p. 11), we have:

$$\frac{Y^{(n)}(u)}{n} \xrightarrow{\mathbb{P}} \left(1 - F_i^{*(j)}(u)\right)\left(1 - G_i^{*(j)}(u^-)\right), \quad J^{(n)}(u) \xrightarrow{\mathbb{P}} 1, \quad (n \to \infty).$$

So that, for all $j \in \{1, \cdots, m\}$, when $n \to \infty$,

$$\begin{aligned}\langle R_n \rangle_t &= \int_0^t \frac{\frac{J^{(n)}(u)}{Y^{(n)}(u)}}{n} \alpha_i^{*(j)}(u) \mathrm{d}u \\ &\xrightarrow{\mathbb{P}} \int_0^t \frac{\alpha_i^{*(j)}(u) \mathrm{d}u}{\left(1 - F_i^{*(j)}(u)\right)\left(1 - G_i^{*(j)}(u^-)\right)} = \beta(t), \quad (n \to \infty),\end{aligned}$$

which is determinist. Thus, the first condition of Robelledo Theorem holds.

To check the second condition, for all $\epsilon > 0$ and $t \geq 0$, define

$$R_{n,\varepsilon}(t) = \int_0^t \sqrt{n} \frac{J^{(n)}(u)}{Y^{(n)}(u)} \mathbb{1}_{\left\{\left|\sqrt{n}\frac{J^{(n)}(u)}{Y^{(n)}(u)}\right| > \epsilon\right\}} \mathrm{d}M^{(n)}(u),$$

where for all $j = 1, \cdots, m$, $M^{(n)}(u) = \sum_{i=1}^{n} M_i^{*(j)}(u)$.

We have to show that as $n \to \infty$, $\langle Z_{n,\epsilon} \rangle_t$ converges to 0 in probability.

One has, for all $t \geq 0$,

$$\begin{aligned}\langle R_{n,\varepsilon} \rangle_t &= \int_0^t n \frac{J^{(n)}(u)}{\left(Y^{(n)}(u)\right)^2} \mathbb{1}_{\left\{\left|\sqrt{n}\frac{J^{(n)}(u)}{Y^{(n)}(u)}\right| > \epsilon\right\}} \mathrm{d}\langle M^{(n)} \rangle_u \\ &= \int_0^t n \frac{J^{(n)}(u)}{\left(Y^{(n)}(u)\right)^2} \mathbb{1}_{\left\{\left|\sqrt{n}\frac{J^{(n)}(u)}{Y^{(n)}(u)}\right| > \epsilon\right\}} Y^{(n)}(u) \alpha_i^{*(j)}(u) \mathrm{d}u \\ &= \int_0^t n \frac{J^{(n)}(u)}{Y^{(n)}(u)} \mathbb{1}_{\left\{\left|\sqrt{n}\frac{J^{(n)}(u)}{Y^{(n)}(u)}\right| > \epsilon\right\}} \alpha_i^{*(j)}(u) \mathrm{d}u \\ &\xrightarrow{\mathbb{P}} 0, \ (n \to \infty),\end{aligned}$$

because

$$n \frac{J^{(n)}(u)}{Y^{(n)}(u)} \xrightarrow{\mathbb{P}} \frac{1}{\left(1 - F_i^{*(j)}(u)\right)\left(1 - G_i^{*(j)}(u^-)\right)}, \quad (n \to \infty).$$

Then

$$\sqrt{n}\frac{J^{(n)}(u)}{Y^{(n)}(u)}=\frac{1}{\sqrt{n}}n\frac{J^{(n)}(u)}{Y^{(n)}(u)}\xrightarrow{\mathbb{P}}0,\quad (n\to\infty).$$

Thus, the second condition of Robelledo Theorem holds.

The conditions of the Rebolledo Theorem are verified and by consequently, for all $t\geq 0$,

$$\left(R_n(t),t>0\right)\Rightarrow\left(\int_0^t f(s)\mathrm{d}W(s),t>0\right),\ (n\to\infty),$$

with $\gamma(t)=\int_0^t f^2(s)\mathrm{d}s$.

Finally, for all $t>0$,

$$R_n(t)\Rightarrow R(t)=\int_0^t f(s)\mathrm{d}W(s)\hookrightarrow\mathcal{N}\left(0,\gamma(t)\right),\quad (n\to\infty).$$

This ends the proof of the Theorem 1.

The following subsection gives the asymptotic law of nonparametric Kaplan-Meier's estimator of the survival function in the competing risks of Njamen and Ngatchou ([10], p. 13).

3.2. Limit Law of Kaplan-Meier's Nonparametric Estimator in Competing Risks

The Kaplan-Meier estimator of the survival function (Kaplan and Meier, [23]) is defined by

$$\hat{S}_n(t)=\prod_{s\leq t}\left(1-\Delta\hat{\Lambda}_n(s)\right)=\prod_{s\leq t}\left(1-\frac{J^{(n)}(s)\Delta N^{(n)}(s)}{Y^{(n)}(s)}\right),$$

where $\hat{\Lambda}_n(t)$ is the Nelson-Aalen estimator and where, for a process $X(t)$ continuous to the right with a left limit such that

$$\Delta X(t)=X(t)-X(t^-).$$

For all $j=1,\cdots,m$, an estimator of the variance of $\hat{S}_n^{(j)}(t)/S^{*(j)}(t)$, where $S^{*(j)}$ is the survival function associated with the subgroup $A^{(j)}$ is given by

$$\hat{\sigma}^{(j)2}(t)=\int_0^t\frac{J^{(n)}(s)}{\left(Y^{(n)}\right)^2(s)}\mathrm{d}N^{(n)}(s).$$

The variance of $\hat{S}_n^{(j)}(t)/S^{(j)}(t)$ approximated by that of $\hat{S}^{(j)}(t)/S^{*(j)}(t)$ is:

$$\begin{aligned}\mathbb{V}\left[\frac{\hat{S}_n^{(j)}(t)}{S^{*(j)}(t)}-1\right]&=\mathbb{E}\left[\left\langle\frac{\hat{S}_n^{(j)}}{S^{*(j)}}-1\right\rangle(t)\right]\\&=\int_0^t\left\{\frac{\hat{S}_n^{(j)}(s^-)}{S^{*(j)}(s)}\right\}^2\times\frac{J^{(n)}(s)}{Y^{(n)}(s)}\alpha_i^{*(j)}(s)\mathrm{d}s\quad\forall i\in\{1,\cdots,n\}.\end{aligned}\tag{12}$$

The estimator of the corresponding variance of $\hat{S}_n^{(j)}(t)$ is given by

$$\hat{\mathbb{V}}\left(\hat{S}_n^{(j)}(t)\right)=\left[\hat{S}_n^{(j)}(t)\right]^2\hat{\sigma}_i^{(j)2}(t)\quad\forall i\in\{1,\cdots,n\}.\tag{13}$$

The following result concerning the asymptotic law of nonparametric Kaplan-Meier estimator and constituted the second fundamental result of this paper:

Theorem 3.

In an area where there is at least one observation, if we assume that for all $j \in \{1,\cdots,m\}$ and $i \in \{1,\cdots,n\}$,

1) for all $s \in [0,t]$,

$$n\int_0^s \frac{J^{(n)}(u)}{Y^{(n)}(u)} \alpha_i^{*(j)}(u)\mathrm{d}u \xrightarrow{\mathbb{P}} \sigma_i^{*(j)2}(u) \quad (n\to\infty),$$

2) for all $\varepsilon > 0$,

$$n\int_0^t \frac{J^{(n)}(u)}{Y^{(n)}(u)} \alpha_i^{*(j)} 1\!\!1_{\left\{\sqrt{n}\left|\frac{J^{(n)}(u)}{Y^{(n)}(u)}\right|>\varepsilon\right\}} \mathrm{d}u \xrightarrow{\mathbb{P}} 0 \quad (n\to\infty),$$

3) for all $t > 0$,

$$\sqrt{n}\int_0^t \left(1 - J^{(n)}(u)\right)\alpha_i^{*(j)}(u)\mathrm{d}u \xrightarrow{\mathbb{P}} 0 \quad (n\to\infty).$$

Then, for all $t > 0$ and $j \in \{1,\cdots,m\}$, the non-parametric estimator $\hat{S}_n^{*(j)}$ checks

$$\sqrt{n}\left(\hat{S}_n^{*(j)}(t) - S^{*(j)}(t)\right) \Rightarrow -U_i^{*(j)}(t) \times S^{*(j)}(t), \quad (n\to\infty),$$

where $U_i^{*(j)}$ is the center Gaussian martingale and where $\Rightarrow$ denotes the weak convergence in the space of continuous functions on the right, having a left-hand boundary with the topology of Skorokhod.

Proof. To prove this theorem, it suffices to show that it satisfies the conditions of the Rebolledo Theorem.

In an area where there is at least one observation, by posing, for all $j = 1,\cdots,m$, $i = 1,\cdots,n$,

$$\tilde{S}_n^{*(j)}(t) = \exp\left(-\tilde{\Lambda}_n^{*(j)}\right)$$

where $\tilde{\Lambda}_n^{*(j)} = \int_0^t J^{(n)}(u)\alpha_i^{*(j)}(u)\mathrm{d}u$.

For $t \in [0,\tau[$ and $\tau > 0$, we have for all $j = 1,\cdots,m$ and $i = 1,\cdots,n$,

$$\sqrt{n}\left\langle\left(\frac{\hat{S}_n^{(j)}}{\tilde{S}_n^{*(j)}} - 1\right)\right\rangle_t = n\int_0^t \frac{\hat{S}_n^{(j)}(u^-)^2}{\tilde{S}_n^{*(j)}(u)^2}\frac{J^{(n)}(u)}{Y^{(n)}(u)}\alpha_i^{*(j)}(u)\mathrm{d}u$$
$$\xrightarrow{\mathbb{P}} \sigma_i^{*(j)2}, \quad (n\to\infty).$$

By the proof of Theorem 3 of Njamen ([12], p.11), we deduce that

$$\frac{\hat{S}_n^{*(j)}(u^-)}{\tilde{S}_n^{*(j)}(u)} \xrightarrow{\mathbb{P}} 1, \quad (n\to\infty).$$

Hence the 1st condition of Robolledo's Theorem.

For the second condition of Robolledo's Theorem, condition B is similar to

the proof of Theorem 1 above, we find that for all $\varepsilon > 0$,

$$n\int_0^t \frac{\hat{S}_n^{(j)}\left(u^-\right)^2}{\tilde{S}_n^{*(j)}(u)^2}\frac{J^{(n)}(u)}{Y^{(n)}(u)}\mathbb{1}_{\left\{\sqrt{n}\left|\frac{J^{(n)}(s)}{Y^{(n)}(s)}\right|>\varepsilon\right\}}\alpha_i^{*(j)}(u)\mathrm{d}u \to 0, \quad (n\to\infty).$$

So, for each $t > 0$,

$$\sqrt{n}\int_0^t \frac{\hat{S}_n^{(j)}\left(u^-\right)}{\tilde{S}_n^{*(j)}(u)}\frac{J^{(n)}(u)}{Y^{(n)}(u)}\mathrm{d}M^{(n)}(u) \Rightarrow U_i^{*(j)}(t),$$

where $M^{(n)}(u) = \sum_{i=1}^n M_i^{*(j)}(u)$ and where

$$U^{*(j)}(t) \hookrightarrow \mathcal{N}\left(0, \sigma_i^{*(j)2}(t)\right).$$

Finally,

$$\sqrt{n}\left(\frac{\hat{S}_n^{(j)}(t)}{\tilde{S}_n^{*(j)}(t)} - 1\right) \Rightarrow -U_i^{*(j)}(t).$$

The fact that $S^{*(j)}(u) \le S_n^{*(j)}(u)$, for all $u \in [0, s[$ and condition C implies:

$$\begin{aligned}\sqrt{n}\left|\frac{S^{*(j)}(s)}{\tilde{S}_n^{*(j)}(u)} - 1\right| &\le \sqrt{n}\int_0^t \frac{S^{*(j)}(u)}{\tilde{S}_n^{*(j)}(u)}\mathrm{d}\left(\Lambda^{*(j)} - \tilde{\Lambda}^{*(j)}\right)(u)\\ &\le \sqrt{n}\int_0^t \left(1 - J(u)\right)\alpha_i^{*(j)}(u)\mathrm{d}u\\ &\xrightarrow{\mathbb{P}} 0 \quad (n\to\infty).\end{aligned}$$

As $\tilde{S}_n^{*(j)}(t) \to S^{*(j)}(t)$ when $n\to\infty$, we deduce that:

$$\sqrt{n}\left(\tilde{S}_n^{*(j)} - S^{*(j)}(t)\right) \xrightarrow{\mathbb{P}} 0, \quad n\to\infty.$$

It follows that:

$$\begin{aligned}&\sqrt{n}\left(\hat{S}_n^{*(j)}(t) - S^{*(j)}(t)\right)\\ &= \sqrt{n}\left(\hat{S}_n^{*(j)}(t) - \tilde{S}_n^{*(j)}(t)\right) + \sqrt{n}\left(\tilde{S}_n^{*(j)}(t) - S^{*(j)}\right)\\ &= \frac{\sqrt{n}\left(\hat{S}_n^{*(j)}(t) - \tilde{S}_n^{*(j)}(t)\right)}{\tilde{S}_n^{*(j)}}\tilde{S}_n^{*(j)} + \sqrt{n}\left(\tilde{S}_n^{*(j)}(t) - S^{*(j)}\right)\\ &\Rightarrow -U_i^{*(j)}(t)S^{*(j)}, \quad (n\to\infty).\end{aligned}$$

This ends the proof of the theorem.

4. Confidence Bands of Survival Function

4.1. Confidence Intervals

For $\alpha \in (0,1)$, we wish to find two random functions b_L and b_U such that $\forall t > 0$,

$$\mathbb{P}\left[b_U(t) \ge S(t) \ge b_L(t)\right] = 1 - \alpha.$$

Recall that from the previous sections, for all $j \in \{1, \cdots, m\}$, $\sqrt{n}\left(\hat{S}_n^{*(j)}(t) - S^{*(j)}(t)\right)\Big/S^{*(j)}(t)$ converges in distribution to a Gaussian

martingale centered (see Theorem 3 above). As a consequence, $\hat{S}_n^{*(j)}(t)$ is asymptotically Gaussian centered on $S^{*(j)}$. Given the above results, the estimated standard deviation of $S^{*(j)}$, noted $\hat{\sigma}_{S_t}$ is given for all $t \geq 0$ by:

$$\hat{\sigma}_{S_t^*}^{*2}(t) = \frac{\hat{\mathbb{V}}\left(\hat{S}_n^{*(j)}(t)\right)}{\left[\hat{S}_n^{*(j)}(t)\right]^2}. \tag{14}$$

Therefore a threshold confidence level $100(1-\alpha)\%$ can be built for all $t \geq 0$ and $j \in \{1,\cdots,m\}$, by:

$$\hat{S}_n^{*(j)}(t) - Z_{1-\alpha/2}\hat{\sigma}_{S_t^*}^{*(j)}(t)\hat{S}_n^{*(j)}(t),\ \hat{S}_n^{*(j)}(t) + Z_{1-\alpha/2}\hat{\sigma}_{S_t^*}^{*(j)}(t)\hat{S}_n^{*(j)}(t). \tag{15}$$

Here $z_{1-\alpha/2}$ is the $1-\alpha/2$ percentile of a standard normal distribution.

A threshold confidence interval $100(1-\alpha)\%$ can also be obtained for all $j \in \{1,\cdots,m\}$, by:

$$\hat{S}_n^{*(j)}(t) \pm z_{\alpha/2}\hat{\sigma}_{S_t^*}^{*(j)}, \tag{16}$$

where $z_{\alpha/2}$ is the rank of fractile $100\times\alpha/2$ of the standardized normal distribution.

A disadvantage of the construction of the confidence interval (CI) with the previous formula is that the bound can be obtained external to the interval $[0,1]$. A solution is to consider a $S^{*(j)}(t)$ $\left(j \in \{1,\cdots,m\}\right)$ transform via a continuous function *g*, differentiable and invertible such that $g\left(S^{*(j)}(t)\right)$ belongs to a more wide space ideally unbounded and best approximate a Gaussian random variable. The delta method then allows for the estimation of the standard deviation of the object created by $\hat{\sigma}_{g\left(S_t^*\right)}^{*(j)}$ defined by $\hat{\sigma}_{g\left(S_t^*\right)}^{*(j)}(t) = g'\left(\hat{S}_n^{*(j)}\right)\hat{\sigma}_{S_t^*}^{*(j)}(t)$. The confidence interval associated with the risk threshold α is built as for all $j \in \{1,\cdots,m\}$,

$$g^{-1}\left(g\left(\hat{S}_n^{*(j)}\right) \pm z_{\alpha/2}g'\left(\hat{S}_n^{*(j)}\right)\hat{\sigma}_{S_t^*}^{*(j)}(t)\right).$$

The most common transformation is $g\left(S_t^*\right) = \log\left[\log\left(S_t^*\right)\right]$, and in this case we have: for all $j \in \{1,\cdots,m\}$,

$$\hat{\sigma}_{\log\left[-\log\left(S_t^*\right)\right]}^{*(j)} = \frac{\hat{\sigma}_{S_t^*}^{*(j)}}{\hat{S}_n^{*(j)}\log\hat{S}_n^{*(j)}} \quad \text{and} \quad \hat{S}_n^{*(j)\exp\left(\pm z_{\alpha/2}\frac{\hat{\sigma}_{S_t^*}^{*(j)}}{\hat{S}_n^{*(j)}\log\left(\hat{S}_t^{*(j)}\right)}\right)}.$$

Remark 1. *It is also possible to use log, square-root or logit-type transformations in most software defined respectively by for all* $j \in \{1,\cdots,m\}$,

$$g\left(S_t^{*(j)}\right) = \log\left[S_t^{*(j)}\right],\quad g\left(S_t^{*(j)}\right) = \sin^{-1}\left[\sqrt{S_t^{*(j)}}\right],\quad g\left(S_t^{*(j)}\right) = \log\left[\frac{S_t^{*(j)}}{1-S_t^{*(j)}}\right].$$

4.2. The Confidence Bands

The challenge now is to find an area containing the survival function with

probability $1-\alpha$, or a set of bounds $b_L(t)$ and $b_U(t)$ which, with probability $1-\alpha$, contains $S^{*(j)}(t)$ for all $t \in [t_L, t_U]$ and $j \in \{1,\cdots,m\}$. Among the proposed solutions, the two most commonly used are firstly Hall and Wellner ([24]) bands and secondly, strips Nair ([25]) ("equal precision bands"). If t_k is the maximum time event observed in the sample, then for the Nair bands, we have the following restrictions $0 < t_L < t_U \le t_k$, however, boter Hall-Wiener may authorize the nullity of t_L, let $0 \le t_L < t_U \le t_k$. Technically obtaining these bands is complex, and their practical utility in relation to the point intervals is not obvious.

Remark 2. *The starting point uses the fact that for all* $j \in \{1,\cdots,m\}$, $\sqrt{n}\left(\frac{\hat{S}_n^{*(j)}(t)}{S^{*(j)}(t)}-1\right)$ *converges to a centered Gaussian martingale. We then go through a transformation making appear a Brownian bridge* $\{W^0(x), x \in [0,1]\}$, *weighted by* $\frac{1}{\sqrt{x(1-x)}}$ *at Nair, to retrieve the suitable critical value.*

In particular, because of the joined character, for a given t their extent is wider than that of the corresponding point IC. In what follows we give the expressions obtained in the absence of transformation.

4.2.1. The Hall-Wellner Confidence Bands

Under the assumption of continuity of survival functions $S^{*(j)}(t)$ and $C^{*(j)}(t)$ respectively related to the event time and the time of censorship, Hall and Wellner show that for every $t \in [t_L, t_U]$, the IC joined the risk threshold α is given for all $j = 1,\cdots,m$ and $t \ge 0$ by:

$$\hat{S}_n^{*(j)}(t) \pm h_\alpha(x_L, x_U) n^{\frac{-1}{2}} \left[1 + n\hat{\sigma}_{S_t^*}^{*(j)2}(t)\right] \hat{S}_n^{*(j)}(t), \tag{17}$$

where x_L and x_U are given by

$$x_i = \frac{n\hat{\sigma}_{S_{t_i}^*}^{*(j)2}(t)}{\left(1 + n\hat{\sigma}_{S_{t_i}^*}^{*(j)2}(t)\right)}, \text{ for } i = L,U$$

and $h_\alpha(x_L, x_U)$ is bounds checking

$$\alpha = \mathbb{P}\left[\sup_{x_L \le x \le x_U} \left|W^0(x)\right| > h_\alpha(x_L, x_U)\right].$$

4.2.2. The Nair Precision Equal Bands

Using a weighted Brownian bridge will notably modify the bounds to IC. For $\alpha \in (0,1)$, $t \in [t_L, t_U]$ and all $j \in \{1,\cdots,m\}$, they are then given by:

$$\hat{S}_n^{*(j)}(t) \pm e_\alpha(x_L, x_U) \hat{\sigma}_{S_t^*}^{*(j)}, \tag{18}$$

where $e_\alpha(x_L, x_U)$ satisfies

$$\alpha = \mathbb{P}\left[\sup_{x_L \le x \le x_U} \frac{\left|W^0(x)\right|}{\sqrt{x(1-x)}} > e_\alpha(x_L, x_U)\right].$$

If we compare (12) and (14), we see that the bounds relating to Nair ([25]) bands are proportional to the bounds IC and simply correspond to a risk adjustment threshold used in the past.

5. Conclusions and Perspectives

In this paper we have studied the asymptotic normality of Nelson-Aalen and Kaplan-Meier type estimators in the presence of independent right-censorship as defined in Njamen and Ngatchou ([10], [11]) and Njamen [12] using Robelledo's theorem that allows applying the central limit theorem to certain types of particular martingales. From the results obtained, confidence bounds for the hazard and the survival functions are provided.

As a perspective, obtaining actual data would allow us to perform numerical simulations to gauge the robustness of our obtained estimators.

Acknowledgements

We thank the publisher and the referees for their comments which allowed to raise considerably the level of this article.

Conflicts of Interest

The author declares no conflicts of interest regarding the publication of this paper.

References

[1] Heckman, J.J. and Honoré, B.E. (1989) The Identifiability of the Competing Risks Models. *Biometrika*, **77**, 325-330. https://www.jstor.org/stable/2336666 https://doi.org/10.1093/biomet/76.2.325

[2] Commemges, D. (2017) Risques compétitifs et modèles multi-états en épidemiologie. *Revue d'épidémiologie et de santé publique Elsevier Masson*, **77**, 605-611.

[3] Com-Nougué, C., Guérin, S. and Rey, A. (1999) Estimation des risques associés à des événements multiples. *Revue d'épidémiologie et de Santé Publique*, **47**, 75-85.

[4] Fine, J.P. and Gray, R.J. (1999) A Proportional Hazards Model for the Subdistribution of a Competing Risk. *Journal of the American Statistical Association*, **94**, 496-509. https://www.jstor.org/stable/2670170 https://doi.org/10.1080/01621459.1999.10474144

[5] Crowder, M. (2001) Classical Competing Risks. Chapman and Hall, London.

[6] Fermanian, J.D. (2003) Nonparametric Estimation of Competing Risks Models with Covariates. *Journal of Multivariate Analysis*, **85**, 156-191. https://doi.org/10.1016/S0047-259X(02)00069-6

[7] Latouche, M. (2004) Modèles de régression en présence de compétition. Thèse de doctorat, Université de Paris, Paris, 6. https://tel.archives-ouvertes.fr/tel-00129238

[8] Geffray, S. (2009) Strong Approximations for Dependent Competing Risks with Independent Censoring with Statistical Applications. *Test*, **18**, 76-95. https://doi.org/10.1007/s11749-008-0113-y

[9] Belot, A. (2009) Modélisation flexible des données de survie en présence de risques concurrents et apports de la mthode du taux en excès. Thèse de doctorat, Université

de la Méditerranée, Marseille.

[10] Njamen, N.D.A. and Ngatchou, W.J. (2014) Nelson-Aalen and Kaplan-Meier Estimators in Competing Risks. *Applied Mathematics*, **5**, 765-776. https://doi.org/10.4236/am.2014.54073

[11] Njamen, N.D.A. and Ngatchou, W.J. (2018) Consistency of the Kaplan-Meier Estimator of the Survival Function in Competiting Risks. *The Open Statistics and Probability Journal*, **9**, 1-17. https://benthamopen.com/TOSPJ/home https://doi.org/10.2174/1876527001809010001

[12] Njamen, N.D.A. (2017) Convergence of the Nelson-Aalen Estimator in Competing Risks. *International Journal of Statistics and Probability*, **6**, 9-23. https://doi.org/10.5539/ijsp.v6n3p9

[13] Njamen, N.D.A. (2018) Study of the Nonparametric Kaplan-Meier Estimator of the Cumulative Incidence Function in Competiting Risks. *Journal of Advanced Statistics*, **3**, 1-13. https://doi.org/10.22606/jas.2018.31001

[14] Aalen, O.O. and Johansen, S. (1978) An Empirical Transition Matrix for Non-Homogeneous Markov Chains Based on Censored Observations. *Scandinavian Journal of Statistics*, **5**, 141-150. https://www.jstor.org/stable/4615704

[15] Peterson, G.L. (1977) A Simplification of the Protein Assay Method of Lowry *et al*. Which Is More Generally Applicable. *Analytical Biochemistry*, **83**, 346-356. https://doi.org/10.1016/0003-2697(77)90043-4

[16] Andersen, P.K., Borgan, Ø., Gill, R.D. and Keiding, N. (1993) Statistical Models Based on Counting Processes. Springer Series in Statistics, Spring-Verlag, New York.

[17] Shorack, G.R. and Wellner, J.A. (1986) Empirical Processes with Applications to Statistics. John Wiley and Sons, Inc., New York.

[18] Breslow, N. and Crowley, J. (1974) A Large Sample Study of the Life Table and Product-Limit Estimates under Random Censorship. *The Annals of Statistics*, **2**, 437-453. https://www.jstor.org/stable/2958131 https://doi.org/10.1214/aos/1176342705

[19] Nelson, W. (1972) A Short Life Test for Comparing a Sample with Previous Accelerated Test Results. *Technometrics*, **14**, 175-185. https://www.jstor.org/stable/1266929 https://doi.org/10.1080/00401706.1972.10488894

[20] Aalen, O.O. (1978) Nonparametric Inference for a Family of Counting Processes. *The Annals of Statistics*, **6**, 701-726. https://www.jstor.org/stable/2958850 https://doi.org/10.1214/aos/1176344247

[21] Fleming, T.R. and Harrington, D.P. (1990) Counting Processes and Survival Analysis. John Wiley and Sons, Hoboken.

[22] Breuils, C. (2003) Analyse de Durées de Vie: Analyse Séquentielle du Modèle des Risques Proportionnels et Tests d'Homogénéité. Thèse de doctorat, Université de Technologie de Compiégne, Compiègne. https://tel.archives-ouvertes.fr/tel-00005524

[23] Kaplan, E.L. and Meier, P. (1958) Nonparametric Estimation from Incomplete Observations. *Journal of the American Statistical Association*, **53**, 457-481. https://www.jstor.org/stable/2281868 https://doi.org/10.1080/01621459.1958.10501452

[24] Hall, W.J. and Wellner, J.A. (1980) Confidence Bands for a Survival Curve. *Biometrika*, **67**, 133-143. https://www.jstor.org/stable/2335326

https://doi.org/10.1093/biomet/67.1.133

[25] Nair, V.N. (1984) Confidence Bands for Survival Functions with Censored Data: A Comparative Study. *Technometrics*, **26**, 265-275.
https://www.jstor.org/stable/1267553
https://doi.org/10.1080/00401706.1984.10487964

Scientific Research Publishing

Applied Mathematics, 2019, 10, 561-567
http://www.scirp.org/journal/am
ISSN Online: 2152-7393
ISSN Print: 2152-7385

Proof of Ito's Formula for Ito's Process in Nonstandard Analysis

Shuya Kanagawa[1], Kiyoyuki Tchizawa[2]

[1]Department of Mathematics, Tokyo City University Setagaya, Tokyo, Japan
[2]Institute of Administration Engineering, Ltd., Tokyo, Japan
Email: skanagaw@tcu.ac.jp, tchizawa@kthree.co.jp

How to cite this paper: Kanagawa, S. and Tchizawa, K. (2019) Proof of Ito's Formula for Ito's Process in Nonstandard Analysis. *Applied Mathematics*, **10**, 561-567.
https://doi.org/10.4236/am.2019.107039

Received: June 17, 2019
Accepted: July 19, 2019
Published: July 22, 2019

Abstract

In our previous paper [1], we proposed a non-standardization of the concept of convolution in order to construct an extended Wiener measure using non-standard analysis by E. Nelson [2]. In this paper, we consider Ito's integral with respect to the extended Wiener measure and extend Ito's formula for Ito's process. Because of doing the extension of Ito's formula, we could treat stochastic differential equations in the sense of nonstandard analysis. In this framework, we need the nonstandardization of convolution again. It was not yet proved in the last paper, therefore we shall provide the proof.

Keywords

Ito's Process, Stochastic Differential Equation, S-Continuity, Nonstandard Analysis

1. Introduction

As for an analysis of stochastic differential equations driven by extended Wiener process in the sense of nonstandard analysis, we need to extend "Ito's formula" for Wiener process or Ito's process. In the previous paper, we extended a concept of convolution in Fourier series to the case of nonstandard analysis. According to the result, we shall extend some theorems in probability theory, for example, the law of large numbers and the central limit theorem, and shall reconstruct Ito's formula by using nonstandard analysis. We shall give the proof of the reconstruction of Ito's formula in the case that the convolution of probability density which functions in a nonstandard extension is convergent for some functional $F(t, X(t))$ of Ito's process $X(t)$. The problem was not solved still now.

If the convolution is not convergent, what kind of problem does it occur? In

Taylor expansion of $F(t,X)$, the higher terms may not vanish. Then, Ito's formula does not be established. As to what we shall give extended law of large numbers and extended central limit theorem, they will be provided precisely in the next paper.

2. Ito's Integral for Extended Wiener Process in Nonstandard

In our previous paper [1], we showed that Fourier series can be described by the convolution in nonstandard analysis, then the series of i.i.d. random variables using Loeb measure [3] converges in L^2 sense under some moment condition. Therefore, the definition of stochastic integral in classical probability theory can be extended by the way of nonstandard analysis [4], [5].

Furthermore, we need to prove some laws of large numbers for i.i.d. random variables to show the convergence to a stochastic integral.

In fact, we use an extended concept of the convolution to investigate the expectation or the distribution of series of i.i.d. random variables for the nonstandardization of the law of large numbers.

In order to prove the convergence of sums of higher order of ΔW_k such as $(\Delta W_k)^3, (\Delta W_k)^5, \cdots$ in the proof of Ito formula, we need to extend the law of large numbers for ΔW_k in the sense of nonstandard.

From the above discussion, we shall define the stochastic integral in nonstandard analysis.

Let Δt be the infinitesimal and $N = \frac{T}{\Delta t}$. The extended Winer process is defined as follows.

Definition 2.1. *Let* $N_t = \frac{t}{\Delta t}, 0 \le t \le T$ *and* $N = N_T$. *Assume that a sequence of i.i.d. random variables* $\{\Delta W_k, k = 1, \cdots, N\}$ *has the distribution*

$$P\{\Delta W_k = \sqrt{\Delta t}\} = P\{\Delta W_k = -\sqrt{\Delta t}\} = \frac{1}{2} \tag{1}$$

for each $k = 1, \cdots, N$. An extended Wiener process $\{W(t), t \ge 0\}$ is defined by

$$W(t) = \sum_{k=1}^{N_t} \Delta W_k, \ 0 \le t \le T. \tag{2}$$

Ito's integral (stochastic integral) in the nonstandard sense is defined as follows.

Definition 2.2. *Let* $\{W(t), 0 \le t \le T\}$ *be an extended Wiener process. Assume that an adapted process* $\{\sigma(t), 0 \le t \le T\}$ *with respect the Wiener process* $W(t)$ *is defined by*

$$\sigma(t) = Y_k, t_k \le t < t_{k+1}, k = 0, 1, \cdots, N, \tag{3}$$

where $t_k = k\Delta t, k = 0, 1, \cdots, N$ and each Y_k is measurable with respect to $\{W(t), 0 \le t \le t_k\}$. Assume that

$$E\left[Y_k^2\right] < \infty, \ k \ge 1. \tag{4}$$

A stochastic integral in nonstandard analysis is defined by

$$\int_0^T \sigma(t)\mathrm{d}W(t) = \sum_{k=1}^{N} Y_{k-1}\Delta W_k, \tag{5}$$

where Y_0 is independent of $\{W(t), t \geq 0\}$ $\{\Delta W_k, k = 1, \cdots, N\}$ is a sequence of i.i.d. random variables with the distribution

$$P\left\{\Delta W_k = \sqrt{\Delta t}\right\} = P\left\{\Delta W_k = -\sqrt{\Delta t}\right\} = \frac{1}{2}. \tag{6}$$

Remark 1. In classical (standard) probability theory, Ito's integral $\int_0^T \sigma(t)\mathrm{d}W(t)$ is well defined under the condition of the existence of the variance of $\sigma(t)$ for each $0 \leq t \leq T$. In nonstandard analysis, the convergence of the series in (5) may not be ensured. On the other hand, take note that we have already given some sufficient conditions for the convergence of the convolution in Fourier series. See [1].

3. Proof of Ito's Formula for Extended Wiener Process in Nonstandard

From the concept of Ito's integral for the extended Wiener process, we provide Ito's formula for the extended Wiener process.

Theorem 3.1. *Let* $F(t,x)$ *be of* C^3. *Assume that the condition* (4) *is satisfied, then we have the following for the extended Wiener Process* $W(t)$. *For any* $T \geq 0$,

$$\begin{aligned} F(t,W(T)) = {} & F(0,W(0)) + \int_0^T F_t(t,W(t))\mathrm{d}t \\ & + \int_0^T F_x(t,W(t))\mathrm{d}W(t) + \frac{1}{2}\int_0^T F_{xx}(t,W(t))\mathrm{d}t. \end{aligned} \tag{7}$$

Proof.

$$\begin{aligned} & F(t+\Delta t, W(t+\Delta t)) - F(t,W(t)) \\ & = F_t(t,W(t))\Delta t + F_x(t,W(t))\{W(t+\Delta t) - W(t)\} \\ & \quad + \frac{1}{2}F_{tt}(t,W(t))(\Delta t)^2 + F_{tx}(t,W(t))\Delta t\{W(t+\Delta t) - W(t)\} \\ & \quad + \frac{1}{2}F_{xx}(t,W(t))\{W(t+\Delta t) - W(t)\}^2 + \frac{1}{3!}F_{ttt}(t,W(t))(\Delta t)^3 \\ & \quad + \frac{3}{3!}F_{ttx}(t,W(t))(\Delta t)^2\{W(t+\Delta t) - W(t)\} \\ & \quad + \frac{3}{3!}F_{txx}(t,W(t))\Delta t\{W(t+\Delta t) - W(t)\}^2 \\ & \quad + \frac{1}{3!}F_{xxx}(t,W(t))\{W(t+\Delta t) - W(t)\}^3 + \cdots \end{aligned} \tag{8}$$

Put

$$N = \left[\frac{T}{\Delta t}\right],\ t_k = k\Delta t,\ k = 0,1,\cdots,N-1,$$

$$\Delta W_k = W(t_k) - W(t_{k-1}),\ k = 0,1,\cdots,N-1$$

and

$$\Delta W_N = W(T) - W(t_{N-1})$$

then,

$$\begin{aligned}
&F(t,W(T)) - F(0,W(0)) \\
&= \sum_{k=1}^{N} F_t(t_{k-1},W(t_{k-1}))\Delta t + \sum_{k=1}^{N} F_x(t_{k-1},W(t_{k-1}))\Delta W_k \\
&\quad + \frac{1}{2}\sum_{k=1}^{N} F_{tt}(t_{k-1},W(t_{k-1}))(\Delta t)^2 + \sum_{k=1}^{N} F_{tx}(t_{k-1},W(t_{k-1}))\Delta t \Delta W_k \\
&\quad + \frac{1}{2}\sum_{k=1}^{N} F_{xx}(t_{k-1},W(t_{k-1}))\Delta t + \frac{1}{3!}\sum_{k=1}^{N} F_{ttt}(t_{k-1},W(t_{k-1}))(\Delta t)^3 \\
&\quad + \frac{3}{3!}\sum_{k=1}^{N} F_{ttx}(t_k,W(t_k))(\Delta t)^2 \Delta W_k + \frac{3}{3!}\sum_{k=1}^{N} F_{txx}(t_k,W(t_k))(\Delta t)^2 \\
&\quad + \frac{1}{3!}\sum_{k=1}^{N} F_{xxx}(t_k,W(t_k))\Delta t \Delta W_k + \cdots \\
&= \int_0^T F_t(t,W(t))\mathrm{d}t + \int_0^T F_x(t,W(t))\mathrm{d}W(t) \\
&\quad + \frac{1}{2}\left\{\int_0^T F_{tt}(t,W(t))\mathrm{d}t\right\}\Delta t + \left\{\int_0^T F_{tx}(t,W(t))\mathrm{d}W(t)\right\}\Delta t \\
&\quad + \frac{1}{2}\int_0^T F_{xx}(t,W(t))\mathrm{d}t + \frac{1}{3!}(\Delta t^2)\left\{\int_0^T F_{ttt}(t,W(t))\mathrm{d}t\right\} \\
&\quad + \frac{3}{3!}\Delta t\left\{\int_0^T F_{ttx}(t,W(t))\mathrm{d}W(t)\right\} + \frac{3}{3!}\Delta t\left\{\int_0^T F_{txx}(t,W(t))\mathrm{d}t\right\} \\
&\quad + \frac{1}{3!}\Delta t\left\{\int_0^T F_{xxx}(t,W(t))\mathrm{d}W(t)\right\} + \cdots \\
&= \int_0^T F_t(t,W(t))\mathrm{d}t + \int_0^T F_x(t,W(t))\mathrm{d}W(t) \qquad (9) \\
&\quad + \frac{1}{2}\int_0^T F_{xx}(t,W(t))\mathrm{d}t
\end{aligned}$$

4. Proof of Ito's Formula for Ito's Process in Nonstandard

Let $X(t)$ be Ito's process defined by

$$X(t) = X_0 + \int_0^t b(s)\mathrm{d}s + \int_0^t \sigma(s)\mathrm{d}W(s), \quad 0 \le t \le T \qquad (10)$$

where $b(s)$ and $\sigma(s)$ are adapted processes with respect to a Wiener process $W(t)$. Then, we have Ito's formula for the Ito's process.

Theorem 4.1. *Let* $F(t,x)$ *be of* C^3, *then we have the following. For any* $T \ge 0$,

$$\begin{aligned}
F(t,X(T)) &= F(0,X(0)) + \int_0^T F_t(t,X(t))\mathrm{d}t \\
&\quad + \int_0^T F_x(t,X(t))b(t)\mathrm{d}t + \int_0^T F_x(t,X(t))\sigma(t)\mathrm{d}W(t) \qquad (11) \\
&\quad + \frac{1}{2}\int_0^T F_{xx}(t,X(t))\sigma(t)^2\mathrm{d}t.
\end{aligned}$$

Proof. We provide the proof by using nonstandard analysis.

From the Taylor expansion for the two-dimensional function $F(t,X(t))$, we

have the following.

$$\begin{aligned}
&F\left(t+\Delta t, X\left(t+\Delta t\right)\right)-F\left(t, X\left(t\right)\right)\\
&=F_t\left(t, X\left(t\right)\right)\Delta t+F_x\left(t, X\left(t\right)\right)\left\{X\left(t+\Delta t\right)-X\left(t\right)\right\}\\
&\quad+\frac{1}{2}F_{tt}\left(t, X\left(t\right)\right)\left(\Delta t\right)^2+F_{tx}\left(t, X\left(t\right)\right)\Delta t\left\{X\left(t+\Delta t\right)-X\left(t\right)\right\}\\
&\quad+\frac{1}{2}F_{xx}\left(t, X\left(t\right)\right)\left\{X\left(t+\Delta t\right)-X\left(t\right)\right\}^2+\frac{1}{3!}F_{ttt}\left(t, X\left(t\right)\right)\left(\Delta t\right)^3\\
&\quad+\frac{3}{3!}F_{ttx}\left(t, X\left(t\right)\right)\left(\Delta t\right)^2\left\{X\left(t+\Delta t\right)-X\left(t\right)\right\}\\
&\quad+\frac{3}{3!}F_{txx}\left(t, X\left(t\right)\right)\Delta t\left\{X\left(t+\Delta t\right)-X\left(t\right)\right\}^2\\
&\quad+\frac{1}{3!}F_{xxx}\left(t, X\left(t\right)\right)\left\{X\left(t+\Delta t\right)-X\left(t\right)\right\}^3+\cdots
\end{aligned}\tag{12}$$

In nonstandard analysis, we can represent the Ito's process $X\left(t\right)$ for the extended Wiener process by

$$\begin{aligned}
X\left(t\right)&=X_0+\int_0^t b\left(s\right)\mathrm{d}s+\int_0^t\sigma\left(s\right)\mathrm{d}W\left(s\right)\\
&=X_0+\sum_{k=1}^{N}b\left(t_{k-1}\right)\Delta t+\sum_{k=1}^{N}\sigma\left(t_{k-1}\right)\Delta W_k,\ \ 0\le t\le T,
\end{aligned}\tag{13}$$

where for infinitesimal Δt

$$N=\left[\frac{T}{\Delta t}\right],\ \ t_k=k\Delta t,\ \ k=0,1,\cdots,N$$

and

$$\Delta W_k=W\left(t_k\right)-W\left(t_{k-1}\right),\ \ k=0,1,\cdots,N.$$

Therefore, the difference of $X\left(t\right)$ can be represented by the following,

$$\Delta X_k=X\left(t_k\right)-X\left(t_{k-1}\right)=b\left(t_{k-1}\right)\Delta t+\sigma\left(t_{k-1}\right)\Delta W_k.\tag{14}$$

On the other hand,

$$\left(\Delta W_k\right)^{2n}=\left(\Delta t\right)^n\ \ a.s.$$

for each $n\ge 1$ from (1).

Thus, we have the following.

$$\begin{aligned}
&F\left(t, X\left(T\right)\right)-F\left(0, X\left(0\right)\right)\\
&=\sum_{k=1}^{N}F_t\left(t_{k-1}, X\left(t_{k-1}\right)\right)\Delta t+\sum_{k=1}^{N}F_x\left(t_{k-1}, X\left(t_{k-1}\right)\right)\Delta X_k\\
&\quad+\frac{1}{2}\sum_{k=1}^{N}F_{tt}\left(t_{k-1}, X\left(t_{k-1}\right)\right)\left(\Delta t\right)^2+\sum_{k=1}^{N}F_{tx}\left(t_{k-1}, X\left(t_{k-1}\right)\right)\Delta tXW_k\\
&\quad+\frac{1}{2}\sum_{k=1}^{N}F_{xx}\left(t_{k-1}, X\left(t_{k-1}\right)\right)\left\{\Delta X_k\right\}^2+\frac{1}{3!}\sum_{k=1}^{N}F_{ttt}\left(t_{k-1}, X\left(t_{k-1}\right)\right)\left(\Delta t\right)^3\\
&\quad+\frac{3}{3!}\sum_{k=1}^{N}F_{ttx}\left(t_k, X\left(t_k\right)\right)\left(\Delta t\right)^2\Delta X_k+\frac{3}{3!}\sum_{k=1}^{N}F_{txx}\left(t_k, X\left(t_k\right)\right)\Delta t\left(\Delta X_k\right)^2\\
&\quad+\frac{1}{3!}\sum_{k=1}^{N}F_{xxx}\left(t_k, X\left(t_k\right)\right)\left(\Delta X_k\right)^3+\cdots\\
&=\sum_{k=1}^{N}F_t\left(t_{k-1}, X\left(t_{k-1}\right)\right)\Delta t
\end{aligned}$$

$$
\begin{aligned}
&+\sum_{k=1}^{N} F_x\left(t_{k-1}, X\left(t_{k-1}\right)\right)\left\{b\left(t_{k-1}\right)\Delta t+\sigma\left(t_{k-1}\right)\Delta W_k\right\}\\
&+\frac{1}{2}\sum_{k=1}^{N} F_{tt}\left(t_{k-1}, X\left(t_{k-1}\right)\right)\left(\Delta t\right)^2\\
&+\sum_{k=1}^{N} F_{tx}\left(t_{k-1}, X\left(t_{k-1}\right)\right)\Delta t\left\{b\left(t_{k-1}\right)\Delta t+\sigma\left(t_{k-1}\right)\Delta W_k\right\}\\
&+\frac{1}{2}\sum_{k=1}^{N} F_{xx}\left(t_{k-1}, X\left(t_{k-1}\right)\right)\left\{b\left(t_{k-1}\right)\Delta t+\sigma\left(t_{k-1}\right)\Delta W_k\right\}^2\\
&+\frac{1}{3!}\sum_{k=1}^{N} F_{ttt}\left(t_{k-1}, X\left(t_{k-1}\right)\right)\left(\Delta t\right)^3\\
&+\frac{3}{3!}\sum_{k=1}^{N} F_{ttx}\left(t_k, X\left(t_k\right)\right)\left(\Delta t\right)^2\left\{b\left(t_{k-1}\right)\Delta t+\sigma\left(t_{k-1}\right)\Delta W_k\right\}\\
&+\frac{3}{3!}\sum_{k=1}^{N} F_{txx}\left(t_k, X\left(t_k\right)\right)\Delta t\left\{b\left(t_{k-1}\right)\Delta t+\sigma\left(t_{k-1}\right)\Delta W_k\right\}^2\\
&+\frac{1}{3!}\sum_{k=1}^{N} F_{xxx}\left(t_k, X\left(t_k\right)\right)\left\{b\left(t_{k-1}\right)\Delta t+\sigma\left(t_{k-1}\right)\Delta W_k\right\}^3+\cdots \qquad (15)\\
&=\int_0^T F_t\left(t, X\left(t\right)\right)\mathrm{d}t+\int_0^T F_x\left(t, X\left(t\right)\right)b\left(t\right)\mathrm{d}t\\
&+\int_0^T F_x\left(t, X\left(t\right)\right)\sigma\left(t\right)\mathrm{d}W\left(t\right)+\frac{1}{2}\int_0^T F_{xx}\left(t, X\left(t\right)\right)\sigma\left(t\right)^2\mathrm{d}t
\end{aligned}
$$

Thus we prove Ito's formula for the extended Ito's process.

Remark 2. Let $X_1, X_2, \cdots, X_n$ be independent random variables with density functions $f_1, f_2, \cdots, f_n$, respectively. Then, the distribution of $\sum_{k=1}^{n} X_k$ can be represented by convolution $f_1 * f_2 * \cdots * f_n$. In standard analysis, for the Fourier transform of the convolution

$$\mathcal{F}\left(f_1 * f_2 * \cdots * f_n\right)=\prod_{k=1}^{n}\mathcal{F}\left(f_k\right) \qquad (16)$$

is established, where $\mathcal{F}\left(f_k\right)$ is the Fourier transform of f_k.

From our previous paper [1], the result can be extended in the sense of nonstandard. See pp.976. Therefore, it is applied for the extension of limit theorems as like central limit theorem, law of large numbers and so on.

5. Conclusions

In classical (standard) probability theory, the stochastic integral

$$\int_0^T \sigma\left(t\right)\mathrm{d}W\left(t\right) \qquad (17)$$

is defined under the condition of the existence of the variance of $\sigma\left(t\right)$ for each $0 \le t \le T$. In nonstandard analysis, the convergence of the series in (5) is proved from the above arguments. On the proof of Ito's formula, it can be applied for other estimations as the same way.

Furthermore, the proof of Ito's formula in nonstandard analysis becomes simple rather than the proof in standard one.

Supported

The first author is supported in part by Grant-in-Aid Scientific Research (C), No.18K03431, Ministry of Education, Science and Culture, Japan.

Conflicts of Interest

The authors declare no conflicts of interest regarding the publication of this paper.

References

[1] Kanagawa, S., Nishiyama, R. and Tchizawa, K. (2018) Extended Wiener Measure by Nonstandard Analysis for Financial Time Series. *Applied Mathematics*, **9**, 975-984. https://doi.org/10.4236/am.2018.98066

[2] Nelson, E. (1977) Internal Set Theory: A New Approach to Nonstandard Analysis. *Bulletin of the American Mathematical Society*, **83**, 1165-1198. https://doi.org/10.1090/S0002-9904-1977-14398-X

[3] Hurd, A.E. and Loeb, P.A. (1985) Introduction to Nonstandard Real Analysis. Acad. Press, New York.

[4] Benot, E. (1989) Diffusions discrètes et mécanique stochastique. Prépubli. Lab. Math. J. Dieudonné, Université de Nice.

[5] Benot, E. (1995) Random Walks and Stochastic Differential Equations. In: Diener, F. and Diener, M., Eds., *Nonstandard Analysis in Practice*, Springer, Berlin, Heidelberg, 71-90. https://doi.org/10.1007/978-3-642-57758-1_4

Applied Mathematics, 2019, 10, 568-577
http://www.scirp.org/journal/am
ISSN Online: 2152-7393
ISSN Print: 2152-7385

Universality Class of the Nonequilibrium Phase Transition in Two-Dimensional Ising Ferromagnet Driven by Propagating Magnetic Field Wave

Ajay Halder, Muktish Acharyya

Department of Physics, Presidency University, Kolkata, India
Email: ajay.rs@presiuniv.ac.in, muktish.physics@presiuniv.ac.in

How to cite this paper: Halder, A. and Acharyya, M. (2019) Universality Class of the Nonequilibrium Phase Transition in Two-Dimensional Ising Ferromagnet Driven by Propagating Magnetic Field Wave. *Applied Mathematics*, **10**, 568-577.
https://doi.org/10.4236/am.2019.107040

Received: June 16, 2019
Accepted: July 20, 2019
Published: July 23, 2019

Abstract

The purpose of this work is to identify the universality class of the nonequilibrium phase transition in the two-dimensional kinetic Ising ferromagnet driven by propagating magnetic field wave. To address this issue, the finite size analysis of the nonequilibrium phase transition, in two-dimensional Ising ferromagnet driven by plane propagating magnetic wave, is studied by Monte Carlo simulation. It is observed that the system undergoes a nonequilibrium dynamic phase transition from a high temperature dynamically symmetric (*propagating*) phase to a low temperature dynamically symmetry-broken (*pinned*) phase as the system is cooled below the transition temperature. This transition temperature is determined precisely by studying the fourth-order Binder Cumulant of the dynamic order parameter as a function of temperature for different system sizes (L). From the finite size analysis of dynamic order parameter ($Q_L \sim L^{-\frac{\beta}{\nu}}$) and the dynamic susceptibility ($\chi_L^Q \sim L^{\frac{\gamma}{\nu}}$), we have estimated the critical exponents $\beta/\nu = 0.146 \pm 0.025$ and $\gamma/\nu = 1.869 \pm 0.135$ (measured from the data read at the critical temperature obtained from Binder cumulant), and $\gamma/\nu = 1.746 \pm 0.017$ (measured from the peak positions of dynamic susceptibility). Our results indicate that such driven Ising ferromagnet belongs to the same universality class of the two-dimensional equilibrium Ising ferromagnet (where $\beta/\nu = 1/8$ and $\gamma/\nu = 7/4$), within the limits of statistical errors.

Keywords

Ising Model, Dynamic Phase Transition, Monte-Carlo Simulation, Propagating Wave, Finite Size Analysis, Critical Exponents, Universality

1. Introduction

The driven Ising ferromagnet shows interesting nonequilibrium phase transitions [1] [2]. This time dependent drive may be of two kinds: 1) an applied magnetic field which is oscillating in time and uniform over the space at any particular instant, 2) the applied magnetic field has a spatio-temporal variation which may be the type of propagating or standing magnetic field wave. The first kind of driving magnetic field has drawn much attention to the researchers and a considerable volume of studies is done in this direction, in last two decades. Here, a few of those may be mentioned as follows: 1) the critical slowing down and the divergence of the specific heat near the dynamic transition temperature [3], 2) the divergence of the fluctuations of the dynamic order parameter [4], 3) the growth of critical correlation near the dynamic transition temperature [5]. These studies are an integrated effort to establish that the nonequilibrium transition in kinetic Ising ferromagnet driven by oscillating magnetic field is indeed a thermodynamic *phase transition*.

The nonequilibrium phase transitions in other magnetic models (e.g., Blume-Capel, Blume-Emery-Griffiths models etc.) driven by oscillating (in time but uniform over the space) magnetic field have been studied [6] [7] [8] also in last few years to present some interesting nonequilibrium behaviors. The nonequilibrium phase transitions were studied in [9] [10] [11] [12] [13] mixed spin systems driven by oscillating magnetic field, recently.

The another kind of external drive may be the magnetic field with spatio-temporal variation. The prototypes of these spatio-temporal drives are propagating or standing magnetic field waves. In the last few years, a number of investigations, on the nonequilibrium phase transitions in Ising ferromagnet driven by propagating and standing magnetic field wave, are done [14] [15] [16] [17] [18] through Monte Carlo methods. Here, the essential findings are the nonequilibrium phase transitions between two phases, namely, the low temperature ordered pinned phase (where the spins do not flip) and a high temperature disordered phase where a coherent propagation (in the case of propagating magnetic field wave) or coherent oscillation (in the case of standing magnetic field wave) of spin bands are observed. The transitions are marked by the divergences of dynamic susceptibility near the transition point.

However, the detailed finite size analyses were not yet performed to know the *universality class* of this nonequilibrium phase transition observed in Ising ferromagnet driven by propagating magnetic field wave. This is the key issue of the present study.

In this paper, we have investigated the nonequilibrium behaviour and the finite size effect of spin-$\frac{1}{2}$ Ising ferromagnet under the influence of propagating magnetic wave by Monte Carlo methods. The paper is organized as follows: The model and the MC simulation technique are discussed in Section II, the numerical results are reported in Section III and the paper ends with a summary in Section IV.

2. Model and Simulation

The *time dependent* Hamiltonian of a two dimensional driven Ising ferromagnet is represented by,

$$H(t) = -J\Sigma\Sigma' s^z(x,y,t)s^z(x',y',t) - \Sigma h^z(x,y,t)s^z(x,y,t). \quad (1)$$

Here $s^z(x,y,t) = \pm 1$, is the Ising *spin variable* at lattice site (x,y) at time *t*. The summation Σ' extends over the nearest neighbour sites (x',y') of a given site (x,y). $J(>0)$ is the *ferromagnetic spin-spin interaction strength* between the nearest neighbour pairs of Ising spins. For simplicity, we have considered the value of *J* to be uniform over the whole lattice. The externally applied driving *magnetic field*, is denoted by $h^z(x,y,t)$, at site (x,y) at time *t*. $h^z(x,y,t)$ has the following form for propagating magnetic wave,

$$h^z(x,y,t) = h_0 \cos\left\{2\pi\left(ft - \frac{x}{\lambda}\right)\right\} \quad (2)$$

Here h_0 and *f* represent *the field amplitude and the frequency* respectively of the propagating magnetic wave, whereas λ represents *the wavelength* of the wave. The wave propagates along the *X*-direction through the lattice.

An $L \times L$ square lattice of Ising spins is taken here as a model system. The boundary conditions applied at both directions are *periodic* which preserve the translational invariances in the system. Using *Monte Carlo Metropolis single spin flip algorithm* with *parallel* updating rule [19], the dynamics of the system are simulated. The initial state of the system is chosen as the high temperature random disordered phase, in which, at any lattice site, both the two states (±1) of the Ising spins have equal probabilities. The system is then slowly cooled down to any lower temperature *T* and the dynamical quantities are calculated. The *Metropolis probability* [19] of single spin flip at temperature *T* is given by,

$$W\left(\left(s^z\right)_i \to \left(s^z\right)_f\right) = \min\left[\exp\left(\frac{-\Delta E}{k_B T}\right), 1\right] \quad (3)$$

where ΔE is the energy change due to spin flip from *i*-th state to *f*-th state and k_B is the Boltzman constant. In a chosen configuration, the probability of flipping of each spin is calculated from the above rule. Then prepared a list of L^2 such values of probability of flipping. On the other hand, a list of L^2 random fraction (collected from a uniformly distributed random numbers) is prepared, keeping in mind that each random fraction is associated to the probability of flipping of each spin. The spins are flipped *simultaneously* where the probability of flipping exceeds (or equal to) the random fraction. This is so called *parallel updating* of spins. Such parallel updating of L^2 spin states in an $L \times L$ square lattice constitute the unit time step and is called *Monte Carlo Step per Spin* (MCSS). The applied magnetic field and the temperature are measured in the units of *J* and J/k_B respectively. The choices of such units of applied magnetic field and the temperatures are very common in the literatures [19] of the simulation of the Statistical Mechanics of Ising ferromagnet in the presence of magnetic field.

3. Results

The nonequilibrium behaviour of the two dimensional Ising ferromagnet is studied here in $L\times L$ square lattices of different sizes (L) where a propagating magnetic wave is passing through the system. The frequency (f) of magnetic field oscillation, wavelength (λ) of the magnetic wave and the amplitude (h_0) of field strength are kept constant throughout the present study. These constant values are respectively $f=0.01(\mathrm{MCSS})^{-1}$, $\lambda=16$ lattice units and $h_0=0.3J$. For $f=0.01$, 100 MCSS is required for a complete time cycle.

Since we have chosen the values of L in the multiple of 16, the wavelength $\lambda=16$ is a reasonable choice. In this case, the smallest system will contain a full wave. The frequency, $f=0.01$, is chosen to have the adequate number of cycles, of the propagating magnetic field, to get a reasonable average value. The choice of the amplitude $h_0=0.3J$ is just to keep the nonequilibrium phase transition in the higher temperature range.

The finite size effect is studied by taking into account four different system sizes (within the limited computational facilities available) such as L = 16, 32, 48 and 128. The system (for any fixed value of L) has been cooled down in small steps ($\Delta T=0.005J/k_B$) from high temperature phase, *i.e.* the dynamical disordered phase, to reach any dynamical steady state at temperature T. The dynamical quantities are calculated when the system has achieved the nonequilibrium steady state. For this we have kept the system in constant temperature for a sufficiently long time; 12,000 (for $L=128$) to 32,000 (for $L=16$) cycles of magnetic oscillations and discarding the initial (or transient) 1000 cycles and taking average over the remaining cycles. We have detected a dynamical phase transition from high temperature symmetric propagating (spin bands) phase to low temperature symmetry-broken pinned phase. The dynamic *Order parameter* for the phase transition is defined as the average magnetisation per spin over a full cycle of external magnetic field, *i.e.*

$$Q=f\times\oint M(t)\mathrm{d}t, \tag{4}$$

where $M(t)$ is the value of instantaneous magnetisation per spin at time t which can be obtained as

$$M(t)=\frac{1}{L^2}\sum_{i=1}^{L^2}s^z(x,y,t) \tag{5}$$

At very high temperature, the flipping probability of the spin, is quite high alongwith the oscillation of the magnetic field. As a result the value of the instantaneous magnetisation is almost close to zero. Consequently, by definition, the value of the dynamic order parameter is very small, thus identifying the dynamically disordered propagating phase ($Q=0$) (see **Figure 1(b)**). It may be noted here, that the instantaneous magnetisation fluctuates symmetrically about zero (see **Figure 1(d)**). Hence, this may be characterised as a dynamically symmetric phase. As the system is cooled down below the critical temperature, which depends on the value of magnetic field strength, the flipping probability of

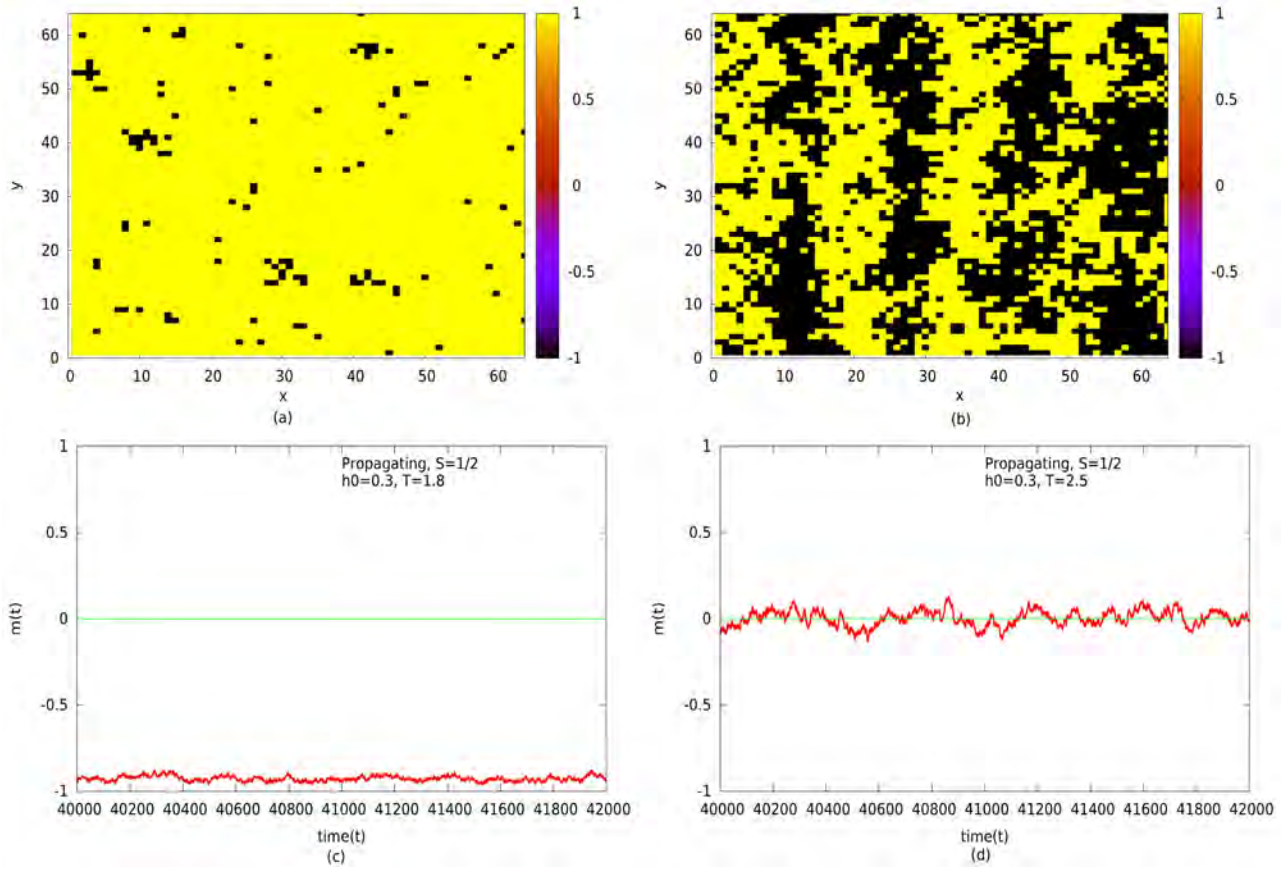

Figure 1. The lattice morphologies of the (a) pinned phase and (b) propagating phase respectively at time $t = 39937$ MCSS for $L = 64$. The dynamical symmetry breaking (change in the value of average magnetisation per spin from non-zero to nearly zero value); (c) at temperature $T = 1.8$ and (d) at temperature $T = 2.5$. The value of the amplitude of the field is $h_0 = 0.3$ in all cases.

the spin gets reduced; also the magnetic field strength may not be adequate to flip the spins and the spins are locked or pinned in a particular orientation giving rise to a large and nearly steady value of average magnetisation. This phase is identified as the dynamically ordered or pinned phase ($Q \neq 0$) (see Figure 1(a)). Unlike, the dynamically symmetric phase (mentioned above), here the instantaneous magnetisation varies asymmetrically about zero (see Figure 1(c)). So, this may be called a dynamically symmetry broken phase. The variation of the order parameter for the dynamic phase transition (DPT) for four different system sizes are shown in Figure 2(a).

The dynamical critical point is determined with high precision by studying the thermal variation of fourth order Binder cumulant ($U_L(T) = 1 - \frac{\langle Q^4 \rangle_L}{3\langle Q^2 \rangle_L^2}$) of dynamic order parameter Q for different system sizes (L). Figure 2(b) shows the variation of the Binder Cumulant ($U_L(T)$) with temperature (T) for different values of L. From this figure we have determined the value of critical temperature as $T_d = 2.011 J/k_B$, which is the value of temperature where the

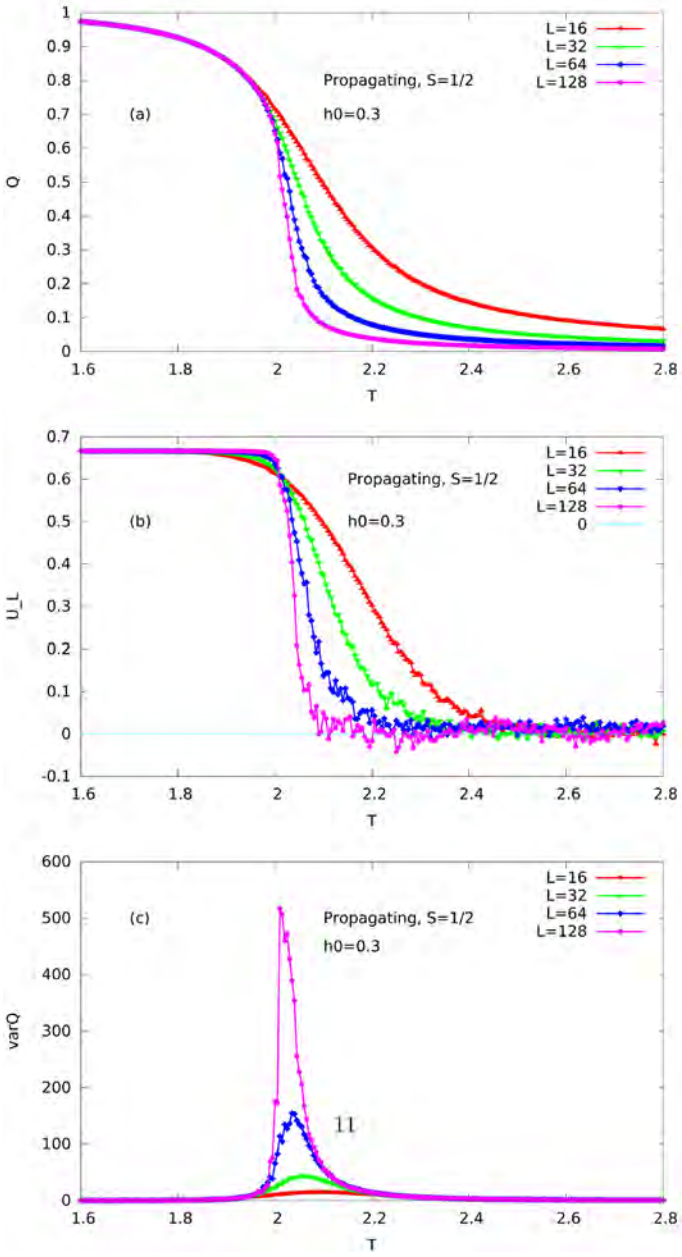

Figure 2. Temperature variation of different quantities for different values of linear system size L: (a) Order parameter Q; (b) Binder cumulant U_L; (c) scaled variance of order parameter $varQ$ or susceptibility χ_L^Q.

Binder cumulants for different lattice sizes have a common intersection. Now it is known from the behaviour of the kinetic Ising model that the scaled variance of the dynamical order parameter may be regarded as the susceptibility of the system, which can be defined as follows:

$$\chi_L^Q = L^2\left(\langle Q^2\rangle - \langle Q\rangle^2\right). \tag{6}$$

Figure 2(c) shows the variation of the scaled variance with the temperature. As we see from the figure that the susceptibility gets peaked near the dynamical

transition temperature showing the tendency of divergence near T_d, as the system size increases. Now we adopt the *finite-size scaling* analysis to determine the critical exponents for the two dimensional kinetic Ising ferromagnet driven by magnetic wave. For this reason we use the usual technique of expressing the measured quantities as a function of the system size. We assume the following scaling forms for the order parameter Q and susceptibility χ^Q at the critical temperature:

$$\langle Q \rangle_L \propto L^{-\beta/\nu} \tag{7}$$

$$\chi_L^Q \propto L^{\gamma/\nu}. \tag{8}$$

It has to be noted here that though we do not have any value measured at the critical temperature which has been determined (as common intersection) from the Binder cumulant versus temperature curves for different L, the values of Q & χ^Q have been read out from the respective graphs which represent the average values at any temperature. Moreover, the detailed investigations done previously [8], show that the above scaling forms are also applicable to classify the universality classes of the driven magnetic systems. **Figure 3(a)** shows the log-log plot of the dynamic order parameter $\langle Q \rangle_L$ as a function of the linear system size L at the dynamic transition temperature. The value of the critical exponent, as estimated from this simulational study, is $\beta/\nu = 0.146 \pm 0.025$ for the dynamic order parameter. From the log-log plot **Figure 3(b)**. of the susceptibility χ_L^Q or the scaled variance of the order parameter χ_L^Q as a function of linear system size L we obtained the estimate of the value of the critical exponent γ/ν. The values are $\gamma/\nu = 1.869 \pm 0.135$ (using the data obtained at $T_d = 2.011 J/k_B$ from the respective graphs) and $\gamma/\nu = 1.746 \pm 0.017$ (using the data obtained at the peak position of susceptibility). It is interesting to note that these estimated values of the critical exponents, for the two dimensional driven Ising ferromagnet, are very close to those of the two dimensional equilibrium Ising ferromagnet, which are $\beta/\nu = 1/8 = 0.125$ and $\gamma/\nu = 7/4 = 1.75$ [20].

4. Summary

In this study, we have mainly focused our attention on the finite size analysis and the critical aspects of the dynamic phase transition near the dynamic transition temperature of an $L \times L$ square type Ising ferromagnet driven by propagating magnetic wave. We have taken four different sizes of square lattice (L = 16, 32, 64 and 128). We have simulated the results using Monte Carlo methods using the Metropolis single spin flip algorithm with parallel updating rules. Our findings suggest that, within the limits of statistical errors obtained in this study, the estimated values of the critical exponents near the dynamic transition temperature are very close to those for the two-dimensional equilibrium Ising ferromagnet. As concluding remarks, we state that the nonequilibrium

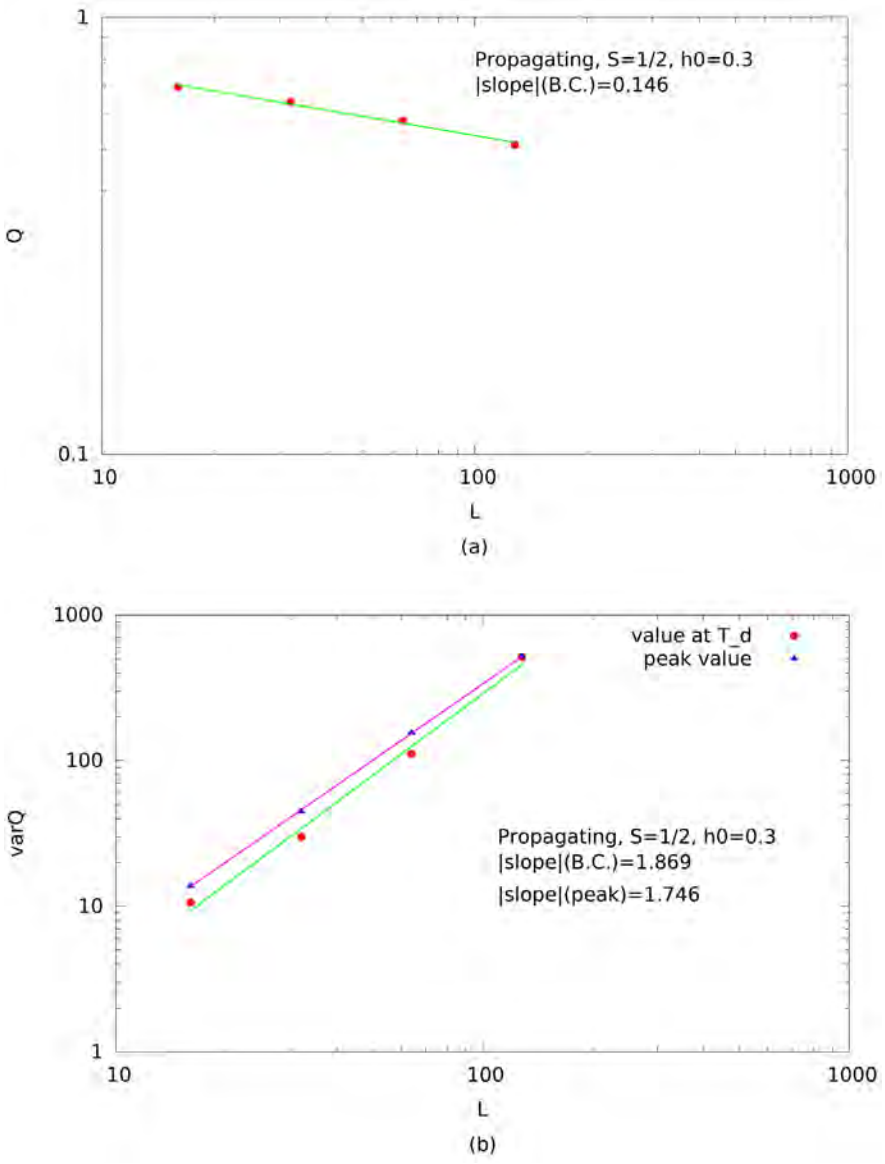

Figure 3. Log-log plot of (a) order parameter Q and (b) scaled variance $varQ$ or susceptibility χ_L^Q as a function of linear system size L. In (b) red dots represent the value of susceptibility at T_d whereas blue triangles represent the same at peak positions.

phase transition, observed in the two-dimensional Ising ferromagnet driven by magnetic field wave, belongs to the same universality class of equilibrium two-dimensional Ising equilibrium ferro-para phase transition. Recently, the nonequilibrium phase transition in the kinetic Ising model via the violation of principle of detailed balance was studied (Manoj Kumar and ChandanDasgupta, IISc, Bangalore) and estimated the exponents in close agreement with the present observations.

Acknowledgements

MA thanks Chandan Dasgupta for helpful discussion and acknowledges financial

support through FRPDF grant provided by Presidency University.

Conflicts of Interest

The authors declare no conflicts of interest regarding the publication of this paper.

References

[1] Chakrabarti, B.K. and Acharyya, M. (1999) Dynamic Transitions and Hysteresis. *Reviews of Modern Physics*, **71**, 847-859. https://doi.org/10.1103/RevModPhys.71.847 https://link.aps.org/doi/10.1103/RevModPhys.71.847

[2] Acharyya, M. (2005) Nonequilibrium Phase Transitions in Model Ferromagnets: A Review. *International Journal of Modern Physics C*, **16**, 1631-1670. https://doi.org/10.1142/S0129183105008266 https://www.worldscientific.com/doi/abs/10.1142/S0129183105008266

[3] Acharyya, M. (1997) Nonequilibrium Phase Transition in the Kinetic Ising Model: Critical Slowing Down and the Specific-Heat Singularity. *Physical Review E*, **56**, 2407. https://link.aps.org/doi/10.1103/PhysRevE.56.2407 https://doi.org/10.1103/PhysRevE.56.2407

[4] Acharyya, M. (1997) Nonequilibrium Phase Transition in the Kinetic Ising Model: Divergences of Fluctuations and Responses near the Transition Point. *Physical Review E*, **56**, 1234. https://doi.org/10.1103/PhysRevE.56.1234

[5] Sides, S.W., Rikvold, P.A. and Novotny, M.A. (1998) Kinetic Ising Model in an Oscillating Field: Finite-Size Scaling at the Dynamic Phase Transition. *Physical Review Letters*, **81**, 834-837. https://link.aps.org/doi/10.1103/PhysRevLett.81.834 https://doi.org/10.1103/PhysRevLett.81.834

[6] Keskin, M., Canko, O. and Deviren, B. (2006) Dynamic Phase Transition in the Kinetic Spin-3/2 Blume-Capel Model under a Time-Dependent Oscillating External Field. *Physical Review E*, **74**, Article ID: 011110. https://doi.org/10.1103/PhysRevE.74.011110

[7] Temizer, U., Kantar, E., Keskin, M. and Canko, O. (2008) Multicritical Dynamical Phase Diagrams of the Kinetic Blume-Emery-Griffiths Model with Repulsive Biquadratic Coupling in an Oscillating Field. *Journal of Magnetism and Magnetic Materials*, **320**, 1787-1801. https://doi.org/10.1016/j.jmmm.2008.02.107

[8] Vatansever, E. and Fytas, N. (2018) Dynamic Phase Transition of the Blume-Capel Model in an Oscillating Magnetic Field. *Physical Review E*, **97**, Article ID: 012122. https://link.aps.org/doi/10.1103/PhysRevE.97.012122 https://doi.org/10.1103/PhysRevE.97.012122

[9] Ertas, M., Deviren, B. and Keskin, M. (2012) Nonequilibrium Magnetic Properties in a Two-Dimensional Kinetic Mixed Ising System within the Effective-Field Theory and Glauber-Type Stochastic Dynamics Approach. *Physical Review E*, **86**, Article ID: 051110. https://doi.org/10.1103/PhysRevE.86.051110

[10] Temizer, U. (2014) Dynamic Magnetic Properties of the Mixed Spin-1 and Spin-3/2 Ising System on a Two-Layer Square Lattice. *Journal of Magnetism and Magnetic Materials*, **372**, 47-58. https://doi.org/10.1016/j.jmmm.2014.07.015

[11] Vatansever, E., Akinci, A. and Polat, H. (2015) Non-Equilibrium Phase Transition Properties of Disordered Binary Ferromagnetic Alloy. *Journal of Magnetism and Magnetic Materials*, **389**, 40-47. https://doi.org/10.1016/j.jmmm.2015.04.042

[12] Ertas, M. and Keskin, M. (2015) Dynamic Phase Diagrams of a Ferrimagnetic Mixed Spin (1/2, 1) Ising System within the Path Probability Method. *Physica A*, **437**, 430-436. https://doi.org/10.1016/j.physa.2015.05.110

[13] Shi, X., Wang, L., Zhao, J. and Xu, X. (2016) Dynamic Phase Diagrams and Compensation Behaviors in Molecular-Based Ferrimagnet under an Oscillating Magnetic Field. *Journal of Magnetism and Magnetic Materials*, **410**, 181-186. https://doi.org/10.1016/j.jmmm.2016.03.028

[14] Acharyya, M. (2014) Polarised Electromagnetic Wave Propagation through the Ferromagnet: Phase Boundary of Dynamic Phase Transition *Acta Physica Polonica B*, **45**, 1027. https://doi.org/10.5506/APhysPolB.45.1027

[15] Acharyya, M. (2014) Dynamic-Symmetry-Breaking Breathing and Spreading Transitions in Ferromagnetic Film Irradiated by Spherical Electromagnetic Wave. *Journal of Magnetism and Magnetic Materials*, **354**, 349-354. https://doi.org/10.1016/j.jmmm.2013.11.037

[16] Halder, A. and Acharyy, M. (2016) Standing Magnetic Wave on Ising Ferromagnet: Nonequilibrium Phase Transition *Journal of Magnetism and Magnetic Materials*, **420**, 290-295. https://doi.org/10.1016/j.jmmm.2016.07.062

[17] Halder, A. and Acharyya, M. (2017) Nonequilibrium Phase Transition in Spin-S Ising Ferromagnet Driven by Propagating and Standing Magnetic Field Wave. *Communications in Theoretical Physics*, **68**, 600. https://doi.org/10.1088/0253-6102/68/5/600

[18] Vatansever, E. (2017) Dynamic Phase Transition Features of the Cylindrical Nanowire Driven by a Propagating Magnetic Field.

[19] Binder, K. and Heermann, D.W. (1997) Monte Carlo Simulation in Statistical Physics. Springer Series in Solid State Sciences, Springer, New York. https://doi.org/10.1007/978-3-662-03336-4

[20] Huang, K. (2010) Onsager Solution. In: *Statistical Mechanics*, Second Edition, John Wiley & Sons Inc., Hoboken, Chapter 15.

Applied Mathematics, 2019, 10, 578-587
http://www.scirp.org/journal/am
ISSN Online: 2152-7393
ISSN Print: 2152-7385

The Structural Relationship between Chinese Money Supply and Inflation Based on VAR Model

Shichang Shen, Xiaoyi Dong

School of Mathematics and Statistics, Qinghai Nationalities University, Xining, China
Email: 13909785766@163.com

How to cite this paper: Shen, S.C. and Dong, X.Y. (2019) The Structural Relationship between Chinese Money Supply and Inflation Based on VAR Model. *Applied Mathematics*, **10**, 578-587.
https://doi.org/10.4236/am.2019.107041

Received: July 3, 2019
Accepted: July 20, 2019
Published: July 23, 2019

Abstract

With the development of economy, more and more attention is paid to the relationship between money supply and inflation in the economic field. This paper chooses consumer price index (*CPI*) as an important index to measure the level of inflation, by choosing between January 2008 and March 2019 money in circulation *M*0, narrow measure *M*1, broad measure *M*2, consumer price index *CPI* monthly data as sample, building a vector autoregressive (VAR) model and using econometric methods of impulse response function and variance decomposition, and finally characterizes money in circulation *M*0, narrow measure *M*1, broad measure *M*2 and the relationship between consumer price index *CPI* and different sizes of the impact of inflation in the money supply relationship.

Keywords

Money Supply, The VAR Model, Inflation

1. Introduction

With the continuous development of China's economy, indicators such as gross national product, consumer price index and money supply have been important indicators to judge the state of macroeconomic development. Consumer price index (*cpi*) [1] is an indicator to measure and judge deflation and inflation. And the control of money circulation has become particularly important, through the control of money circulation will directly affect inflation, affect the development of the whole economy. The influence of money supply on inflation is higher than that of fiscal deficit on inflation. The relationship between fiscal stimulus plan, money supply, public expectation and inflation, and finally the money

supply is the most important factor affecting inflation mainly in [2] [3]. There is a close relationship between money supply and inflation. There is no inflation in their short term, but we should also guard against the pressure brought by stagflation. Yang Zihui *et al.* [4] studied the directed acyclic graph and found that the fiscal deficit had a certain impact on inflation but was not the most important one. Somethings can be inspected in [4] [5]. And the money supply has a strong asymmetric influence on CPI and does not depend on the state of the economy. Inflation is closely related to China's monetary policy [6] and asset inflation. This paper is based on the VAR model to show that the impact of different money supply on inflation is different.

2. Materials and Methods

2.1. The VAR Model

Vector autoregression (VAR) [7] is to establish a model based on the statistical properties of data. The VAR model constructs the model by taking each endogenous variable in the system as the lagged value function of all endogenous variables in the system, thus extending the univariate autoregressive model to the "vector" autoregressive model composed of multivariate time series variables.

In 1980, C. A. Sims introduced VAR model into economics, promoting the wide application of dynamic analysis of economic system. The mathematical expression of VAR (P) model is:

$$y_t = \Phi_1 y_{t-1} + \cdots + \Phi_p y_{t-p} + Hx_t + \varepsilon_t, \quad t = 1, 2, \cdots, T \tag{1}$$

y_t is the column vector of endogenous variables in k dimension, x_t is the column vector of exogenous variables in d dimension, p is the lag order, and T is the number of samples. $k \times k$ dimensional matrix $\Phi_1, \cdots, \Phi_p$ and $k \times d$ dimensional matrix H are coefficient matrices to be estimated. ε_t is a k dimensional disturbance column vector, which can be correlated with each other synchronously, but not with its own lag value and not with the variables on the right-hand side of the equation.

2.2. Granger Causality Test

Proposed by Granger (1969) [7], another important application of VAR model is to analyze the causal relationship between economic time series variables. Granger solved the problem of whether x caused y, mainly looking at the extent to which the present y could be explained by the past x, and whether the addition of the lag value of x improved the explanation degree. If x is helpful in y prediction, or if the correlation coefficient between x and y is statistically significant, it can be said that "y is caused by x Granger".

Consider the mean square error (MSE) of the march period prediction:

$$\mathrm{MSE} = \frac{1}{s}\sum_{i=1}^{s}\left(\hat{y}_{t+i} - y_{t+i}\right)^2 \tag{2}$$

This can be expressed as follows: if the mean square error obtained by pre-

dicting y_{t+s} based on $(y_t, y_{t-1}, \cdots)$ for all $s > 0$ is the same as the mean square error obtained by y_{t+s} based on both $(y_t, y_{t-1}, \cdots)$ and $(x_t, x_{t-1}, \cdots)$, then y is not caused by x Granger.

2.3. Impulse Response Function

Vector autoregression model (VAR) [8] is a non-theoretical model, so it is not necessary to analyze the mutual influence between its variables when it is analyzed, but the impact on the explained variable when it is impacted by an error term. Therefore, for the VAR model, it is difficult to explain the economic value of a single parameter estimate. In addition to prediction, an important aspect of its application is the dynamic characteristics of the system, that is, the response of an endogenous variable to residual shock (response). The impulse response function can be used to describe the impact of the random error on the current and future values of endogenous variables.

First i endogenous variable of an impact not only directly affect the first i variable, and pass through the dynamic structure of the VAR model to other endogenous variables, impulse response function attempts to depict the influence of trajectory, shows how an arbitrary variable disturbance affect all other variables through model, finally and feedback to the process itself.

2.4. Variance Decomposition

In 1980 [8], Sims proposed the variance decomposition method according to the expression of VAR (∞), and provided the influencing relationship between variables in the VAR model:

$$y_{it} = \sum_{j=1}^{k}\left(\theta_{ij}^{(0)}\varepsilon_{jt} + \theta_{ij}^{(1)}\varepsilon_{jt-1} + \theta_{ij}^{(2)}\varepsilon_{jt-2} + \theta_{ij}^{(3)}\varepsilon_{jt-3} + \cdots\right), i = 1, 2, \cdots, k; t = 1, 2, \cdots, T \quad (3)$$

$$Var(y_i) = \sum_{j=1}^{k}\left\{\sum_{q=0}^{\infty}\left(\theta_{ij}^{(q)}\right)^2\sigma_{jj}\right\}, i = 1, 2, \cdots, k \quad (4)$$

We know that the contents of the brackets are the sum of the influences of the j disturbance term ε_j from the infinite past to the present time point on y_i.

In this paper, the consumer price index (CPI) cover 8 types of goods and services consumed nationwide, and the calculation formula of CPI is

$$CPI = \sum_{i=1}^{n} CPI_i \times Weight_i$$

3. Empirical Analysis

3.1. Data Preprocessing

Data are derived from Wind database. **Figures 1-4** are the sequential trend charts of *CPI*, *M*0, *M*1 and *M*2 from January 2008 to March 2019. As the observed trend charts are not stable, the stationarity of unit root test series is further adopted.

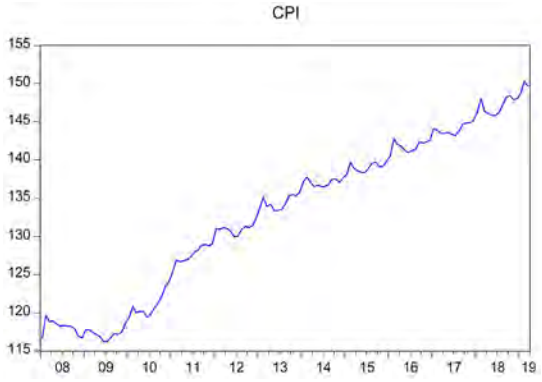

Figure 1. *CPI* trend chart.

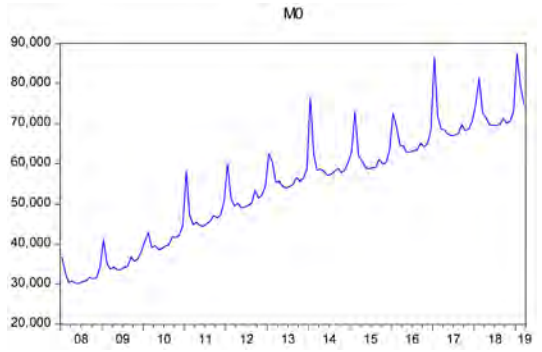

Figure 2. *M*0 trend chart.

Figure 3. *M*1 trend chart.

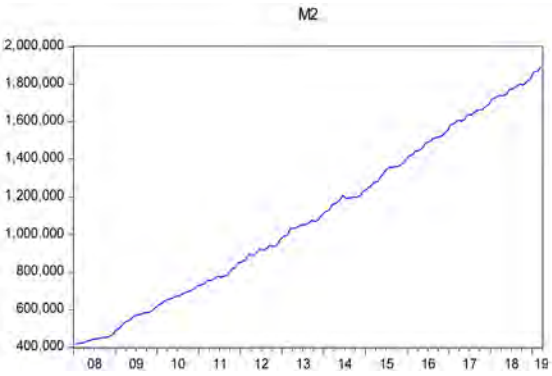

Figure 4. *M*2 trend chart.

3.2. Stationarity Test

In this paper, ADF unit root test was adopted to test the stationarity of the original sequence. The test results are shown in Table 1. By observing Table 1, *CPI*, *M*0, *M*1 and *M*2 sequences failed the stationarity test.

Therefore, the first-order difference is carried out for the above sequences, and then the unit root test is carried out for the new sequences. The obtained results are shown in Table 2, and the new sequences after the first-order difference have been stabilized.

3.3. Order Determination and Stability Test of the Model

As can be seen from Table 3, the likelihood ratio (LR) is an indicator reflecting authenticity, which is a compound indicator reflecting both sensitivity and specificity. The final prediction error statistic (FPE) is a tool that provides prediction accuracy and high imitation, as well as a more general prediction checking capability. *DCPI*, *DM*0, *DM*1 and *DM*2 are first-order integral sequences, so they can be judged according to the results of LR test statistics, final prediction error (FPE), AIC information criterion, SC information criterion and HQ information criterion, and there are enough lag terms and enough degrees of freedom at the same time. According to the results in Table 3, the optimal order of the VAR model is finally selected as order 2. By using EViews7.2 to establish the VAR (2) model, the vector autoregression expression about *CPI* can be obtained as follows:

$$\begin{aligned} DCPI = {} & 6.4339e{-}05 * DM0(-1) + 3.4488e{-}05 * DM0(-2) \\ & + 0.1177 * DCPI(-1) + 0.080 * DCPI(-2) \\ & + 4.9877e{-}05 * DM1(-1) + 1.9733e{-}05 * DM1(-2) \\ & - 3.8129e{-}07 * DM2(-1) - 3.6004e{-}06 * DM2(-2) - 0.0062 \end{aligned}$$

Table 1. ADF test results of *CPI*, *M*0, *M*1 and *M*2 sequences.

Variable	ADF test value	The critical value at the 1% level	The critical value at the 5% level	The critical value at the 10% level	P values	Conclusion
CPI	−320194	−3.479656	−2.883073	−2.578331	0.9177	Non-stationary
M0	−2.488793	−3.484653	−2.885249	−2.579491	0.1207	Non-stationary
M1	0.225702	−3,480038	−2.883239	−2.578402	0.9733	Non-stationary
M2	2.070928	−3.484653	−2.885249	−2.579491	0.9999	Non-stationary

Table 2. ADF test results of *DCPI*, *DM*0, *DM*1 and *DM*2 sequences.

Variable	ADF test value	The critical value at the 1% level	The critical value at the 5% level	The critical value at the 10% level	P values	Conclusion
CPI	−11.21752	−3.480038	−2.883239	−2.578420	0.0000	Non-stationary
M0	−9.797663	−3.484653	−2.885249	−2.579491	0.0000	Non-stationary
M1	−13.92312	−3.480038	−2.578420	−2.578420	0.0000	Non-stationary
M2	−3.258272	−3.484653	−2.885249	−2.579491	0.0191	Non-stationary

Table 3. Delay order judgment results.

	LogL	LR	FPE	AIC	SC	HQ
0	−4152.109	NA	2.62e+22	62.97134	63.05870	63.00684
1	−4076.024	146.4052	1.05e+22	62.06097	62.49776*	62.23846
2	−4048.308	51.65193*	8.83e+21*	61.88346*	62.66968	62.20294*

Note: *represents the optimal lag order of the corresponding criterion; LR represents likelihood ratio statistic; FPE represents the final prediction error statistic; AIC represents the chi information criterion statistics; SC represents Schwartz statistic; HQ represents the hannan-quinn information statistic.

After the estimation of the model, the inverse roots of the AR characteristic polynomial of the model should be tested, and the AR root diagram and tables can be obtained, as shown in Figure 4 and Figure 5.

According to Figure 5 and Table 4, the inverse roots of AR characteristic roots are all within the unit circle, and the overall stability of the model indicates that the VAR model composed of these indicators is effective, that is, there is a stable relationship between the money supply index and the inflation index.

3.4. Granger Causality Test

Granger causality test can further determine the causal relationship between each variable. The Granger causality test is conducted below, and the test results are shown in Table 5.

According to the data in Table 5, at the significant level of 10%, there is a causal relationship between *CPI* and *M*0, *M*1 and *M*2, but it is not mutual. Instead, there is a one-way granger causal relationship, and the change of money supply is the cause of inflation.

3.5. Impulse Response Function

According to the impulse response diagram in Figure 6 and Figure 7, when *M*0 increases, the *CPI* changes very little, indicating that *M*0 has a lag effect on *CPI*. In the 6th, 7th and 8th phases, *CPI* has a negative effect on *M*0, and reaches its maximum in the 9th phase.

By observing the impulse response diagram in Figure 8, it can be concluded that the maximum value reached in the second phase produced a positive boost, and the negative effect was generated in the fifth phase, and the amplitude fluctuation decreased and tended to be near the 0 value in the end.

By observing the impulse response diagram in Figure 9, it can be concluded that in the first period, *M*2 had no effect on *CPI*, and the impulse response value was 0. After that, there was a negative impact in the fourth period, and then the fluctuation was gradually reduced until the response value approached 0.

Variance Decomposition

Figure 10 is the variance decomposition graph of *CPI*, which is used in the VAR model to analyze the contribution to the change of endogenous variables. In this paper, the contribution of *M*0, *M*1 and *M*2 to *CPI* is adopted in anova. In

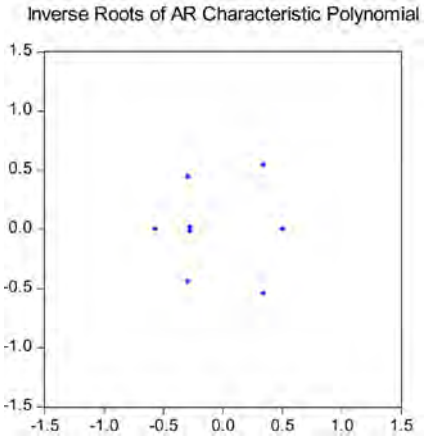

Figure 5. AR root diagram of VAR (2) model.

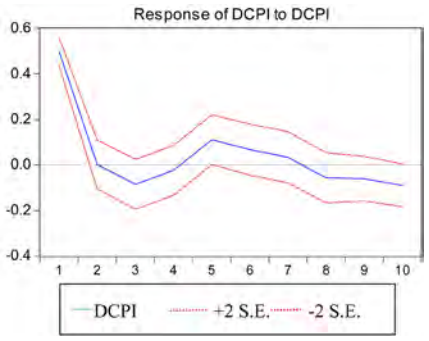

Figure 6. Impulse response of DCPI to DCPI.

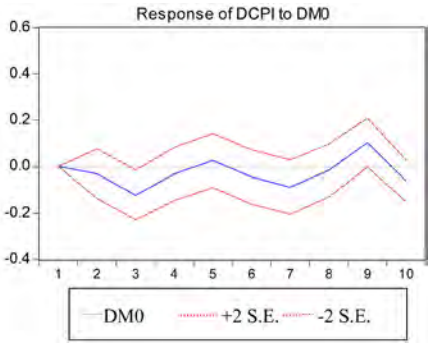

Figure 7. Pulse response of DCPI to DM0.

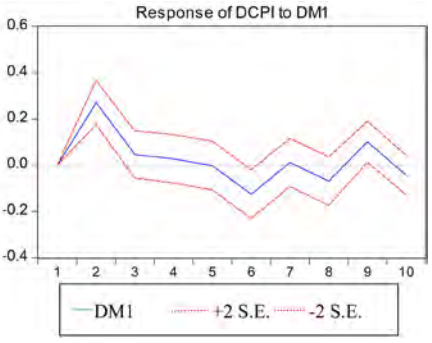

Figure 8. DCPI impulse response to DM1.

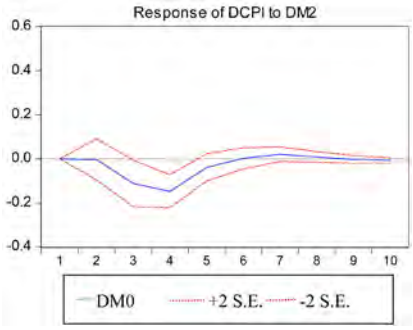

Figure 9. Impulse response of DCPI to DM2.

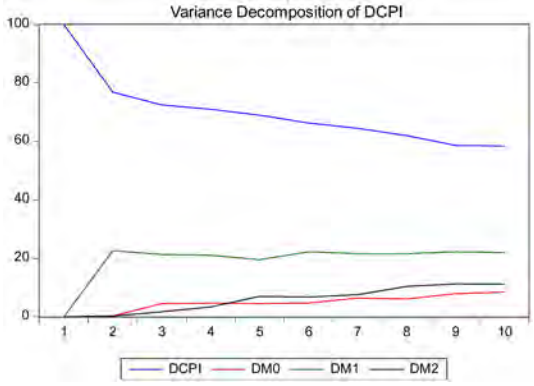

Figure 10. Variance decomposition.

Table 4. AR root table of VAR model.

Root	Modulus
0.343647 − 0.543592i	0.643106
0.343647 + 0.543592i	0.643106
−0.564894	0.564894
−0.290970 − 0.442758i	0.529809
−0.290970 + 0.442758i	0.529809
0.505074	0.505074
−0.272000 − 0.017187i	0.272543
−0.272000 + 0.017187i	0.272543

Table 5. Results of Granger causality test.

The null hypothesis	The F value	Probability (P value)	Conclusion
DCPI is not the granger cause of DM0	0.810061	0.6670	Accept
DCPI is not the granger cause of DM0	17.99314	0.0001	Refuse
DCPI is not the granger cause of DM0	0.029371	0.9854	Accept
DCPI is not the granger cause of DM0	40.54574	0.0000	Refuse
DCPI is not the granger cause of DM0	3.940281	0.1394	Accept
DCPI is not the granger cause of DM0	0.394868	0.0008	Refuse

the first period, *CPI* was only affected by itself. With the passage of time, the contribution rate of *CPI* itself is gradually decreasing and the contribution rate of money supply variance is steadily rising.

4. Conclusions and Recommendations

Through correlation analysis such as impulse response function and variance as impulse response function and variance decomposition, the following conclusions can be drawn.

It is observed that the cumulative effect values of the corresponding impulse response functions *M*0, *M*1 and *M*2 are greater than 0, and it can be concluded that the increase of *M*0, *M*1 and *M*2 will increase *CPI*. From the variance decomposition, it can be concluded that contribution rate of different money supply to *CPI* is different.

The impact of *CPI* is a certain lag, and the lag index *M*1 is the leading indicator. Therefore, from the perspective of money supply, we should pay more attention to the change of *M*1 indicator, and then pay attention to the change of *M*2 indicator.

However, there is a significant short-term relationship between China's inflation and money supply, and money supply has a significant impact on inflation. This relationship is very obvious in the short run. In the long run, the influence of money supply on inflation will gradually weaken and stabilize at a relative level, and the volatility will gradually stabilize.

Therefore, it can be concluded that there is no inflation in China's economy in a short time, but it does not mean that the economy will develop steadily in the future, and stagflation may occur. At the same time, the monetary policy also has some lag and limitations. Therefore, we should establish a preventive mechanism in advance, and constantly improve some fiscal policies, formulate relevant systems, laws and regulations, so as to avoid some adverse impacts brought by inflation.

Fund

This work is supported by the National Natural Science Foundation of China (No. 11561056) and Natural Science Foundation of Qinghai (No. 2016-ZJ-914).

Conflicts of Interest

The authors declare no conflicts of interest regarding the publication of this paper.

References

[1] Zhang, W. and Su, J. (2010) Empirical Analysis of Output and Inflation Effect of Chinese Money Supply. *Economic Issues*, No. 5, 72-75.

[2] Gao, Y. (2010) Fiscal Stimulus Plan, Money Supply, Public Expectation and Inflation. *Research on Fiscal and Economic Issues*, No. 3, 8-16.

[3] Guo, S.H., Li, X.X. and Wu, W.L. (2016) Research on the Relationship between Money Supply and Inflation. *Productivity Research*, No. 8, 15-17.

[4] Yang, Z.H. Zhou, T.Y. and Huang, X.F. (2014) Whether China's Fiscal Deficit Has Inflation Effect—New Evidence from the Study of Directed Acyclic Graph. *Financial Research*, No. 12, 55-70.

[5] Liu, L. and Zhu, M.N. (2013) Monetary Supply, Broad Money Velocity and Price Level—An Empirical Study on Chinese Data Based on Nonlinear LSTVAR Model. *International Finance Research*, No. 10, 20-32.

[6] Wu, Z.W. and Ju, F. (2003) Deflation, Asset Inflation and Monetary Policy—On the Current Monetary Aggregate and Monetary Structure in China. *Management World*, No. 11, 7-18.

[7] Yi, D.H. (2008) Data Analysis and Application of Eviews. China Renmin University Press, Beijing.

[8] Gao, T.M. (2009) Econometric Analysis Methods and Modeling—E Views Applications and Examples. 2nd Edition, Tsinghua University Press, Beijing.

Applied Mathematics, 2019, 10, 588-604
http://www.scirp.org/journal/am
ISSN Online: 2152-7393
ISSN Print: 2152-7385

Global Dynamics of an SEIRS Compartmental Measles Model with Interrupted Vaccination

Dominic Otoo, Justice A. Kessie, Elvis K. Donkoh, Eric Okyere, Williams Kumi

Department of Mathematics & Statistics, University of Energy & Natural Resources, Sunyani, Ghana
Email: dominic.otoo@uenr.edu.gh, justice.kessie.stu@uenr.edu.gh, elvis.donkor@uenr.edu.gh, williams.kumi@uenr.edu.gh, eric.okyere@uenr.edu.gh

How to cite this paper: Otoo, D., Kessie, J.A., Donkoh, E.K., Okyere, E. and Kumi, W. (2019) Global Dynamics of an SEIRS Compartmental Measles Model with Interrupted Vaccination. *Applied Mathematics*, **10**, 588-604.
https://doi.org/10.4236/am.2019.107042

Received: May 21, 2019
Accepted: July 21, 2019
Published: July 24, 2019

Abstract

Measles is a reemerging disease that has a devastating impact, especially among children under 5. In this paper, an SEIRS model is developed to investigate a possible outbreak among the population of children under 5 in the Sunyani Municipality. We consider waning immunity or loss of immunity among those who were vaccinated, which leads to secondary attacks among some in the population. Using Routh-Hurwitz criterion, Matrix Theoretic and Goh-Volterra Lyapunov functions, the stability of the model was investigated around the equilibria. We have computed the threshold parameter, R_0, using the Next Generation Matrix method. The disease-free equilibrium is globally stable whenever $R_0 \le 1$ and unstable otherwise. The endemic equilibrium is globally stable when $R_0 > 1$.

Keywords

Global Stability, Lyapunov Function, Matrix Theoretic Method, Next Generation Matrix, SEIRS

1. Introduction

Measles, a recurrent virus infection has a short term outbreak but its impact is devastating especially among children under five. Severe measles results in pneumonia, which is the disease with high mortality rate in Ghana. Found in [1], the graphs show the mortality during an outbreak of measles. In this research paper, the authors looked at a case study of the dynamics of measles disease in the case of interrupted vaccination in Sunyani, a thriving metropolis in Ghana, a country where only 57% deliveries are handled by qualified health personnel [2]. In the Sunyani city and its immediate environs, new deliveries are commonly

done in the hospital, clinics and maternity homes but significantly some cases of new births are successfully done without the presence of qualified trained health practitioner, usually in their homes. The health program in Ghana makes it necessary for regular attendant mothers with newborns to vaccinate their children against the six childhood killer diseases including measles in any health facility. The first dose of MMR (mumps, measles, rubella) vaccine is given at 12 - 13 months of age. The second dose is usually taken when the child is 3 years and 4 months old. This can be taken in later years in the management of a disease outbreak. The irregular attendants do not successfully vaccinate their children against measles. New deliveries done outside a health facility make it difficult to track these children for vaccination. There are some children who missed the first and second doses, and there are some still who also missed the second dose because of irregularity in attending a health facility and for immigration, too [3]. There is also among the population a strong believe that MMR vaccines are leaving children with autism. Thereby, there are many who do not have a strong immunity against measles and many have their immunity wane in time. Their development of a strong immunity is interrupted so several children are susceptible to the disease and several still may have secondary infection. We seek to investigate the nature of a possible outbreak of measles in a population with dynamics such as this. Many researchers have studied the global dynamics of infectious diseases in general (see [4] [5]) while others also studied the dynamics of specific infectious diseases such as measles, chickenpox, mumps and rubella (see [6] [7]). In this paper, we also study the dynamics of measles with a relapse in a varying population where birth, death and immigration dynamics are considered. [8] [9] [10] studied the global stability of disease models and inculcated immigration and/or births and death dynamics into the population system. Again much work has already been done (see [11] [12]) defining what measles is and the symptoms and the effect of chronic infection of measles. It is mentioned that measles is severe among children under five (5) years.

Mathematical models are strong instruments used extensively to study the spread and control of infectious diseases. One important measure that determines the dynamics of disease models is the threshold parameter known as *basic reproductive number* R_0. This parameter measures the number of infectives generated by a single infectious individual introduced into the susceptible population. In measuring the foregoing, researchers in recent literature use the NGM approach. When $R_0 \le 1$ (usually when the disease-free equilibrium exists) the introduction of infectious individual can not generate a large outbreak. On the other hand, when $R_0 > 1$, (where the endemic equilibrium exists), the disease will persist in the population. [4] [13] have mentioned in their works that establishing global properties of dynamical systems using Lyapunov functions is not a trivial problem because there is no systematic procedure in constructing Lyapunov functions for infectious diseases. But one of the most successful procedures used to construct Lyapunov functions by many researchers is the

quadratic function of the form $\mathcal{D}_i = \sum_{i=1}^{n} c_i \left(x - x^*\right)^2$ (see [14]) or the nonlinear Goh-Volterra function $\mathcal{D}_i = \sum_{i=1}^{n} c_i \left(x - x^* - x^* \ln \frac{x}{x^*}\right)$ (see [15] [16]).

In this paper, the matrix theoretic method, a type of Lyapunov function, is used to establish the stability in the disease free system. Later in this study, the Goh-Volterra method is used to establish the stability of the endemic equilibrium. [4] [17] used this matrix theoretic method to study the global dynamics of several specific disease models.

2. The Model

We consider a susceptible-exposed-infectious-recovered-susceptible (SEIRS) model with relapse since there is a vaccination parameter that provides a near-permanent immunity against the disease with non-negative initial conditions. E represents the number of latent(exposed) individuals, $\sigma > 0$ represents the rate at which the *exposed* individuals become infectious (*i.e.*) $1/\sigma$ represents the average latent period. $\lambda > 0$ represents the rate at which the susceptible individual become immune and gain near-permanent immunity and $\gamma > 0$ also represents the rate at which the infectious individuals go through the successful treatment process of the disease. Near-permanent immunity because there exist a rate $\epsilon > 0$ of the recovered individuals falling back into the susceptible compartment. It is considered that this ϵR individual have a waning immunity over time so they fall back susceptible to the infectious disease. Already, [18] studied the "Global Stability Results in an SVIR Epidemic Model with Immunity Loss Rate Depending on the Vaccine-Age" where it is assumed that the waning rate of vaccine-induced immunity is depending on the vaccine-age. α represents a vital dynamics-birth and immigration rates. The total number of new infections at a time t is given by $\beta SI/N$. It is also considered that the natural immunity of some exposed individuals δ_E moves them into the recovered population. While μ is the natural death rate for the susceptible and recovered compartments, $\mu_E = \mu + k_E$ and $\tau = \mu + k_I$ represent the death rates for the exposed and infected classes respectively.

$N(t) = S(t) + E(t) + I(t) + R(t)$ is a growing population since births and immigration rates are added at any time *t*. The schematic diagram as shown in **Figure 1** is drawn or developed to depict the interactions in the thriving metropolis, Sunyani of Ghana. The schematic diagram above in **Figure 1** has the following as its system of equations;

$$\begin{aligned} S' &= \alpha N + \epsilon R - \left(\mu + \beta I/N + \lambda\right) S \\ E' &= \beta SI/N - \left(\mu_E + \sigma + \delta_E\right) E \\ I' &= \sigma E - \left(\tau + \gamma\right) I \\ R' &= \gamma I - \left(\mu + \epsilon\right) R + \lambda S + \delta_E E \end{aligned} \tag{1}$$

3. Model Transformation & Analysis

The total population size N_t can be determined by $N = S(t) + E(t) + I(t) + R(t)$

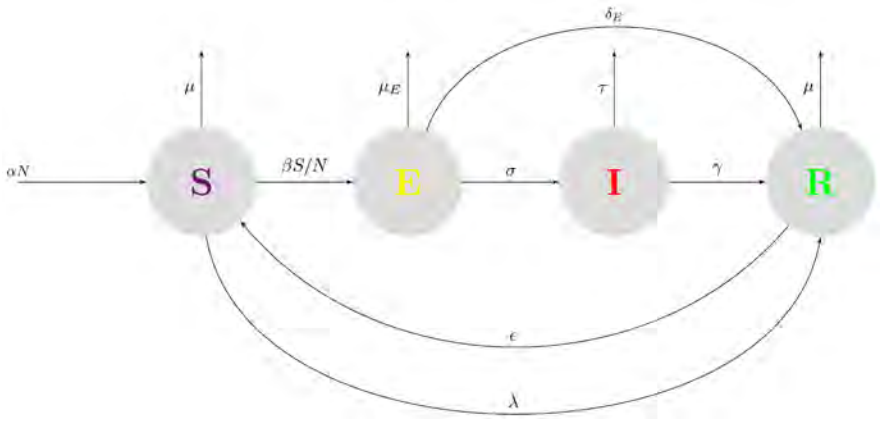

Figure 1. Schematic diagram of the SEIRS model.

or from the differential equation $N' = (\alpha - \mu)N - k_E E - k_I I$, which is derived by adding the equations in (1). Let $s = S/N$, $e = E/N$, $i = I/N$ and $r = R/N$ denote the fractions of the classes *S*, *E*, *I* and *R* in the population, respectively. Then for $s' = (N \cdot S' - S \cdot N')/N^2$, $e' = (N \cdot E' - E \cdot N')/N^2$, $i' = (N \cdot I' - I \cdot N')/N^2$ and $r' = (N \cdot R' - R \cdot N')/N^2$ respectively, the following assignments are appropriate;

$$\begin{aligned}
s' &= \frac{N \cdot (\alpha N + \epsilon R - (\mu + \beta I/N + \lambda) S) - S \cdot ((\alpha - \mu) N - k_E E - k_I I)}{N^2} \\
&= \alpha + \epsilon r - (\alpha + \lambda) s - (\beta - k_I) si + k_E se \\
e' &= \frac{N \cdot (\beta SI/N - (\mu_E + \sigma + \delta_E) E) - E \cdot ((\alpha - \mu) N - k_E E - k_I I)}{N^2} \\
&= \beta si - (\alpha + \sigma + k_E + \delta_E) e + k_E e^2 + k_I ie \\
i' &= \frac{N \cdot (\sigma E - (\tau + \gamma) I) - I \cdot ((\alpha - \mu) N - k_E E - k_I I)}{N^2} \\
&= \sigma e - (\alpha + k_I) i + k_E ei + k_I i^2 \\
r' &= \frac{N \cdot (\gamma I - (\mu + \epsilon) R + \lambda S + \delta_E E) - R \cdot ((\alpha - \mu) N - k_E E - k_I I)}{N^2} \\
&= \gamma i - (\alpha + \epsilon) r + \lambda s + \delta_E e + k_E er + k_I ir
\end{aligned} \tag{2}$$

From the transformation above, the following equations are derived

$$\begin{aligned}
s' &= \alpha + \epsilon r - (\alpha + \lambda) s - (\beta - k_I) si + k_E se \\
e' &= \beta si - (\alpha + \sigma + k_E + \delta_E) e + k_E e^2 + k_I ie \\
i' &= \sigma e - (\alpha + k_I) i + k_E ei + k_I i^2 \\
r' &= \gamma i - (\alpha + \epsilon) r + \lambda s + \delta_E e + k_E er + k_I ir
\end{aligned} \tag{3}$$

subject to the restriction that $s + e + i + r = 1$. Let us hereon refer to (3) as the full model. It is also worthy to note that the total population $N(t)$ does not appear in Equation (2). We can attribute that to the homogeneity in the system (1). Also, since *r* appears in the first equation of the Equation (3), we substitute $r = 1 - s - e - i$ into the first equation to get:

$$\begin{aligned} s' &= \alpha + \epsilon - (\alpha + \lambda + \epsilon)s - (\beta - k_I)si + k_E se - \epsilon e - \epsilon i \\ e' &= \beta si - (\alpha + \sigma + k_E + \delta_E)e + k_E e^2 + k_I ie \\ i' &= \sigma e - (\alpha + k_I)i + k_E ei + k_I i^2 \end{aligned} \tag{4}$$

so that we can focus our attention on the subsystem (4).

$$\begin{aligned} s' &= (\alpha + \epsilon) - (\alpha + \lambda + \epsilon)s - (\beta - k_I)si + k_E se - \epsilon e - \epsilon i \\ e' &= \beta si - (\alpha + \sigma + k_E + \delta_E)e + k_E e^2 + k_I ie \\ i' &= \sigma e - (\alpha + k_I)i + k_E ei + k_I i^2 \end{aligned} \tag{5}$$

The transformation has revealed some dynamics and interactions embedded in our model which is not intended to be measured in this study. Let us rewrite system (5) by making these substitutions; $h_1 = \alpha + \epsilon$; $h_2 = \alpha + \lambda + \epsilon$, $h_3 = \alpha + \sigma + k_E + \delta_E$; and $h_4 = \alpha + k_I$ to obtain the system of equations:

$$\begin{aligned} s' &= h_1 - h_2 s - (\beta - k_I)si \\ e' &= \beta si - h_3 e \\ i' &= \sigma e - h_4 i \end{aligned} \tag{6}$$

For biological considerations we study the system (6) in the region

$$\Omega = \left\{ (s, e, i) \in \Re_+^3 \mid 0 \le s + e + i \le 1 \right\}$$

It can be shown that Ω is positively invariant. In the latter part of this study, we show that the transformed model (3) is similar to the new model (6) by numerical simulation. [19] also did this transformation in their study and used the full model, but for the purpose of this study, with the established equality of the models (3) and model (6) by numerical computation we turn our attention to the latter model.

4. Equilibria & Stability

It can be seen that Equation (6) has a disease-free equilibrium is $DFE = \left(\frac{h_1}{h_2}, 0, 0 \right)$. The Jacobian matrix evaluated at the DFE is given thus,

$$DFE = \begin{pmatrix} -h_2 & 0 & \frac{h_1(k_I - \beta)}{h_2} \\ 0 & -h_3 & \frac{\beta h_1}{h_2} \\ 0 & \sigma & -h_4 \end{pmatrix}$$

The characteristic polynomial of the *DFE* system $F(\lambda)$ is given as,

$$\begin{aligned} F(\lambda) = \lambda^3 + (h_2 + h_3 + h_4)\lambda^2 + \left(h_2 h_3 + h_2 h_4 + h_3 h_4 - \frac{\beta \sigma h_1}{h_2} \right)\lambda \\ + h_2 h_3 h_4 - \beta \sigma h_1 \end{aligned} \tag{7}$$

From the characteristic polynomial above,

$$b_1 = h_2 + h_3 + h_4 \tag{8}$$

$$b_2 = h_2h_3 + h_2h_4 + h_3h_4 - \frac{\beta\sigma h_1}{h_2} \tag{9}$$

$$b_3 = h_2h_3h_4 - \beta\sigma h_1 \tag{10}$$

By the Routh-Hurwitz's criterion, for the characteristic equation to have negative eigenvalues, then $b_1 > 0$, $b_3 > 0$ and $b_1b_2 > b_3$. The Routh-Hurwitz's criterion is a tool used to establish the negativity or otherwise of the roots of a characteristic equation. Let us first introduce our threshold parameter R_0.

4.1. Basic Reproductive Number, R_0

Following the theory made explicit in [4] on R_0 above, we use the features of the model under study to carve out an appropriate measure for the R_0. Let $\mathcal{F}$, $\mathcal{V}$ F, V and $f(x,y)$ be defined as in [4]. From the system (6),

$$\mathcal{F} = \begin{bmatrix} (\beta - k_I)si \\ 0 \end{bmatrix} \quad \text{and} \quad \mathcal{V} = \begin{bmatrix} h_3 e \\ -\sigma e + h_4 i \end{bmatrix} \tag{11}$$

From (11), we proceed to find F and V as defined in [4] above.

$$F = \begin{bmatrix} 0 & (\beta - k_I)s \\ 0 & 0 \end{bmatrix} \quad \text{and} \quad V = \begin{bmatrix} h_3 & 0 \\ -\sigma & h_4 \end{bmatrix} \tag{12}$$

It can be easily shown that

$$V^{-1} = \frac{1}{h_3h_4}\begin{bmatrix} h_4 & 0 \\ \sigma & h_3 \end{bmatrix} \tag{13}$$

Consequently,

$$\begin{aligned} R_0 = \rho\left(FV^{-1}\right) &= \frac{1}{h_3h_4}\begin{bmatrix} 0 & (\beta - k_I)s \\ 0 & 0 \end{bmatrix} \times \begin{bmatrix} h_3 & 0 \\ -\sigma & h_4 \end{bmatrix} \\ &= \frac{(\beta - k_I)\sigma s_{DFE}}{h_3h_4}, \text{ but } s_{DFE} = \frac{h_1}{h_2} \\ R_0 &= \frac{(\beta - k_I)h_1\sigma}{h_2h_3h_4} \end{aligned} \tag{14}$$

Another construction of the measure R_0 mostly considered by researchers long before the introduction of the new generation matrix (NGM) method was introduced is

$$R_0 = \frac{DFE}{EE}$$

where EE is the endemic equilibrium.

$$R_0 = \frac{DFE}{EE} = \frac{\beta\sigma h_1}{h_2h_3h_4} \tag{15}$$

We remark that, the NGM's measure of R_0 (as shown in 14) is equivalent to this measure (15) *if and only if* $k_I = 0$. But for the purpose of this study, we choose (14) as our measure for R_0.

Theorem 1. *Denote* $R_0 = \frac{(\beta - k_I)h_1\sigma}{h_2h_3h_4}$. *When* $R_0 \le 1$, *then the system* (6)

has only a $DFE = \left(\frac{h_1}{h_2}, 0, 0\right)$ *on the set* Ω. *When* $R_0 > 1$ *then besides the DFE, there exist a unique endemic equilibrium EE where the disease is persistent.*

4.2. Routh-Hurwitz's Criterion

Theorem 2 (Routh-Hurwitz's Criterion) *Consider the characteristic equation*

$$|\lambda I - A| = \lambda^n + b_1\lambda^{(n-1)} + \cdots + b_{(n-1)}\lambda + b_n = 0 \tag{16}$$

determining the n eigenvalues λ of a real $n \times n$ square matrix A, where I is the identity matrix. Then the eigenvalues λ all have negative real parts if $\Delta_1 > 0$, $\Delta_2 > 0$, $\cdots$, $\Delta_n > 0$, where

$$\Delta_k = \begin{vmatrix} b_1 & 1 & 0 & 0 & 0 & 0 & \cdots & 0 \\ b_3 & b_2 & b_1 & 1 & 0 & 0 & \cdots & 0 \\ b_5 & b_4 & b_3 & b_2 & b_1 & 1 & \cdots & 0 \\ \vdots & \vdots & \vdots & \vdots & \vdots & \vdots & \ddots & \vdots \\ b_{2k-1} & b_{2k-2} & b_{2k-3} & b_{2k-4} & b_{2k-5} & b_{2k-6} & \cdots & b_k \end{vmatrix}$$

The above theorem (2) is reproduced from [20] and used in the article [21].

Theorem 3. *The disease-free equilibrium DFE is locally stable as* $R_0 \le 1$ *and unstable as* $R_0 > 1$.

Proof. It is easy to show from (7) that $b_1 > 0$ and $b_2 > 0$ whenever $R_0 \le 1$. Now for $b_1 b_2 > b_3$,

$$\Rightarrow b_1 b_2 > b_3$$

$$\Rightarrow (h_2 + h_3 + h_4)\left(h_2 h_3 + h_3 h_4 - \frac{\beta\sigma h_1}{h_2}\right) > h_2 h_3 h_4 - \beta\sigma h_1$$

$$\Rightarrow h_2^2 h_3 + h_2 h_3 h_4 - \beta\sigma h_1 + h_2 h_3^2 + h_3^2 h_4 - \frac{\beta\sigma h_1 h_3}{h_2} + h_2 h_3 h_4 + h_3 h_4^2 - \frac{\beta\sigma h_1 h_4}{h_2}$$

$$> h_2 h_3 h_4 - \beta\sigma h_1$$

And since $R_0 \le 1$,

$$h_2^2 h_3 + h_2 h_3^2 + h_3^2 h_4 + h_3 h_4^2 + h_2 h_3 h_4 > \frac{\beta\sigma h_1}{h_2}(h_3 + h_4)$$

therefore $b_1 b_2 > b_3$. The DF system has negative eigenvalues, hence the DF system is locally stable when $R_0 \le 1$. Again, when $R_0 > 1$, then the condition 2 of the Routh-Hurwitz's criterion is violated; *thus* b_2 may become less than 0 and therefore the system becomes unstable.

4.3. Global Stability of the DFE

The matrix theoretic method is used to prove the global stability of the DFE.

A Matrix-Theoretic Method

The matrix-theoretic method is used to prove the sharp threshold statement in theorem (5). It is a systematic method, and it is presented to guide the

construction of a Lyapunov function. Taking the same path as [4] [22] [23], let us set

$$f(x,y) := (F-V)x - \mathcal{F}(x,y) + \mathcal{V}(x,y) \tag{17}$$

Then the equation for the disease compartment can be written as

$$x' = (F-V)x - f(x,y) \tag{18}$$

Let $\psi^{\mathrm{T}} \le 0$ be the left eigenvector of the non-negative matrix $V^{-1}F$ corresponding to the eigenvalue $\rho(V^{-1}F) = \rho(FV^{-1}) = R_0$. The following result provides a general method to construct a Lyapunov function for [1.1]. [17] [24] used this Lyapunov function involving the Perron eigenvectors to study the global dynamics of several specific disease models while [4] used it to consider a general case for infectious diseases. In this paper, this method reproduces to establish the global stability of our system.

Theorem 4 *Let F, V and* $f(x,y)$ *be defined as in* (1.2) *and* (2.1) *in* [4] *respectively. If* $f(x,y) \ge 0$, *in the* $\Omega \subset \Re_+^{n+m}$, $F \ge 0$, $V^{-1} \ge 0$ *and* $R_0 \le 1$, *then the function* $\mathcal{D} = \psi^{\mathrm{T}} V^{-1} x$ *is a Lyapunov function for the system* (1.1) (*again in* [4]) *on* Ω.

Proof. The proof as followed in [4] gives

$$\begin{aligned} \mathcal{D}' = \mathcal{D}' | &= \psi V^{-1} x' = \psi V^{-1}(F-V)x - \psi V^{-1} f(x,y) \\ &= (R_0 - 1)\psi^{\mathrm{T}} x - \psi^{\mathrm{T}} V^{-1}(x,y) \end{aligned} \tag{19}$$

Since $\psi^{\mathrm{T}} \ge 0$, $V^{-1} \ge 0$, and $f(x,y) \ge 0$ in the region Ω, the last term is non-positive. If $R_0 \le 1$, then $\mathcal{D}^1 \le 0$ in Ω and thus $\mathcal{D}$ is a Lyapunov function for the system [1.1] as defined in [4].

[4] has proven that the Lyapunov function used to prove the global stability of the DFE in Ω can also be extended to establish a uniform persistence and thus establish the existence of an EE in $\Re_+^{n+m}$. Find the *theorem* 2.2 in [4] and the proof thereof.

Theorem 5. *The DFE is globally stable.*

Proof. Taking the left side expansion of (19), the Lyapunov function $\mathcal{D}$ as defined in theorem (4) therefore is

$$\mathcal{D} = \psi^{\mathrm{T}} V^{-1} x = \left(\frac{\sigma}{h_4^2} + \frac{\sigma}{h_3 h_4}\right) e + \frac{1}{h_3} i \tag{20}$$

$$\mathcal{D}' = (R_0 - 1)\left(\frac{\sigma}{h_4} e + i\right) - \left(\frac{2\sigma}{h_3 h_4} + \frac{1}{h_4}\right) f(x,y)$$

it is easy to prove that

$$f(x,y) = 0 \tag{21}$$

$$\mathcal{D}' = (R_0 - 1)\left(\frac{\sigma}{h_4} e + i\right) \tag{22}$$

It is obvious from this equation that when $R_0 \le 1$ then $\mathcal{D}' < 0$ and therefore the *DFE* is globally asymptotically stable and unstable when $R_0 > 1$.

4.4. Existence and Stability of the Endemic Equilibrium

Referring to theorem (1), there exists a unique *EE*. In this section, we establish the stability of the *EE* using Routh-Hurwitz's criterion for the proof of local stability and Lyapunov functions for the global stability.

4.4.1. Local Stability of Endemic Equilibrium

Theorem 6. *The EE is locally stable.*

Proof. The Jacobian of the *EE* is given thus

$$J_{EE}=\begin{pmatrix} -\dfrac{(\beta-k_I)(\beta h_1\sigma-h_2h_3h_4)}{(\beta-k_I)h_3h_4}-h_2 & 0 & -\dfrac{h_3h_4(\beta-k_I)}{\beta\sigma} \\ \dfrac{\beta(\beta h_1\sigma-h_2h_3h_4)}{(\beta-k_I)h_3h_4}-h_2 & -h_3 & \dfrac{h_3h_4}{\sigma} \\ 0 & \sigma & -h_4 \end{pmatrix}$$

Then the characteristic polynomial of the EE would be

$$\begin{aligned} F(\lambda)=&-\frac{\beta h_1h_3h_4k_I\sigma}{h_3h_4k_I-\beta h_3h_4}-\frac{\lambda\beta h_1h_4k_I\sigma}{h_3h_4k_I-\beta h_3h_4}-\frac{\lambda\beta h_1h_3k_I\sigma}{h_3h_4k_I-\beta h_3h_4}-\frac{\lambda^2\beta h_1k_I\sigma}{h_3h_4k_I-\beta h_3h_4}\\ &+\frac{\beta^2h_1h_3h_4\sigma}{h_3h_4k_I-\beta h_3h_4}+\frac{\lambda\beta^2h_1h_4\sigma}{h_3h_4k_I-\beta h_3h_4}+\frac{\lambda\beta^2h_1h_3\sigma}{h_3h_4k_I-\beta h_3h_4}+\frac{\lambda^2\beta^2h_1\sigma}{h_3h_4k_I-\beta h_3h_4}\\ &+\frac{h_2h_3^2h_4^2k_I}{h_3h_4k_I-\beta h_3h_4}+\frac{\lambda h_2h_3h_4^2k_I}{h_3h_4k_I-\beta h_3h_4}+\frac{\lambda h_2h_3^2h_4k_I}{h_3h_4k_I-\beta h_3h_4}+\frac{\lambda^2h_2h_3h_4k_I}{h_3h_4k_I-\beta h_3h_4}\\ &-\frac{\beta h_2h_3^2h_4^2}{h_3h_4k_I-\beta h_3h_4}-\frac{\lambda\beta h_2h_3h_4^2}{h_3h_4k_I-\beta h_3h_4}-\frac{\lambda\beta h_2h_3^2h_4}{h_3h_4k_I-\beta h_3h_4}-\frac{\lambda^2\beta h_2h_3h_4}{h_3h_4k_I-\beta h_3h_4}\\ &-\lambda h_2h_4-\lambda^2h_4-\lambda h_2h_3-\lambda^2h_3-\lambda^2h_2-\lambda^3 \end{aligned} \tag{23}$$

which is of the form $F(\lambda)=\lambda^3+b_1\lambda^2+b_2\lambda+b_3$ where b_1, b_2 and b_3 are simplified from Equation (23) as

$$b_1=h_3+h_4+\frac{\beta\sigma h_1}{h_3h_4}$$

$$b_2=\beta\sigma h_1+\frac{h_1}{h_3}\sigma$$

$$b_3=\beta\sigma h_1-h_2h_3h_4$$

when $F(\lambda)=0$. It can be seen that b_1, b_2 and b_3 are all positive. For $b_1b_2>b_3$,

$$\begin{aligned} b_1b_2&=\left(h_3+h_4+\frac{\beta\sigma h_1}{h_3h_4}\right)\left(\beta\sigma h_1+\frac{h_1}{h_3}\sigma\right)>\beta\sigma h_1-h_2h_3h_4=b_3\\ &=\beta\sigma h_1h_3+h_1\sigma+\beta\sigma h_1h4+\frac{h_1h_4}{h_3}\sigma+\frac{(\beta\sigma h_1)^2}{h_3h_4}+\frac{\beta(\sigma h_1)^2}{h_3^2h_4}\\ &>\beta\sigma h_1-h_2h_3h_4=b_3\\ &=(h_3+h_4)\beta\sigma h_1+h_1\sigma+\frac{h_1h_4}{h_3}\sigma+\frac{(\beta\sigma h_1)^2}{h_3h_4}+\frac{\beta(\sigma h_1)^2}{h_3^2h_4}\\ &>\beta\sigma h_1-h_2h_3h_4=b_3 \end{aligned} \tag{24}$$

Now $h_1<h_3+h_4$ and by extension $(h_3+h_4)\beta\sigma h_1>\beta\sigma h_1$. The rest of the

terms in the left hand side of this inequality are non-negative and therefore obviously greater than $-h_2h_3h_4$. Therefore the EE is locally stable.

4.4.2. Global Stability Analysis of the Endemic Equilibrium

A general form of Lyapunov functions coined from the first integral form of the Goh-Volterra system which is often used in the literature of mathematical biology is used to prove the global stability of the EE. This function takes the form

$$\mathcal{L}_i = \sum_{i=1}^{n} c_i \left(x_i - x_i^* - x_i^* \ln \frac{x_i}{x_i^*} \right) \tag{25}$$

where x is the variables and c_i are carefully selected constants. This criterion has been used many times in establishing the stability or otherwise of many disease models and also present in [4, 13, 15].

Theorem 7. *The EE is globally stable.*

Proof. Let $s > s^*$ and $i > i^*$,

$$\mathcal{L}_1 = s - s^* - s^* \ln \frac{s}{s^*} \tag{26}$$

$$\mathcal{L}_1' = -\left(\frac{s^* - s}{s} \right) s' \tag{27}$$

$$= -\left(\frac{s^* - s}{s} \right) \left(h_1 - h_2 s - (\beta - k_I) si \right), \tag{28}$$

and the equilibrium relation for $h_1 = h_2 s^* + (b - k_I) s^* i^*$

$$\leq -\left(\frac{s^* - s}{s} \right) \left(h_2 (s^* - s) + (\beta - k_I) (s^* i^* - si) \right) \tag{29}$$

$$\mathcal{L}_1' \leq 0, \text{ whenever } s > s^* \text{ and } i > i^* \text{ in the region } \Re_+ \tag{30}$$

In line (26), we define the Goh-Volterra function for the first variable s and differentiate it in the second line (27). In the following line, s' is substituted for its relation in (6) and evaluated at the equilibrium relation for h_1 in line (29). Consider that $s > s^*$ and $i > i^*$, (which is a necessary condition for (26) to hold). Then the inequality in line (29) is justified. Therefore, $\mathcal{L}_1$ defined above is a Lyapunov function.

Again, let $e > e^*$ and $\mathcal{L}_2 = e - e^* - e^* \ln \frac{e}{e^*}$

$$\mathcal{L}_2 = e - e^* - e^* \ln \frac{e}{e^*} \tag{31}$$

$$\mathcal{L}_2' = -\left(\frac{e^* - e}{e} \right) e' \tag{32}$$

$$\mathcal{L}_2' = -\left(\frac{e^* - e}{e} \right) (\beta si - h_3 e) \tag{33}$$

$$= -(e^* - e) \left(\frac{\beta si}{e} - h_3 \right) \tag{34}$$

$$\leq -\left(e^* - e\right)\left(\frac{\beta s^* i^*}{e^*} - h_3\right), \tag{35}$$

then from the system under study, (6), $\frac{i^*}{e^*} = \frac{s}{h_4}$ and $s^* = \frac{h_3 h_4}{bs}$

$$\leq -\left(e^* - e\right)\left(\frac{\beta h_3 h_4 \sigma}{\beta h_4 \sigma} - h_3\right) = -\left(e^* - e\right) \times 0 = 0 \tag{36}$$

$$\mathcal{L}_2' \leq 0 \tag{37}$$

The next Lyapunov function for the e variable is given in line (31), differentiated and evaluated in lines (32) and (33) respectively. The equilibrium relation for $\frac{\beta s^* i^*}{e^*}$ is introduced in lines (35) and (36). Again, the inequality is obviously justified whenever $e > e^*$. The function defined as $\mathcal{L}_2 = e - e^* - e^* \ln \frac{e}{e^*}$ is successful Lyapunov function.

Lastly, let us set $i > i^*$ and $\mathcal{L}_3 = i - i^* - i^* \ln \frac{i}{i^*}$,

$$\mathcal{L}_3 = i - i^* - i^* \ln \frac{i}{i^*} \tag{38}$$

$$\mathcal{L}_3' = -\left(\frac{i^* - i}{i}\right) i' \tag{39}$$

$$\mathcal{L}_3' = -\left(\frac{i^* - i}{i}\right)\left(\sigma e - h_4 i\right) \tag{40}$$

$$= -\left(i^* - i\right)\left(\sigma \frac{e}{i} - h_4\right) \tag{41}$$

$$\leq -\left(i^* - i\right)\left(\sigma \frac{e^*}{i^*} - h_4\right), \frac{e^*}{i^*} = \frac{h_4}{s} \tag{42}$$

$$\leq -\left(i^* - i\right)\left(\sigma \frac{h_4}{\sigma} - h_4\right) = 0 \tag{43}$$

$$\mathcal{L}_3' \leq 0 \tag{44}$$

The Lyapunov function for the last variable understudy is introduced in line (38) and differentiated in the following line (39). The equilibrium relation for e^* / i^* is substituted in lines (42) and (43) thereby justifying the inequality.

Therefore $\mathcal{L}$ defined as

$$\mathcal{L} = \sum_{i=1}^{n}\left(x_i - x_i^* - x_i^* \ln \frac{x_i}{x_i^*}\right) = \mathcal{L}_1 + \mathcal{L}_2 + \mathcal{L}_3$$

is a Lyapunov function for the system (6). Arbitrary constants c_i can be chosen from $\Re_+$ and any linear combination of $\mathcal{L}$ would be a Lyapunov function for the system. Hence the proof.

5. Numerical Simulations

In this section, we simulate our model to demonstrate the theoretic results found by this study. We only talk about susceptibility and recovery over time since they explain the rest of the compartments. Note that from the schematic diagram (figure [1]), individuals in the exposed compartments are recruited from the susceptible and the infectious individuals are also recruited from the exposed compartment. We wish you to see that we have shown by this numerical simulation that the first system (1) which was transformed to give the full system (3) is mathematically the same as the reduced model (6). Parameters used for this simulation are shown in **Table 1**. With all other parameters held constant, we vary vaccination from 0.2 to 0.8 with a step size of 0.2 to see when the disease would die out of the system.

From **Figure 2**, we can see that the higher the vaccination cover in the population, the lesser the susceptibility to the measles disease in the population. Some significant fraction of the population remains susceptible to measles at a 20% yearly vaccination cover after ten-year span. This means then that in the wake of an outbreak there would still be some that would be impacted by the disease. At a 40% vaccination cover yearly, the susceptible individuals reduce sharply. The same can be said of a vaccination cover of 60% and 80% vaccination cover. It can be drawn from here that when vaccination cover is aimed at 80%, the number of susceptible individuals approaches zero.

In **Figure 3**, it can be seen that awareness of the disease is already in the population and control steps for treatment and vaccination do not allow for an outbreak to get worse before it becomes better. It can be seen that no matter the

Table 1. Parameter and variable definition & values.

Parameters	Value	Sources
α	0.045	GHS & GIS
μ	0.00875	GHS
μ_E	0.0111	GHS
β	0.005	Estimated
σ	0.9913	Estimated
γ	0.9912	Estimated
δ_E	0.015	Assumed
τ	0.0025	Assumed
ϵ	0.0003	Assumed
$S_0(**) = y1\_0(*)$	10000	Assumed
$E_0(**) = y2\_0(*)$	3000	Assumed
$I_0(**) = y3\_0(*)$	326	Assumed
$R_0(**) = y4\_0(*)$	2965	Assumed

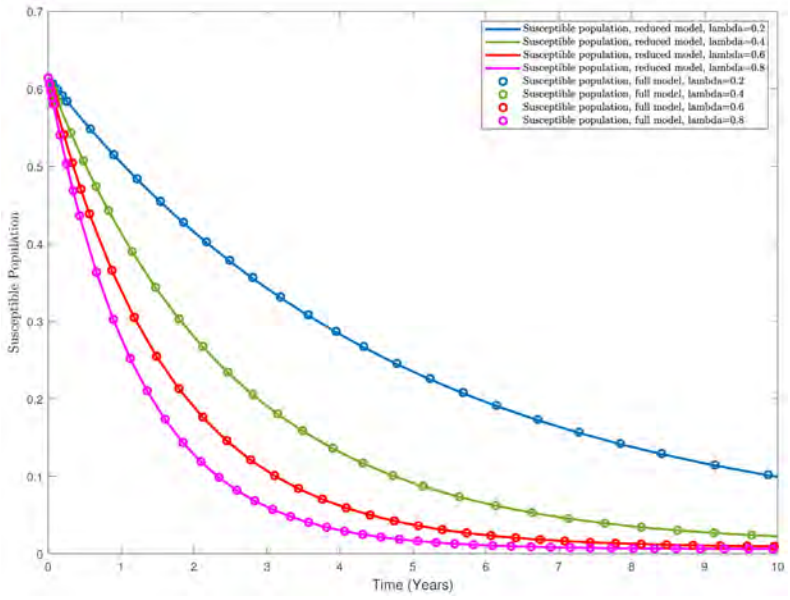

Figure 2. Plot of the susceptible individuals with time.

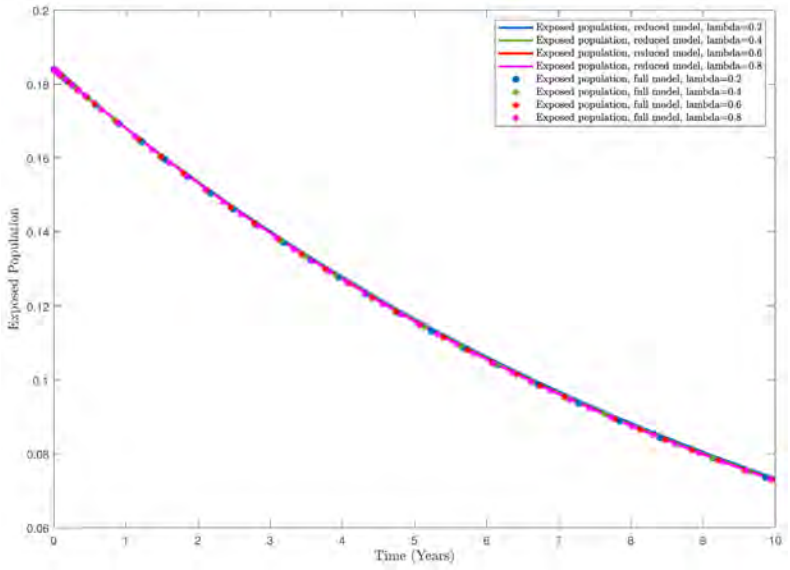

Figure 3. Plot of the exposed individuals with time.

vaccination cover in the population, the disease will persist in the population for a while and die out. When the time is extended, it would be seen that the disease will completely die out of the system as the exposed individuals approaches zero. It makes sense because, from the schematic diagram (4.1) of the model, the exposed individuals are assumed to go through the infectious stage or attained a natural cure against the disease and move into the recovery stage. Again, we see that the full model and the reduced model are the same.

In Figure 4 also, with time, measles would no longer be seen in the population. At any level of vaccination cover, the disease will die out of the population. Only that, at a higher vaccination rate, more susceptible individuals

do not have to get the disease but will gain a strong immunity against the disease.

In Figure 5, the higher the vaccination rate, the more susceptible individuals gain immunity against the disease so that more people fall into the safe haven of being recovered. But it can be seen at 60% vaccination cover is comparable to an 80% vaccination cover. It would therefore be a good practice if vaccination in a population whose system can be compared to that which is studied in this paper vaccinate 80% of its people, newborns and new immigrants so that in any case of an outbreak of measles, the disease will be eradicated in the shortest possible time.

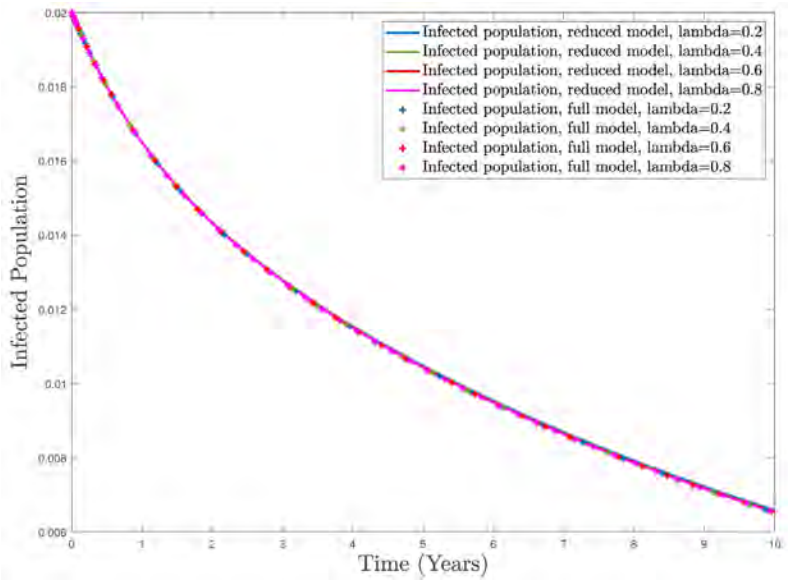

Figure 4. Plot of the infectious individuals with time.

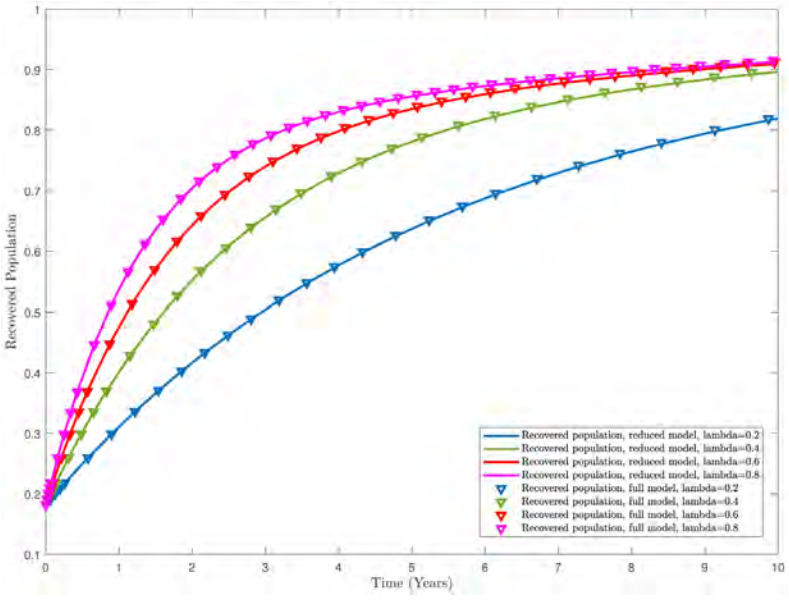

Figure 5. Plot of the recovered individuals with time.

6. Conclusion

In this paper, the global dynamics of measles has been studied in a varying population system such as could be compared to the thriving metropolis of Sunyani in Ghana. A matrix theoretic method and Goh-Volterra types of Lyapunov function were used to establish the stability of the disease-free and endemic equilibria respectively. The basic reproductive number R_0 is defined using the New Generation Matrix method and proved as the threshold parameter. The DFE is globally stable whenever $R_0 \leq 1$ and unstable otherwise. The EE is globally stable when $R_0 > 1$. Also, the transformation of the original system (1) uncovered some unnecessary measures embedded in the model which was removed to give the approximate system (6). The latter system was used to replace the former and towards the end of this paper, we showed by numerical simulation that approximate system (3) is the same as (6). The numerical simulation also showed the theoretic dynamics discussed in this paper. It showed that more people will gain immunity against the measles and by extension, an outbreak of measles would not impact the community if vaccination cover is 80% annually.

Conflicts of Interest

The authors declare no conflicts of interest regarding the publication of this paper.

References

[1] Earn, D.J.D. (2008) A Light Introduction to Modelling Recurrent Epidemics. In: *Mathematical Epidemiology*, Springer, Berlin, 317. https://doi.org/10.1007/978-3-540-78911-6_1

[2] Ghana Health Service and UNICEF Encourage Mothers to Deliver with Help from Skilled Birth Attendants UNICEF. https://www.unicef.org/infobycountry/ghana_62444.html

[3] NHS Public Health Functions Agreement 2015-16, Service Specification No. 10 Measles, Mumps and Rubella (mmr) Immunisation Programme. https://assets.publishing.service.gov.uk/government/uploads/system/uploads/attachment_data/file/383184/1516_No10_Measles_Mumps_and_Rubella__MMR__Immunisation_Programme_FINAL.pdf

[4] Shuai, Z. and van den Driessche, P. (2013) Global Stability of Infectious Disease Models Using Lyapunov Functions. *SIAM Journal on Applied Mathematics*, **73**, 1513-1532. https://doi.org/10.1137/120876642

[5] Smith, H.L., Wang, L. and Li, M.Y. (2001) Global Dynamics of an SEIR Epidemic Model with Vertical Transmission. *SIAM Journal on Applied Mathematics*, **62**, 58-69. https://doi.org/10.1137/S0036139999359860

[6] Abdelhadi, A. and Hassan, L. (2013) Optimal Control Strategy for SEIR with Latent Period and a Saturated Incidence Rate. *ISRN Applied Mathematics*, **2013**, Article ID: 706848. https://doi.org/10.1155/2013/706848

[7] Onyejekwe, O.O. and Kebede, E.Z. (2015) Epidemiological Modeling of Measles Infection with Optimal Control of Vaccination and Supportive Treatment. *Applied*

and Computational Mathematics, **4**, 264-274.
https://doi.org/10.11648/j.acm.20150404.15

[8] Henshaw, S. and McCluskey, C.C. (2015) Global Stability of a Vaccination Model with Immigration. *Electronic Journal of Differential Equations*, **92**, 110.

[9] Wang, W., Xin, J. and Zhang, F. (2010) Persistence of an SEIR Model with Immigration Dependent on the Prevalence of Infection. *Discrete Dynamics in Nature and Society*, **2010**, Article ID: 727168. https://doi.org/10.1155/2010/727168

[10] Li, J. and Ma, Z. (2002) Qualitative Analyses of SIS Epidemic Model with Vaccination and Varying Total Population Size. *Mathematical and Computer Modelling*, **35**, 1235-1243. https://doi.org/10.1016/S0895-7177(02)00082-1

[11] Clements, C.J. and Cutts, F.T. (1995) The Epidemiology of Measles: Thirty Years of Vaccination. In: *Measles Virus*, Springer, Berlin, Heidelberg, 13-33.
https://doi.org/10.1007/978-3-642-78621-1_2

[12] Centers of Disease Control (CDC) (1989) Measles Prevention. *MMWR Supplements*, **38**, 1.

[13] Safi, M.A. and Garba, S.M. (2012) Global Stability Analysis of SEIR Model with Holling Type II Incidence Function. *Computational and Mathematical Methods in Medicine*, **2012**, Article ID: 826052. https://doi.org/10.1155/2012/826052

[14] Lahrouz, A., Omari, L. and Kiouach, D. (2011) Global Analysis of a Deterministic and Stochastic Nonlinear SIRS Epidemic Model. *Nonlinear Analysis*: *Modelling and Control*, **16**, 59-76.

[15] Melesse, D.Y. and Gumel, A.B. (2010) Global Asymptotic Properties of an SEIRS Model with Multiple Infectious Stages. *Journal of Mathematical Analysis and Applications*, **366**, 202-217. https://doi.org/10.1016/j.jmaa.2009.12.041

[16] Adewale, S.O., Podder, C.N. and Gumel, A.B. (2009) Mathematical Analysis of a TB Transmission Model with DOTS. *Canadian Applied Mathematics Quarterly*, **17**, 1-36.

[17] Shuai, Z. and Van den Driessche, P. (2011) Global Dynamics of Cholera Models with Differential Infectivity. *Mathematical Biosciences*, **234**, 118-126.
https://doi.org/10.1016/j.mbs.2011.09.003

[18] Peralta, R., Vargas-De-Len, C. and Miramontes, P. (2015) Global Stability Results in a SVIR Epidemic Model with Immunity Loss Rate Depending on the Vaccine-Age. *Abstract and Applied Analysis*, **2015**, Article ID: 341854.
https://doi.org/10.1155/2015/341854

[19] Li, J. and Cui, N. (2013) Dynamic Analysis of an SEIR Model with Distinct Incidence for Exposed and Infectives. *The Scientific World Journal*, **2013**, Article ID: 871393. https://doi.org/10.1155/2013/871393

[20] Weisstein, E.W. (2000) Routh-Hurwitz Theorem. From MathWorld—A Wolfram Web Resource. http://mathworld.wolfram.com/Routh-HurwitzTheorem.html

[21] Li, M.Y., Graef, J.R., Wang, L. and Karsai, J. (1999) Global Dynamics of a SEIR Model with Varying Total Population Size. *Mathematical Biosciences*, **160**, 191-213.
https://doi.org/10.1016/S0025-5564(99)00030-9

[22] Castillo-Chavez, C., Feng, Z. and Huang, W. (2002) On the Computation of RO and Its Role on Global Stability. In: Castillo-Chavez, P.C., Blower, S., Driessche, P., Kirschner, D. and Yakubu, A.-A., Eds., *Mathematical Approaches for Emerging and Reemerging Infectious Diseases*: *An Introduction*, Springer, Berlin, 229.
https://doi.org/10.1007/978-1-4757-3667-0_13

[23] Van den Driessche, P. and Watmough, J. (2008) Further Notes on the Basic Repro-

duction Number. In: *Mathematical Epidemiology*, Springer, Berlin, 159-178.

[24] Guo, H., Li, M. and Shuai, Z. (2008) A Graph-Theoretic Approach to the Method of Global Lyapunov Functions. *Proceedings of the American Mathematical Society*, **136**, 2793-2802. https://doi.org/10.1090/S0002-9939-08-09341-6

Applied Mathematics, 2019, 10, 605-618
http://www.scirp.org/journal/am
ISSN Online: 2152-7393
ISSN Print: 2152-7385

Wrong Use of Averages Implies Wrong Results from Many Heuristic Models

Michael Grabinski, Galiya Klinkova

Department of Business and Economics, Neu-Ulm University, Neu-Ulm, Germany
Email: michael.grabinski@uni-neu-ulm.de, galiya.klinkova@uni-neu-ulm.de

How to cite this paper: Grabinski, M. and Klinkova, G. (2019) Wrong Use of Averages Implies Wrong Results from Many Heuristic Models. *Applied Mathematics*, **10**, 605-618.
https://doi.org/10.4236/am.2019.107043

Received: June 30, 2019
Accepted: July 21, 2019
Published: July 24, 2019

Abstract

In a linear world, averages make perfect sense. Something too big is compensated by something too small. We show, however that the underlying differential equations (e.g. unlimited growth) rather than the equations themselves (e.g. exponential growth) need to be linear. Especially in finance and economics non-linear differential equations are used although the input parameters are average quantities (e.g. average spending). It leads to the sad conclusion that almost all results are at least doubtful. Within one model (diffusion model of marketing) we show that the error is tremendous. We also compare chaotic results to random ones. Though these data are hardly distinguishable, certain limits prove to be very different. Implications for finance can be important because e.g. stock prices vary generally, chaotically, though the evaluation assumes quite often randomness.

Keywords

Mean, Median, Chaos, Finance, Random, Fractals

1. Introduction

Almost everybody knows how to calculate an average or (arithmetic) mean, and its use is widespread. Its interpretation is quite often questionable and sometimes ludicrous, see e.g. [1]. Though such remarks are important, this paper focuses on a different, more mathematical point.

Sometimes an average makes perfect sense. The average weight of an airline passenger times the number of passengers gives a perfect measure for the weight of all passengers. The average size of a screw in a warehouse does not make sense. Probably nobody will be fooled by this extreme example. However, there are more sophisticated examples in [1] like designing the cockpit of a fighter jet in accordance to the height of an average pilot, which turned out to be hardly

existent.

Sometimes the problem is solved by using the median instead of the mean or average. But this is not the point here. The median size of a screw in a warehouse is as useless as its average size. From Chapter 2 one can see that the arithmetic mean is a number that minimizes the sum of the quadratic deviations from all data points. So the actual data points may be bigger or smaller than the average, but the (linear) deviations to the bigger and smaller side are the same. If being bigger than the average can be canceled out by being smaller, an average does make sense. It is the case in the example of the average weight of a passenger. A heavier passenger can be compensated by a lighter one. This is in contrast to screws in a warehouse. One that is too small is as bad as one that is too big.

So the pivotal point is the *use* of the arithmetic mean. In the example of the average weight of an airline passenger, the *use* was to calculate the total passenger load. The total passenger load is a positive real number. The use of the screw was to fit. Such function has only two values: does fit and does not fit. For "does not fit", it is irrelevant whether the screw is too small or too big. Mathematically speaking such a use-function must be strictly linear.

So far for a complicated explanation of a maybe trivial issue. However, most long-term considerations take into account non-linear equations. As an archetype consider exponential population growth. Obviously, it is not a linear function. Its exponent is essentially the birthrate. A larger birthrate implies higher population growth and vice versa, but it is highly non-linear. A ten percent higher birthrate in one part of the population cannot be compensated by a ten percent lower one in another one. However, almost everywhere an average birthrate is used to forecast the future population. Chapter 3 scrutinizes this example. Surprisingly, one may use average birthrates in the normal (unlimited) population growth formula. In Chapter 3 we prove generally that average parameters such as average birthrates can be used in linear differential equations only.

A further application are financial markets. Mankind is far away from having proper differential equations determining the future profit of a company and with it the future stock price. However, people try to build estimates. In these calculations, one uses averages from mean inflation over mean spending on R & D to mean productivity of the employees. Everything else would make the considerations impossible for practical reasons as it is not possible to consider and determine millions of variables. However, nobody doubts that the financial word is governed by non-linear differential equations. If it was not, the solutions would have to be plane waves in contrast to all observations. We will discuss this in more detail in Chapter 4. It leads to the sad conclusion that almost all quantitative analyses in financial markets are at least doubtful.

In Chapter 5 we will consider the diffusion model in marketing, a mathematical tool to forecast the future market share. There, also average quantities are used. And due to that, one (sometimes) gets completely wrong results. Even chaos effects have been predicted [2] though they do not exist [3]. In Chapter 5

we also show how one can use a continuum limit to overcome the problem of knowing average parameters only. It is quite important to notice that in almost all financial models a continuum limit is not possible. This has been stated for the first time in [4]. It is due to the fact that typical financial data such as e.g. stock prices are, unlike the market share, not conserved. This led to the suggestion of a conserved value [5] in finance. Eventually it has been proven mathematically in [6].

We close with a look to further research in Chapter 6. Here we consider chaos in contrast to randomness. Though chaos appears random, it is not. However, it *seems* so random that chaotic functions are sometimes used to create "random" numbers. Building arithmetic means in chaotically varying quantities sometimes (but not always) gives identical results to random variations as one might expect. But sometimes it does not. This is an open question. It is of special relevance whenever something varies chaotically such as prices in financial markets. Is a statistical analysis allowed at all? Can one modify ordinary statistics in order to cope with it?

2. Definition of Mean and Median

It is assumed that arithmetic mean (here also called average) and median are well-known to any potential reader of this publication. Else it can be found in any mathematical handbook such as [7]. Here we take a route different from most textbooks. It is important to understand what mean and median means.

Given is a set of real number x_i with i running from 1 to N. We *define* the average $\langle x \rangle$ as a number so that

$$\sum_{i=1}^{N} \left(x_i - \langle x \rangle \right)^2 \to \text{minimal} \tag{1}$$

To find this minimum, Equation (1) can be differentiated with respect to $\langle x \rangle$ and set to zero. It leads to the well-known formula for the average

$$\langle x \rangle = \frac{1}{N} \sum_{i=1}^{N} x_i \tag{2}$$

The average is therefore a special least square fit. The data points are fitted by a constant. As with the least square fit, taking the squares in Equation (1) is by no means justified. It is practical for getting positive numbers and keeping an analytic function. However, it is arbitrary. Why not take the fourth power? Taking squares makes small numbers smaller and larger ones larger. The error of a least square fit is given by Equation (1). This does not make sense if the x_i have a dimension such as €. The error thus has the dimension €² which has no meaning. Taking the square root of Equation (1) does not help either. Squares and roots are non-linear functions which must not be interchanged with the sum. Therefore, the least square fit is an approximation only. A least absolute value fit is the correct procedure. However, dealing with it becomes horribly complicated, and the result can be obtained numerically only in most cases. This is the reason why a least square fit is so popular though strictly speaking it is

wrong. The difference between a (wrong) least square fit and the (correct) absolute value fit is small in many cases. However, if the data points are varying over orders of magnitude (e.g. in exponential growth) the error becomes significant. This logic brings us to the definition of the median:

Given is a set of real number x_i with i running from 1 to N. We *define* the median $\{x\}$ as a number so that

$$\sum_{i=1}^{N}\left|x_i-\{x\}\right| \to \text{minimal} \tag{3}$$

Equation (3) is a non-analytic function of $\{x\}$. Of course, the minimum can be determined. One way is to use differentiation *carefully*: differentiating from the right and left, respectively, at non-analytic points. Either way the minimization problem of Equation (3) has the solution

$$\sum_{i=1}^{N}\operatorname{sgn}\left(x_i-\{x\}\right)=0 \tag{4}$$

where sgn denotes the signum function defined as −1 for negative arguments, +1 for positive ones and zero else. As one sees, $\{x\}$ must be in "the middle" of the numbers x_i in order to fulfill Equation (4). $\{x\}$ is therefore exactly what one calls median.

Mean and median are least square fits or least absolute value fit, respectively, where the fit function is a constant. In order to find means or medians for a continuous distribution one has to change the sum signs into integrals.

From this definition of mean and median it becomes clear that the use of mean and median is not optional depending on the situation. Median is the correct way and mean is the approximation. If median and mean are similar, mean is a good approximation. However, sometimes mean gives something *exact*. Knowing the mean weight and the number of passengers, one knows the exact weight of all passengers combined. This may be practical, but it has nothing to do with a statistical interpretation, what mean and median are meant for.

3. Why the Underlying Differential Equation Must Be Considered

In this chapter we want to show that averages can be used even in non-linear functions as long as the underlying differential equation is linear. As a starting example consider the formula for unlimited population growth:

$$N(t)=N_0\cdot \mathrm{e}^{(b-\beta)\cdot\frac{t}{\tau}} \tag{5}$$

$N(t)$ denotes the population at a time t and N_0 is the population at $t=0$. b is the birth rate (number of children per woman) and β is the birthrate when the population stays constant (typically $\beta\approx 2.1$). τ is a constant depending essentially on the lifespan of the population. Because $N(t)$ depends exponentially on the birthrate b, it appears doubtful to use an average birthrate. Some years ago we used Equation (5) as an exercise for graduate students: Half of the population has a birthrate $b=0$ and half of it $b=2\beta$. On average it

yields $\langle b \rangle = \beta$. Of course, the population does not stay constant, because only in the beginning $\langle b \rangle = \beta$ holds. Half of the population becomes extinct and the other half is reproducing rapidly. In a properly weighted average we have a time dependent average birthrate of

$$\langle b \rangle(t) = \beta \cdot \left(1 + \tanh\left(\beta \cdot \frac{t}{\tau}\right)\right) \text{ with } \tanh(x) \equiv \frac{e^{x} - e^{-x}}{e^{x} + e^{-x}} \tag{6}$$

Of course, one must not insert $\langle b \rangle(t)$ of Equation (6) directly into Equation (5). Equation (5) is the solution of the differential equation

$$\frac{dN(t)}{dt} = \frac{b - \beta}{\tau} \cdot N(t) \tag{7}$$

So one has to insert the $\langle b \rangle(t)$ of Equation (6) for b into Equation (7). The solution is:

$$N(t) = N_0 \cdot \cosh\left(\beta \cdot \frac{t}{\tau}\right) \text{ and } \cosh(x) \equiv \frac{1}{2} \cdot \left(e^{x} + e^{-x}\right) \tag{8}$$

If one took a realistic growth model with e.g. limited growth, the corresponding differential equation would be non-linear. A weighted average like in Equation (6) will not be possible in that case. This is an important information for any person dealing with population growth or decrease. Such people use much more sophisticated models compared to Equation (7). Their differential equations are non-linear in almost all cases. Nevertheless they use average birth rates only. So their results are generally wrong—yet it is hard to tell by how much. In order to check, one must have the distribution of birthrates. Such distributions cannot be found in statistical data banks. It is left to the reader to try some examples or it would be an exercise for advanced graduate students. In what follows we will prove that the linearity of the underlying differential equation is essential for using averages.

Instead of Equation (7) we use a very general model for a function $f(x)$:

$$f'(x) = g\left(f(x)\right) \tag{9}$$

In a linear model, $g(f) = a \cdot f$ holds. The function g corresponds to the parameters of the differential equation. Without limitation we are just considering two functions g_1 and g_2. If we are able to prove that the averaging is wrong for all non-linear functions, we have for sure shown that it will not work out for more than two functions. Furthermore, our proof can be extended easily to an arbitrary number of functions. Therefore we consider only two functions:

$$f_1'(x) = g_1\left(f_1(x)\right) \text{ and } f_2'(x) = g_2\left(f_2(x)\right) \tag{10}$$

Needless to say that the functions g are analytic functions. Therefore a Taylor expansion is possible:

$$g(f) = a^0 + a^1 f + a^2 f^2 + \cdots = \sum_{i=0}^{\infty} a^i f^i \tag{11}$$

Please note that the a's in Equation (11) have upper indices rather than exponents in contrast to the f's in Equation (11). For the average f one can write by

using Equations (10) and (11).

$$\begin{aligned}\langle f\rangle' &= \frac{f_1'(x)+f_2'(x)}{2} = \frac{1}{2}\left(\sum_{i=0}^{\infty} a_1^i f_1^i + \sum_{i=0}^{\infty} a_2^i f_2^i\right)\\ &= \sum_{i=0}^{\infty} \frac{a_1^i f_1^i + a_2^i f_2^i}{\left(\frac{1}{2}\right)^{i-1}(f_1+f_2)^i}\left(\langle f\rangle\right)^i\end{aligned} \tag{12}$$

On the other hand, the average coefficient $\langle a^i\rangle$ is given by

$$\langle a^i\rangle = \frac{a_1^i\cdot f_1 + a_2^i\cdot f_2}{f_1+f_2} \tag{13}$$

Comparing with the average coefficient from Equation (12) we have the following equation to hold:

$$\frac{a_1^i f_1^i + a_2^i f_2^i}{\left(\frac{1}{2}\right)^{i-1}(f_1+f_2)^i} = \frac{a_1^i\cdot f_1 + a_2^i\cdot f_2}{f_1+f_2} \tag{14}$$

Equation (14) is equivalent to

$$a_1^i f_1^i + a_2^i f_2^i = \left(a_1^i\cdot f_1 + a_2^i\cdot f_2\right)\cdot 2^{i-1}\cdot(f_1+f_2)^{i-1} \tag{15}$$

Because the different powers of f in Equation (15) are linearly independent, all corresponding powers must fulfill Equation (15) separately. This is generally impossible except we have only one exponent $i=1$. In other words, the Taylor expansion of g contains only the linear term. This concludes the proof that only in linear differential equations averages can be used.

In this chapter we have shown that averages can be used even in non-linear equations as long as the underlying differential equation is linear. It is a plausible result, because the differential equation governs the situation. If it is linear, averages are fine to use. The solution of the differential equation is just the sum (integral) of the underlying microscopic interactions. If each interaction may use averages, so does its sum.

4. Financial Markets

Finance is far away from having models like population growth. At most one has heuristic models. The goal is to predict prices or at least probabilities for it. These models have grown more and more complex. The ultimate model has not been established, and the authors are convinced that it will never be (For more details see below and also [3] or [6]). However, there is no doubt that these models will consist of non-linear differential equations. If the governing differential equations were linear, their solutions would be plane waves. This is in contrast to any observation of financial data. Furthermore, the used "tools" are based on non-linear differential equations in most cases. Just as an example consider the Black-Scholes model [8]. It is a model for pricing options. The details are not important here, but it is a non-linear (partial) differential equation. (There are many more such models, also or especially in quantitative economics,

see e.g. [9]).

In order to use these models one needs parameters such as inflation rates, interest rates, investments for e.g. R & D, and so forth. For all these parameters one uses averages. Some are even defined as averages such as the inflation of a basket of goods over a year. Everything else would be virtually impossible. One would have to consider a huge number of variables changing every day or maybe every second. At first glance averaging appears reasonable because there is an interest in e.g. average prices. However, we have shown in Chapter 3 that one must not use average quantities in non-linear differential equations.

We come to the sad conclusion that almost all work in finance and quantitative economics suffers from these shortcomings. That such (wrong) calculations lead to at least sometimes correct results is of course far from being a justification: Ex falso quodlibet![1] Especially in finance there maybe also some herd effect if sufficiently many people believe in a certain model. Then it is nothing but a self-fulfilling prophecy, e.g. cf. [10].

However, there are many more shortcomings besides using averages in non-linear differential equations. There exist plenty of additional variables than usually considered and these variables appear to be important. It leads to the almost ludicrous result that the weather on Wall Street is an essential influencer on stock prices [11]. This comes as no surprise as it has been proven that prices of most financial products vary chaotically [12]. Within chaos tiny changes in seemingly unimportant parameters have big effects in the end. Therefore, financial markets work similarly to gambling. However, it is not considered gambling. Else there would be regulations to give the same odds to anybody.

To overcome these difficulties one has to:

- Use individual data instead of averages.
- Use many more presently unknown variables.
- Know any parameter/variable up to an extremely high accuracy due to chaos.

That is the reason why the authors are convinced that there will never be a proper model for financial markets. Please be aware that "extremely high accuracy" is quite often much more than 10^{1000} digits. From this, another problem arises. A computer has to perform these highly accurate calculations. In a very simple chaotic situation as mentioned in Chapter 6, we estimate calculation times of 10^{276} times the age of the universe on a 3.5 GHz processor. Even quantum computing would not help because it is currently *only* 100 million times faster than an ordinary computer. Our very simple chaotic calculation would still take 10^{268} times the age of the universe.

Calculating next week's lottery numbers is comparably simple to the above. That is the main reason why considering conserved values has been suggested in [5] and proven in [6]. By using it, all problems disappear. However, gaining

[1]It is not possible to show the exact margin of error due to averaging without considering a particular model. Even then we do not know the correct result in order to calculate an error. As the mathematical expression *ex falso quodlibet* indicates, making a wrong assumption can "prove" *anything*. 1 = 2 implies not only 2 = 3 but also $10^{30} = 0$.

money due to trading financial products will also disappear. This comes as no surprise as such trading is nothing but a special form of gambling [12].

Furthermore, it is important to note that prices of financial products vary chaotically. As we will explain in Chapter 6, it will make use of statistics (e.g. averages) not without flaws.

5. Diffusion Model in Market Forecast

In this chapter we will comment on the use of the diffusion model of marketing. It is a tool for forecasting the future market share. Using averages in this model may lead to completely wrong results under certain circumstances [2]. However, here we can present a way out by using a continuum limit, which is the reason why we comment on this particular model. Unfortunately, the continuum limit cannot be applied to the world of finance because stock prices and the like are not conserved quantities.

The use of the diffusion model in marketing started in the 1960 and it is used ever since. There are several versions. We will consider the so-called logistic diffusion model. It is an iterating formula calculating the market share N_t at time t from the market share N_{t-1} at time $t-1$. The main idea behind it is that the product diffuses into the market, like the smell of sold waffles in a shopping mall attracts more customers. The formula of the logistic diffusion model takes the form

$$N_t = b \cdot N_{t-1} \cdot \left(M - N_{t-1}\right)$$

b is a diffusion constant. A large b means that one will gain market share rapidly, and a small b implies slow growth or even shrinking. The constant M in the term $M - N_{t-1}$ is the natural limitation. Else the market share will grow to infinity, which is unrealistic. It is similar to a growth limitation in a realistic growth model. From a mathematical point of view, one may always set $M = 1$. In doing so, one will get the following formula for the logistic diffusion model, which has also been used in [2]:

$$N_t = b \cdot N_{t-1} \cdot \left(1 - N_{t-1}\right) \tag{16}$$

If b approaches a certain value (≈3.5699) something strange happens. N is changing very rapidly and seemingly randomly between 0 and 1. This comes as no surprise since Equation (16) is nothing but the logistic map, cf. Equation (19) of Chapter 6. This has been described as *the end of the diffusion model* in [2]. But how can it be? Why is the market share "jumping" if it is growing sufficiently fast? How can a market share change chaotically though it is a conserved quantity?[2] Why is the market share varying between $-\infty$ and $+\infty$ for $b > 4$?

As already mentioned in [2], the constant b of Equation (16) is generally speaking a different one for each customer buying or not buying something. So one would probably have millions of different constants b. With such a huge number of fit parameters reality is described perfectly. On the sad side, it would

[2]Admittedly conserved quantities in this sense were first mentioned in 2011 in [5], many years after 1993 when [2] has been published.

make forecasts impossible by using Equation (16). Nobody can estimate so many parameters. Therefore, one uses an average b in Equation (16). However, with the same proof as in Chapter 2 (but much simpler) one can show that one must not use averages in Equation (16). Using numbers one will find, however, that for small values of b there is only a minor error. If b is approaching 4, the error becomes huge. As a conclusion, using an average b in Equation (16) produced the in reality not existing chaos effects. This is a good example to show that using averages may produce tremendous errors. The huge error has to do with the fact that Equation (16) shows chaos in a mathematical sense. Though we cannot calculate the corresponding error in the financial world (as argued in Footnote 1), it is assumed to be very large due to the fact that chaos is also present in e.g. stock prices [12].

Unlike the models of finance of the last chapter, in this example one can easily overcome the problem of using averages. The approach is the same as in diffusion in the physical world. The analog to Equation (16) is called the ballistic regime. There single molecules are considered. They scatter on each other or with other molecules. Depending on the details of each scattering the exchange of energy and momentum within each scattering is different. It makes thorough considerations next to impossible in the same way one cannot use Equation (16) with many different b. Because the number of molecules, the exchanged energy and momentum are conserved quantities, one may take averages over long time spans and long distances. The time spans and distances have to be so large, that within them many scatterings will take place, so that one can consider the average exchange of momentum and energy. Taking also into account symmetry considerations, this will lead to what is called hydrodynamics in physics.

Unfortunately, a similar approach is not possible in finance if one considers stock prices and the like. These are non-conserved quantities. The problem was first addressed in [4] and let to further research and eventually to the definition of a conserved value in finance and economics ([5], [6]).

The market share is a perfectly conserved quantity. If the market share of one person or company goes up, it must go down somewhere else accordingly. Building upon this, it is now easy to perform a continuum limit in Equation (16). Details can be found in [3], though it can be considered common sense. Equation (16) transforms into a differential equation:

$$\frac{\mathrm{d}N(t)}{\mathrm{d}t} = (b-1)\cdot N(t) - b\cdot N(t)^2 \tag{17}$$

Unlike Equation (16) one can easily solve Equation (17) in a closed form:

$$N(t) = \frac{N(0)\cdot(b-1)\mathrm{e}^{bt}}{\left(b\cdot(1-N(0))-1\right)\mathrm{e}^{t} + b\cdot N(0)\cdot\mathrm{e}^{bt}} \tag{18}$$

For small values of b the iterative solution of Equation (16) gives almost an identical result compared to Equation (18). Of course, Equation (18) is reasonable for any (positive) value of b. Similar formulas for other diffusion models and

also for $M \neq 1$ are easily obtained in the same way or can be found in [3]. Though there is no chaos within a properly used diffusion model, chaos effects may be present in market forecast. As it is impossible that the market share itself varies chaotically, the time to reach that market share can vary chaotically, because time is no conserved quantity.[3] The diffusion model of marketing has an artificial time variable because each time step has the length one. However, there are other market forecast procedures such the one suggested in [13]. There one explicitly determines the market share and the time to reach it. Depending on the detailed numbers, one may or may not find chaos effects. In the example in [3] they are explicitly proven.

So we can conclude that the never is chaos within the diffusion model. The wrong usage of averages seemingly produced chaos effects. Though one cannot show that the wrong use of averages produces a similar tremendous effect in finance, it is at least highly plausible.

6. Further Research

The purpose of this last chapter is to give some general remarks about the often mentioned word chaos. It is especially puzzling that chaotic variations appear so randomly that one can use them to produce random numbers. However, there are differences which we will point out. Hausdorff dimension or the Lyapunov exponent (see e.g. [7] or [14]) are the correct tools to evaluate chaos besides its random look. They clarify and quantify the difference between chaos and randomness. Unfortunately, they can only be used if the chaotically varying variable is given by a mathematical formulation (equation). It is impossible to use them by considering a finite number of data points. Though we know at least from [12] that stock prices are varying chaotically in many cases, we cannot see chaos in the stock prices quoted at the stock exchange. Evaluating them statistically is therefore far from being flawless with no solution at hand. Therefore we leave it to further research. Here we are just explaining the problem.

Chaos effects are known to mathematicians for more than a century. In the 1960 Edward Lorenz found that long term weather forecast is impossible due to chaos (butterfly effect). In the 1980 it has become common in physics. Starting from the 1990 it has been scrutinized in business and economics. Just as an example consider [15] or [16]. Furthermore, chaos has also be used to explain less quantitative but nevertheless important things like the origin of war. In this context the phrase "drop of honey effect" has been framed in [17].

In this chapter we will introduce the maybe simplest mathematical model which shows chaos. It is the logistic map:

$$f_a(x,n) = a \cdot f_a(x,n-1) \cdot \left(1 - f_a(x,n-1)\right) \tag{19}$$

Equation (19) is mathematically identical to the logistic diffusion model of

[3]The chaos effects in the weather forecast show the same behavior. As the amount of rain is a conserved quantity, it is well predictable. The exact time when (and where) the rain starts is by no means conserved. And indeed this time is practically unpredictable over a sufficiently long time period.

Equation (16). We have $x \in [0,1]$ and $n \in \mathbb{N}$ as an iteration index. Starting with $f_4(0.6,0) = 0.6$ we will have $f_4(0.6,1) = 0.96$, $f_4(0.6,2) = 0.1536$, $\cdots$, $f_4(0.6,999) \approx 0.81141$, and $f_4(0.6,1000) \approx 0.61209$. The first iterations are obtained easily. The last ones are already much more complicated. Typically one has to take into account 10^{300} digits in order to get the correct results. These 1,000 numbers look like random numbers between 0 and 1. Indeed one finds

$$\frac{1}{1000} \cdot \sum_{n=1}^{1000} f_4(0.6,n) \approx 0.5055$$

and also a nearly perfect equal distribution. One can also plot e.g. $f_4(x,1000)$ as a function of *x*. It looks identical to plotting a random number.

The strange (chaotic) behavior will start at $a \approx 3.5699$ and is fully developed at $a = 4$. $a > 4$ leads to a divergence. For $a = 4$ one can show by e.g. complete induction that

$$f_4(x,n) = \frac{1}{2} \cdot \left(1 - \cos\left(2^n \cdot \arccos(1 - 2 \cdot x)\right)\right) \tag{20}$$

Equation (20) makes it possible to calculate the 1,000 values of $f_4(0.6,n)$ within a quite short computing time. Using Equation (19) directly, which is necessary if e.g. $a = 3.9$ is chosen, one needs *10^{276} times the age of the universe* as mentioned in Chapter 4. Please note that for any finite *n* Equations (19, 20) are strictly speaking non-chaotic, though they look very chaotic for e.g. $n = 1000$. Only for $n \to \infty$ real chaos is present in a mathematical sense. One can also calculate the average of $f_4(x,n)$ in the limit $n \to \infty$. As expected one will get

$$\frac{1}{y} \cdot \lim_{n \to \infty} \int_0^y \mathrm{d}x \, f_4(x,n) = \frac{1}{2} \tag{21}$$

It proves that there really is an equal distribution of the functional values between 0 and 1.

In order to see the difference between randomness and chaos we will introduce two common methods to detect chaos mathematically. The first is the Lyapunov exponent, which one will find in most textbooks about chaos such as [14]. The Lyapunov exponent $\lambda(x)$ is defined as

$$\lambda(x) = \lim_{n \to \infty} \frac{1}{n} \ln \left| \frac{\mathrm{d}f(x,n)}{\mathrm{d}x} \right| \tag{22}$$

Equation (22) holds for every function *f* not just the logistic map. However, *f* must be an iterative function. $\lambda > 0$ means chaos. By inserting f_4 from Equation (20) into Equation (22) the Lyapunov exponent for the logistic map ($a = 4$) is easily calculated to $\lambda = \ln(2) \approx 0.693$. It is (almost) independent of *x*. For certain values of *x* the logistic map will give 0 after a finite number of iterations. The values are:

$$x = \frac{1}{2}\left(1 - \cos\left(\frac{\pi}{2^m}\right)\right) \; m \in \mathbb{N} \Rightarrow \lambda \to -\infty \tag{23}$$

As f_4 becomes a constant function after a finite number of operations, the

differentiation in Equation (22) gives zero and the logarithm minus infinity.

Because an iterative function is a function of a function of a function …, and so forth, one may apply the chain rule for the differentiation in Equation (22) yielding a product. The logarithm transforms the product into a sum. After some rearrangement one finally gets

$$\lambda(x) = \lim_{n\to\infty} \frac{1}{n} \sum_{i=1}^{n} \ln \left| \frac{\mathrm{d}f\left(f\left(x, n-i\right), 1\right)}{\mathrm{d}f\left(x, n-i\right)} \right| \tag{24}$$

Inserting for f the logistic map of Equation (19) yields

$$\lambda_{\log\,\mathrm{map}}(x) = \ln a + \lim_{n\to\infty} \frac{1}{n} \sum_{i=1}^{n} \ln \left| 1 - 2 \cdot f\left(x, n-i\right) \right| \tag{25}$$

Equation (25) is the only reasonable way to calculate the Lyapunov exponent of the logistic map for $a \neq 4$. Please note that a numerical calculation of the Lyapunov exponent for $a \neq 4$ via Equation (25) is numerically still *very* challenging. For $a = 4$ we know from above that Equation (25) will yield $\ln(2)$. The $f\left(x, n-i\right)$ in Equation (25) look like random numbers between zero and one as stated above. So one might come up with the idea to calculate the Lyapunov exponent of random numbers via Equation (25). Naively trying it, one will get a result around 0.4. More careful considerations show that the limit in Equation (25) does not exist for random numbers. This has to do with the fact that random numbers come arbitrarily close to 0.5. Avoiding the values for x given in Equation (23), the values of the logistic map may come close to 0.5 but not arbitrarily close.

So we have shown that the limit of Equation (25) does exist for a chaotically varying f. It is $\ln(2)$ for $a = 4$. Using the seemingly identical varying random numbers yields a non-existing limit in Equation (25). Here the explanation for it is easy as stated in the last paragraph. However, having numerical data like e.g. stock prices one has to decide: Is it a random variation or a chaotic one? For sure any limits one will build may be completely different.[4] If one decides for a chaotic variation, one has to know how this chaos works. As stated, Lyapunov exponents are positive when chaos is present, but they may take any value.

Scrutinizing some measured data not being created by a known (or assumed) mathematical procedure is therefore highly risky. Ordinary statistics is at least doubtful. Therefore we called this last chapter *further research*, though it appears to be far from straight forward.

As mentioned above there is a second method to quantify chaos. The results there do not have the same dire consequences for finance as we got from considering the Lyapunov exponent. It may be however important for engineering and related sciences. The next method is the Hausdorff dimension. Its detailed definition can be found in any advanced textbook such as [7] or [14]. Though the Hausdorff dimension is defined in any spatial dimension, we here just consider two dimensions. In a two-dimensional plane one may have objects of dimension 0 (dots), dimension 1 (lines or curves), or dimension 2 (e.g. a filled triangle). The Hausdorff dimension is a generalization of this approach which al-

[4]Please note that a differentiation, integration, or Fourier transformation also implies building limits.

lows non-integer dimensions. Its definition goes as follows. One has to cover the objects in a plane with N circles of diameter l. When l goes to zero, N will go to infinity—at least in most cases. In that limit one may write

$$N(l \to 0) = A \cdot \left(\frac{1}{l}\right)^D \tag{26}$$

The exponent D determines how fast the number of circles goes to infinity. It is called the Hausdorff dimension. If one has M dots in a plane, one needs M circles to cover the dots. So with $A = M$ and $D = 0$ Equation (26) is fulfilled. The Hausdorff Dimension is in this case identical to the ordinary dimension. Considering a square with side length c, Equation (26) is fulfilled for $A = c^2$ and $D = 2$ as it should because a square is a two-dimensional object.

In order to get non-integer Hausdorff dimensions, consider $f_4(x,n)$ from Equation (20). For any finite n it is a curve oscillating 2^n times up and down between 0 and 1. This line has a Hausdorff dimension of 1. Taking the limit $n \to \infty$ is slightly tricky but a rigorous calculation yields $D = 4/3$ [18]. So in the limit $n \to \infty$ $f_4(x,n)$ from Equation (20) becomes truly chaotic showing a fractal dimension. A fractal dimension is a rigorous proof of chaos like a positive Lyapunov exponent. Please note that a positive Lyapunov exponent and a fractal Hausdorff dimension both prove chaos, but there is no algebraic connection between them, because the Hausdorff dimension is a global measure while the Lyapunov exponent depends on the variable (here x).

Instead of considering $f_4(x, n \to \infty)$ from Equation (20) one may consider a function mapping the interval $(0,1)$ to a random number between 0 and 1 (and 1 and 0 to 0). As stated, this function *looks* identical to $f_4(x, n \to \infty)$. However, it is a filled square having a Hausdorff dimension of 2. So we have a second difference between randomness and chaos. In this case we have $D = 2$ or $D = 4/3$, respectively.

As a result, chaotically varying quantities look random. Some limits and averages are identical whether random numbers or chaotically varying ones are considered. Others are completely different such as e.g. Lyapunov exponent or Hausdorff dimension. A statistical analysis of experimental data such as stock prices is therefore generally impossible, because one does not know whether they are random or chaotic. Even if one has proven or at least has assumed chaos, it is impossible to decide the mathematical form of this chaos such as its Lyapunov exponent or Hausdorff dimension.

Acknowledgements

We are indebted to our colleague Sascha Fabian who showed in his lectures that averages are sometimes complete nonsense. He also gave us the hint to [2] where chaos effects in the diffusion model are discussed.

Conflicts of Interest

The authors declare no conflicts of interest regarding the publication of this paper.

References

[1] Rose, T. (2017) The End of Average. Penguin Books, London.

[2] Weiber, R. (1993) Chaos: Das Ende der klassischen Diffusionsmodellierung. *Marketing ZFP*, **1**, 35-46. https://doi.org/10.15358/0344-1369-1993-1-35

[3] Klinkova, G. (2018) The Effects of Chaos on Business Operations, PhD Thesis, Neu-Ulm. http://uni-neu-ulm.de/Klinkova_PhD

[4] Grabinski, M. (2004) Is There Chaos in Management or Just Chaotic Management? Complex Systems, Intelligence and Modern Technology Applications, Paris. http://www.h-n-u.de/Veroeffentlichungen/CSIMTA%202004.pdf

[5] Appel, D. and Grabinski, M. (2011) The Origin of Financial Crisis: A Wrong Definition of Value, *PJQM*, **2**, 33-51. http://www.h-n-u.de/Veroeffentlichungen/PJQM_2_I_2011.pdf

[6] Klinkova, G. and Grabinski, M. (2017) Conservation Laws Derived from Systemic Approach and Symmetry. *The International Journal of Latest Trends in Finance and Economic Sciences*, **7**, 1307-1312. http://h-n-u.de/systemic.pdf

[7] Bronshtein, I.N., Semenddyayev, K.A., Musiol, G. and Muehlig, H. (2007) Handbook of Mathematics. 5th English Edition, Springer, Berlin Heidelberg.

[8] Black, F. and Scholes, M. (1973) The Pricing of Options and Corporate Liabilities. *Journal Political Economy*, **81**, 637-654. https://doi.org/10.1086/260062

[9] Sato, R. and Ramaschandran, R.V. (2014) Symmetry and Economic Invariance. Springer, New York.

[10] Appel, D., Dziergwa, K. and Grabinski, M. (2012) Momentum and Reversal: An Alternative Explanation by Non-Conserved Quantities. *The International Journal of Latest Trends in Finance and Economic Sciences*, **2**, 8-16. http://www.h-n-u.de/Veroeffentlichungen/momentum.pdf

[11] Saunders, E.M. (1993) Stock Prices and Wall Street Weather. *American Economic Review*, **83**, 1337-1345.

[12] Klinkova, G. and Grabinski, M. (2017) Due to Instability Gambling Is the Best Model FOR Most Financial Products. *Archives of Business Research*, **5**, 255-261. https://doi.org/10.14738/abr.53.3029

[13] Klinkova, G. and Grabinski, M. (2012) Learning Curves with Two Frequencies for Analyzing All Kinds of Operations. Yasar University Publication, Bornova. http://www.h-n-u.de/Veroeffentlichungen/learning.pdf

[14] Schuster, H.G. (1984) Deterministic Chaos. Physik Verlag, Weinheim.

[15] Filipe, J.A., Ferreira, M.A.M., Coelho, M. and Pedro, M.I. (2010) Chaos, Anti-Chaos and Resources: Dealing with Complexity. *Aplimat-Journal of Applied Mathematics*, **3**, 83-90.

[16] Ferreira, M.A.M., Filipe, J.A., Coelho, M. and Pedro, M.I. (2010) Chaos Effect in Fisheries Management. *Journal of Economics and Engineering*, **2**, 36-43.

[17] Filipe, J.A. and Ferreira, M.A.M. (2013) Social and Political Events and Chaos Theory—The "Drop of Honey Effect". *Emerging Issues in the Natural and Applied Sciences*, **3**, 126-137.

[18] Grabinski, M. (2018) Calculations of Lyapunov Exponent and Hausdorff Dimension. (Unpublished)

Applied Mathematics, 2019, 10, 619-625
http://www.scirp.org/journal/am
ISSN Online: 2152-7393
ISSN Print: 2152-7385

A Study on Exact Travelling Wave Solutions of Generalized *KdV* Equations

Jing Chen

Department of Mathematics, Southwest University of Science and Technology, Mianyang, China
Email: mychenjing2007@sina.com

How to cite this paper: Chen, J. (2019) A Study on Exact Travelling Wave Solutions of Generalized *KdV* Equations. *Applied Mathematics*, **10**, 619-625.
https://doi.org/10.4236/am.2019.107044

Received: June 6, 2019
Accepted: July 26, 2019
Published: July 29, 2019

Abstract

In this paper, generalized *KdV* equations are investigated by using a mathematical technique based on the reduction of order for solving differential equations. The compactons, solitons, solitary patterns and periodic solutions for the equations presented in this paper are obtained. For these generalized *KdV* equations, it is found that the change of the exponents of the wave function u and the coefficient a, positive or negative, leads to the different physical structures of the solutions.

Keywords

Generalized *KdV* Equations, Compactons, Solitons, Physical Structures

1. Introduction

Late in the 19th century, Korteweg and de Vries developed a theory to describe weakly nonlinear wave propagation in shallow water. The classical Korteweg-de Vries (*KdV*) equation is usually written as

$$u_t + 6uu_x + u_{xxx} = 0. \tag{1}$$

After a long time, the *KdV* equation has been found to be involved in a wide range of physics phenomena, especially those exhibiting shock waves, travelling waves, and solitons. Certain theoretical physics phenomena in the quantum mechanics domain can be explained by means of *KdV* model.

As is well known, the classical *KdV* equation has been played a central role in the study of nonlinear phenomena, especially solitons phenomena which exist due to a balance between weak nonlinearity and dispersion. As one of the most fundamental equations of solitons phenomena, Equation (1) has caused great attention from many researchers, all forms of modified *KdV* equations have been studied extensively (see [1]-[10]).

Tzirtzilakis, *et al.* [1] discussed second and third order approximations of water wave equations of *KdV* type. Analytical expression for solitary wave solutions for some special equations was derived. By using a Fourier pseudospectral method combined with a finite-difference scheme, a detailed numerical study of these solutions obtained in [1] was carried out. The stability of these solitary wave solutions was also established.

Rosenau and Hyman [2] introduced and studied a class of *KdV* equations—$K(m,n)$ equation. They discovered that the solitary solutions of these equations, for certain m and n, have compact support, namely they vanish outside a finite core region. Solitons with finite wavelength are called compactons.

In [3], Rosenau subsequently studied the model

$$u_t + a\left(u^{n+1}\right)_x + \left[u\left(u^n\right)_{xx}\right]_x = 0, \quad n \geq 1, \tag{2}$$

where $a > 0$. This model emerged in nonlinear lattices and was used to describe the dispersion of dilute suspensions for $n = 1$. But Rosenau [3] only got general formulas in terms of the cosine for model (2). With the use of new ansatze methods, Wazwaz [4] examined model (2) for two cases, $a > 0$ and $a < 0$. And the exact travelling solutions in terms of sine, cosine function, the hyperbolic function sinh and cosh were derived.

Wazwaz investigated variants of the *KdV* equations respectively in [5] and [6] as follows:

$$u_t + au\left(u^n\right)_x + \left[u\left(u^n\right)_{xx}\right]_x = 0, \quad n > 1, \tag{3}$$

$$u_t + au^n\left(u\right)_x + \left[u^n\left(u\right)_{xx}\right]_x = 0, \quad n \geq 3, \tag{4}$$

where a is a nonzero constant. The compactons and solitary pattern solutions were presented.

The present work aims to extend the work made by Wazwaz [5] [6]. We desire to seek another method to solve nonlinear equations. For this purpose, the wave variable $\xi = \mu x - ct$ is introduced to carry the PDEs into ODEs. By using this variable replacement method, some new exact solutions including solitons can be obtained. In fact, the method in this paper is efficient to solve many nonlinear equations. It avoids tedious algebra and guesswork and also can be used in higher dimensional space.

In this paper, we will discuss generalized *KdV* equations, Equaiton (3) and Equaiton (4) and the following equations with negative exponents:

$$u_t + au\left(u^{-n}\right)_x + \left[u\left(u^{-n}\right)_{xx}\right]_x = 0, \quad n > 1, \tag{5}$$

$$u_t + au^{-n}\left(u\right)_x + \left[u^{-n}\left(u\right)_{xx}\right]_x = 0, \quad n \geq 3, \tag{6}$$

where a is a nonzero constant. In the sense of ignoring the constants of integration resulted from solving Equations (3)-(6), the exact travelling solutions have been obtained which contain the main results made in [5] [6] as special cases.

2. The Generalized *KdV* Equations with Positive Exponents

2.1. Exact Travelling Wave Solutions for Equation (3)

Firstly, we assume that the travelling wave solutions of Equation (3) take the form

$$u(x,t)=u(\xi),\quad \xi=\mu x-ct, \tag{7}$$

in which $\mu\neq 0$, $c\neq 0$.

Notice that

$$\frac{\partial}{\partial t}=-c\frac{\mathrm{d}}{\mathrm{d}\xi},\quad \frac{\partial}{\partial x}=\mu\frac{\mathrm{d}}{\mathrm{d}\xi},\quad \frac{\partial^3}{\partial x^3}=\mu^3\frac{\mathrm{d}^3}{\mathrm{d}\xi^3}. \tag{8}$$

Substituting (7) and (8) into Equation (3) gives the following nonlinear ODE

$$-cu_{\xi}+a\mu u\left(u^n\right)_{\xi}+\mu^3\left[u\left(u^n\right)_{\xi\xi}\right]_{\xi}=0. \tag{9}$$

Integrating Equation (9) once and setting the constant of integration to be zero, we find

$$\mu^3 u\left(u^n\right)_{\xi\xi}+\frac{an\mu}{n+1}u^{n+1}-cu=0. \tag{10}$$

Considering $u\neq 0$, we get

$$\mu^3\left(u^n\right)_{\xi\xi}+\frac{an\mu}{n+1}u^n-c=0. \tag{11}$$

Set $V=u^n$, then

$$\mu^3 V_{\xi\xi}+\frac{an\mu}{n+1}V-c=0. \tag{12}$$

Letting $\frac{\mathrm{d}V}{\mathrm{d}\xi}=Z$, we get $\frac{\mathrm{d}^2V}{\mathrm{d}\xi^2}=Z\frac{\mathrm{d}Z}{\mathrm{d}V}$. So Equation (12) becomes

$$\mu^3 Z\frac{\mathrm{d}Z}{\mathrm{d}V}+\frac{an\mu}{n+1}V-c=0. \tag{13}$$

By using the separating variants method, we have

$$\frac{\mu^3}{2}Z^2=cV-\frac{an\mu}{2(n+1)}V^2. \tag{14}$$

That is

$$\left(\frac{\mathrm{d}V}{\mathrm{d}\xi}\right)^2=\frac{V}{\mu^3}\left(2c-\frac{an\mu}{n+1}V\right). \tag{15}$$

Case 1. $a>0$: Solving Equation (15) gives

$$V=\frac{2c(n+1)}{an\mu}\sin^2\left(\frac{1}{2\mu}\sqrt{\frac{an}{n+1}}\xi\right), \tag{16}$$

and

$$V=\frac{2c(n+1)}{an\mu}\cos^2\left(\frac{1}{2\mu}\sqrt{\frac{an}{n+1}}\xi\right). \tag{17}$$

Hence, we limit the domain of ξ, obtain the following compacton solutions:

$$u(x,t)=\begin{cases}\left\{\dfrac{2c(n+1)}{an\mu}\sin^2\left[\dfrac{1}{2\mu}\sqrt{\dfrac{an}{n+1}}(\mu x-ct)\right]\right\}^{\frac{1}{n}}, & |\xi|\le 2|\mu|\pi\Big/\sqrt{\dfrac{an}{n+1}},\\ 0, & \text{otherwise,}\end{cases} \tag{18}$$

and

$$u(x,t)=\begin{cases}\left\{\dfrac{2c(n+1)}{an\mu}\cos^2\left[\dfrac{1}{2\mu}\sqrt{\dfrac{an}{n+1}}(\mu x-ct)\right]\right\}^{\frac{1}{n}}, & |\xi|\le |\mu|\pi\Big/\sqrt{\dfrac{an}{n+1}},\\ 0, & \text{otherwise.}\end{cases} \tag{19}$$

Case 2. $a<0$: Solving Equation (15), we get the solitary pattern solutions as follows:

$$u(x,t)=\left\{-\frac{2c(n+1)}{an\mu}\sinh^2\left[\frac{1}{2\mu}\sqrt{-\frac{an}{n+1}}(\mu x-ct)\right]\right\}^{\frac{1}{n}}, \tag{20}$$

and

$$u(x,t)=\left\{\frac{2c(n+1)}{an\mu}\cosh^2\left[\frac{1}{2\mu}\sqrt{-\frac{an}{n+1}}(\mu x-ct)\right]\right\}^{\frac{1}{n}}. \tag{21}$$

Remark 1. Letting $\mu=1$ in (18) and (19), we have

$$u(x,t)=\begin{cases}\left\{\dfrac{2c(n+1)}{an}\sin^2\left[\dfrac{1}{2}\sqrt{\dfrac{an}{n+1}}(x-ct)\right]\right\}^{\frac{1}{n}}, & |-ct|\le 2\pi\Big/\sqrt{\dfrac{an}{n+1}},\\ 0, & \text{otherwise,}\end{cases} \tag{22}$$

and

$$u(x,t)=\begin{cases}\left\{\dfrac{2c(n+1)}{an}\cos^2\left[\dfrac{1}{2}\sqrt{\dfrac{an}{n+1}}(x-ct)\right]\right\}^{\frac{1}{n}}, & |-ct|\le \pi\Big/\sqrt{\dfrac{an}{n+1}},\\ 0, & \text{otherwise.}\end{cases} \tag{23}$$

which just are the main results for Equation (3) obtained by Wazwaz [5]. In other words, solutions (22), (23) made in [5] are special cases of formulas (18), (19).

2.2. Exact Travelling Wave Solutions for Equation (4)

Following the analysis presented above, we use the wave variable $\xi=\mu x-ct$ into Equation (4) to get the following ODE:

$$\mu^3 u_{\xi\xi\xi}+\frac{a\mu}{n+1}u-cu^{1-n}=0. \tag{24}$$

Letting $Y=\dfrac{\mathrm{d}u}{\mathrm{d}\xi}$, we get $\dfrac{\mathrm{d}^2u}{\mathrm{d}\xi^2}=Y\dfrac{\mathrm{d}Y}{\mathrm{d}u}$. Then

$$\mu^3 Y\frac{\mathrm{d}Y}{\mathrm{d}u}+\frac{a\mu}{n+1}u-cu^{1-n}=0. \tag{25}$$

Solving Equation (25) yields

$$\left(\frac{\mathrm{d}u}{\mathrm{d}\xi}\right)^2 = \frac{1}{\mu^3}\left(\frac{2c}{2-n}u^{-n} - \frac{a\mu}{n+1}\right)u^2. \tag{26}$$

Setting $W = u^{-n}$, we have

$$u = W^{-\frac{1}{n}}, \tag{27}$$

$$\mathrm{d}u = -\frac{1}{n}W^{-\frac{1}{n}-1}\mathrm{d}W. \tag{28}$$

Substituting (27) and (28) into Equation (26) gives

$$\left(\frac{\mathrm{d}W}{\mathrm{d}\xi}\right)^2 = \frac{n^2}{\mu^3}\left(\frac{2c}{2-n}W - \frac{a\mu}{n+1}\right)W^2. \tag{29}$$

Case 1. $a > 0$: For this case, solving Equation (29), we get

$$W = \frac{a\mu(2-n)}{2c(n+1)}\sec^2\left(\frac{n}{2\mu}\sqrt{\frac{a}{n+1}}\xi\right), \tag{30}$$

and

$$W = \frac{a\mu(2-n)}{2c(n+1)}\csc^2\left(\frac{n}{2\mu}\sqrt{\frac{a}{n+1}}\xi\right). \tag{31}$$

Therefore, we obtain the following compacton solutions:

$$u(x,t) = \begin{cases} \left\{\dfrac{2c(n+1)}{a\mu(2-n)}\sin^2\left[\dfrac{n}{2\mu}\sqrt{\dfrac{a}{n+1}}(\mu x - ct)\right]\right\}^{\frac{1}{n}}, & |\xi| \le 2|\mu|\pi \Big/ n\sqrt{\dfrac{a}{n+1}}, \\ 0, & \text{otherwise}, \end{cases} \tag{32}$$

and

$$u(x,t) = \begin{cases} \left\{\dfrac{2c(n+1)}{a\mu(2-n)}\cos^2\left[\dfrac{n}{2\mu}\sqrt{\dfrac{a}{n+1}}(\mu x - ct)\right]\right\}^{\frac{1}{n}}, & |\xi| \le |\mu|\pi \Big/ n\sqrt{\dfrac{a}{n+1}}, \\ 0, & \text{otherwise}. \end{cases} \tag{33}$$

Case 2. $a < 0$: Solving Equation (29), we have the solitary pattern solutions given by

$$u(x,t) = \left\{-\frac{2c(n+1)}{a\mu(2-n)}\sinh^2\left[\frac{n}{2\mu}\sqrt{-\frac{a}{n+1}}(\mu x - ct)\right]\right\}^{\frac{1}{n}}, \tag{34}$$

and

$$u(x,t) = \left\{\frac{2c(n+1)}{a\mu(2-n)}\cosh^2\left[\frac{n}{2\mu}\sqrt{-\frac{a}{n+1}}(\mu x - ct)\right]\right\}^{\frac{1}{n}}. \tag{35}$$

3. The Generalized *KdV* Equations with Negative Exponents

In fact, Equation (3) and Equation (4) and Equation (5) and Equation (6) have

the symmetric property about n respectively. We replace n by $-n$ in Equation (3) and Equation (4) and the corresponding travelling wave solutions in Section 2. So we have the following results:

3.1. Exact Travelling Wave Solutions for Equation (5)

Case 1. $a>0$: The periodic solutions are given by

$$u(x,t)=\left\{\frac{an\mu}{2c(n-1)}\sec^2\left[\frac{1}{2\mu}\sqrt{\frac{an}{n-1}}(\mu x-ct)\right]\right\}^{\frac{1}{n}}, \tag{36}$$

and

$$u(x,t)=\left\{\frac{an\mu}{2c(n-1)}\csc^2\left[\frac{1}{2\mu}\sqrt{\frac{an}{n-1}}(\mu x-ct)\right]\right\}^{\frac{1}{n}}. \tag{37}$$

Case 2. $a<0$: The soliton solutions have the forms of

$$u(x,t)=\left\{\frac{an\mu}{2c(n-1)}\operatorname{sech}^2\left[\frac{1}{2\mu}\sqrt{-\frac{an}{n-1}}(\mu x-ct)\right]\right\}^{\frac{1}{n}}, \tag{38}$$

and

$$u(x,t)=\left\{-\frac{an\mu}{2c(n-1)}\operatorname{csch}^2\left[\frac{1}{2\mu}\sqrt{-\frac{an}{n-1}}(\mu x-ct)\right]\right\}^{\frac{1}{n}}. \tag{39}$$

3.2. Exact Travelling Wave Solutions for Equation (6)

Case 1. $a>0$: In this case, we get the following soliton solutions:

$$u(x,t)=\left\{\frac{a\mu(n+2)}{2c(1-n)}\operatorname{sech}^2\left[\frac{n}{2\mu}\sqrt{-\frac{a}{1-n}}(\mu x-ct)\right]\right\}^{\frac{1}{n}}, \tag{40}$$

and

$$u(x,t)=\left\{-\frac{a\mu(n+2)}{2c(1-n)}\operatorname{csch}^2\left[\frac{n}{2\mu}\sqrt{-\frac{a}{1-n}}(\mu x-ct)\right]\right\}^{\frac{1}{n}}. \tag{41}$$

Case 2. $a<0$: We have the following periodic solutions:

$$u(x,t)=\left\{\frac{a\mu(n+2)}{2c(1-n)}\sec^2\left[\frac{n}{2\mu}\sqrt{\frac{a}{1-n}}(\mu x-ct)\right]\right\}^{\frac{1}{n}}, \tag{42}$$

and

$$u(x,t)=\left\{\frac{a\mu(n+2)}{2c(1-n)}\csc^2\left[\frac{n}{2\mu}\sqrt{\frac{a}{1-n}}(\mu x-ct)\right]\right\}^{\frac{1}{n}}. \tag{43}$$

4. Conclusions

The method based on the reduction of order is a powerful tool for acquiring

some special solutions of nonlinear PDEs. In this paper, we study three types of generalized *KdV* equations with positive and negative exponents by using this mathematical technique. Different from others, this technique carries some partial differential equations into ordinary equations which are easier to be solved. And the analytical expression of travelling wave solutions, containing compactons, solitons, solitary patterns and periodic solutions, are derived.

The obtained results in Section 2 and Section 3 each represent two completely different sets of models, which has been shown that the variation of exponents and coefficient, positive or negative, could cause the quantitative change in the physical structure of the solutions. The physical structures of the compactons solutions and the solitary patterns solutions deepen our understanding of many scientific processes, such as the super deformed nuclei, preformation of cluster in hydrodynamic models, the fission of liquid drops, and the inertial fusion.

Conflicts of Interest

The author declares no conflicts of interest regarding the publication of this paper.

References

[1] Tzirtzilakis, E., Mrinakis, V., Apokis, C. and Bountis, T. (2002) Soliton-Like Solutions of Higher Order Wave Equations of the Korteweg-de Vries Type. *Journal of Mathematical Physics*, **43**, 6151-6165. https://doi.org/10.1063/1.1514387

[2] Rosenau, P. and Hyman, J.M. (1993) Compactons: Solitons with Finite Wavelength. *Physical Review Letters*, **70**, 564-567. https://doi.org/10.1103/PhysRevLett.70.564

[3] Rosenau, P. (2000) Compact and Noncompact Dispersive Structures. *Physics Letters A*, **275**, 193-203. https://doi.org/10.1016/S0375-9601(00)00577-6

[4] Wazwwaz, A.M. (2002) Compactons Dispersive Structures for Variants of the K (m, n) and the KP Equations. *Chaos, Solitons and Fractals*, **15**, 1053-1062. https://doi.org/10.1016/S0960-0779(01)00109-6

[5] Wazwwaz, A.M. (2003) Compactons and Solitary Patterns Structures for Variants of the KdV and KP Equations. *Applied Mathematics and Computation*, **139**, 37-54. https://doi.org/10.1016/S0096-3003(02)00120-0

[6] Wazwwaz, A.M. (2004) Dinstinct Variants of the KdV Equation with Compact and Nocompact Structures. *Applied Mathematics and Computation*, **150**, 365-377. https://doi.org/10.1016/S0096-3003(03)00238-8

[7] Taogetusang, S. (2006) New Exact Wave Solutions to Generalized mKdV Equation and Generalized Zakharov-Kuzentsov Equation. *Chinese Physics*, **15**, 1143-1148. https://doi.org/10.1088/1009-1963/15/6/004

[8] Zhu, Z. (1996) Exact Solutions for a Two-Dimensional KdV-Burgers Equation. *Chinese Journal of Physics*, **34**, 1101-1105.

[9] Fan, E.G. and Zhang, H.Q. (1998) New Exact Solutions for a System of Coupled KdV Equation. *Physics Letters A*, **245**, 389-392. https://doi.org/10.1016/S0375-9601(98)00464-2

[10] Fan, E.G. (2006) Soliton Solutions for a Generalized Hirota-Satsuma Coupled KdV Equation and a Coupled mKdV Equation. *Physics Letters A*, **348**, 244-250.

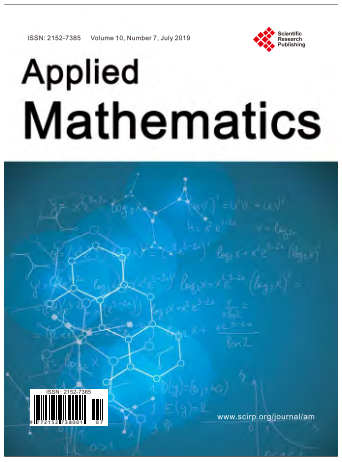

Call for Papers

Applied Mathematics (AM)

ISSN Print: 2152-7385 ISSN Online: 2152-7393
http://www.scirp.org/journal/am

Applied Mathematics **(AM)** is an international journal dedicated to the latest advancement of applied mathematics. The goal of this journal is to provide a platform for scientists and academicians all over the world to promote, share, and discuss various new issues and developments in different areas of applied mathematics.

Subject Coverage

All manuscripts must be prepared in English, and are subject to a rigorous and fair peer-review process. Accepted papers will immediately appear online followed by printed hard copy. The journal publishes original papers including but not limited to the following fields:

- Applied Probability
- Applied Statistics
- Approximation Theory
- Chaos Theory
- Combinatorics
- Complexity Theory
- Computability Theory
- Computational Methods in Mechanics and Physics
- Continuum Mechanics
- Control Theory
- Cryptography
- Discrete Geometry
- Dynamical Systems
- Elastodynamics
- Evolutionary Computation
- Financial Mathematics
- Fuzzy Logic
- Game Theory
- Graph Theory
- Information Theory
- Inverse Problems
- Linear Programming
- Mathematical Biology
- Mathematical Chemistry
- Mathematical Economics
- Mathematical Physics
- Mathematical Psychology
- Mathematical Sociology
- Matrix Computations
- Neural Networks
- Nonlinear Processes in Physics
- Numerical Analysis
- Operations Research
- Optimal Control
- Optimization
- Ordinary Differential Equations
- Partial Differential Equations
- Probability Theory
- Statistical Finance
- Stochastic Processes
- Theoretical Statistics

We are also interested in: 1) Short Reports—2-5 page papers where an author can either present an idea with theoretical background but has not yet completed the research needed for a complete paper or preliminary data; 2) Book Reviews—Comments and critiques.

Notes for Intending Authors

Submitted papers should not have been previously published nor be currently under consideration for publication elsewhere. Paper submission will be handled electronically through the website. All papers are refereed through a peer review process. For more details about the submissions, please access the website.

Website and E-mail

http://www.scirp.org/journal/am **E-mail: am@scirp.org**

What is SCIRP?

Scientific Research Publishing (SCIRP) is one of the largest Open Access journal publishers. It is currently publishing more than 200 open access, online, peer-reviewed journals covering a wide range of academic disciplines. SCIRP serves the worldwide academic communities and contributes to the progress and application of science with its publication.

What is Open Access?

All original research papers published by SCIRP are made freely and permanently accessible online immediately upon publication. To be able to provide open access journals, SCIRP defrays operation costs from authors and subscription charges only for its printed version. Open access publishing allows an immediate, worldwide, barrier-free, open access to the full text of research papers, which is in the best interests of the scientific community.

- High visibility for maximum global exposure with open access publishing model
- Rigorous peer review of research papers
- Prompt faster publication with less cost
- Guaranteed targeted, multidisciplinary audience

Scientific Research Publishing

Website: http://www.scirp.org

Subscription: sub@scirp.org

Advertisement: service@scirp.org